Hybrid adaptive observer for controlling a Brushless DC Motor

(MASTER THESIS BY GROUP 1032C)

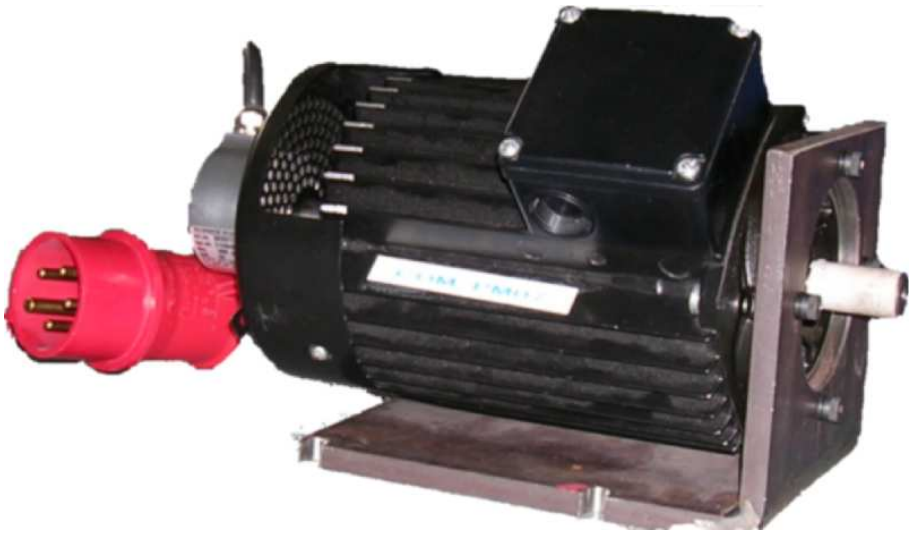

AALBORG UNIVERSITY · AAU
Department of Electronic Systems

Master Thesis, May 2007
Group 1032c

This page is left intentionally blank

Intelligent Autonomous Systems
Fredrik Bajers Vej 7C
9220 Aalborg Ø, Denmark
Telephone +45 96 35 87 00
Fax +45 98 15 17 39

Title:

Hybrid adaptive observer for controlling a Brushless DC Motor

Semester:

10th, IAS

Project group:

1032c

Supervisors:

Jan Dimon Bendtsen
Carsten Skovmose Kallesøe

Group Members:

Piotr Niemczyk
Thomas Porchez

Copies: 7

Report pages: 98

Appendices pages: 21

Finished: 24^{th} May 2007

Abstract:

This report documents the work conducted on the development of hybrid adaptive observers for a BLDCM. The goal of the project is to investigate the possibilities of using those observers in the control of brushless DC motors.
A previously designed observer was improved by changing its structure and decreasing its computational demands. Various optimization techniques for finding the observers' parameters were investigated and suitable methods were selected.
An observer that uses only one current sensor to estimate the rotor's angle and speed was designed. A new hybrid automaton and continuous equations for this observer were derived. Both of the observers were tested and have shown good results in open loop estimation.
Simulations were run to verify the possibility of controlling the motor using the observers' estimates. Then the observers were tested to control a real BLDCM. The observer that utilizes two current sensors was found to be able to provide sufficient information for control in a reduced operating region than. The single sensor observer estimates did not remain stable; thus it is concluded that it is not possible to remove the second sensor in the current setup.

This page is left intentionally blank

PREFACE

This is Master Thesis report that documents the 10th semester project work done by group 1032c from the Department of Electronic Systems, Intelligent Autonomous Systems specialization at Aalborg University. The project work spanned the period of 1^{st} of February 2007 - 7^{th} of June 2007.

Throughout the report, chapters are numbered sequentially. Sections, figures, tables and equations are numbered sequentially according to the chapter in question. Literature references are presented as [Chi05], which refers to "Modeling and High-Performance Control of Electric Machines" by John Chiasson. Sections, figures, tables and equations are referred to using the chapter and index number, e.g. Section 6.2, Figure 6.2, Table 6.2 and Equation 6.2. A nomenclature and acronym lists are included at the end of the report to explicate the terms and notations that were used.

The enclosed CD-ROM contains this report in .pdf format. Data sheets, various sources and MATLAB® / Simulink® implementations are also included. For readers with an interest in this CD-ROM, attention is turned towards the file Readme.txt located in the root folder. A part of previous work [NP06] is also included in this report, mostly in Chapters 2 and 3, to explain the methods developed earlier.

We would like to thank Rasmus K. Ursem from Grundfos for his help on optimization algorithms used in this report.

Special thanks to our supervisors Jan Dimon Bendtsen and Carsten Skovmose Kallesøe for their time, important feedback and very good cooperation during the two semesters of our studies at AAU.

Aalborg, the 24^{th} of May, 2007

Piotr Niemczyk Thomas Porchez

This page is left intentionally blank

CONTENTS

1 Introduction **1**

1.1 Motivation . . . 3

1.2 Background . . . 4

1.3 Test setup . . . 5

1.4 Objectives . . . 5

1.5 Report outline . . . 6

2 Introduction to the Brushless DC Motor (BLDCM) **9**

2.1 Construction . . . 9

2.2 Three phase inverter . . . 10

2.3 Pulse Width Modulation . . . 11

2.4 Control strategy . . . 14

2.5 Back-ElectroMotive Force (EMF) sensing method . . . 15

2.6 Dynamics of the BLDCM . . . 16

2.7 Conclusion . . . 22

3 Hybrid model **23**

3.1 Definition of a hybrid system . . . 23

3.2 Hybrid automaton . . . 24

3.3 Continuous time equations . . . 27

3.4 Formal description of the model . . . 31

3.5 Test of the hybrid model . . . 33

3.6 Conclusion . . . 35

4 Hybrid observer **37**

4.1 Location automaton . . . 37

4.2 Structure of the continuous observer 38
4.3 Calculation of the angle and the speed 40
4.4 Continuous observer equations 41
4.5 Conclusion 43

5 Optimization of observer feedback **45**
5.1 Problem overview 45
5.2 Random search methods 46
5.3 Particle Swarm Optimization 47
5.4 Evolutionary Computation 47
5.5 Implementation and verification 56
5.6 Conclusion 63

6 Verification of the observer **65**
6.1 Test setup 65
6.2 Test results 66
6.3 Proportional correction of the estimates 68
6.4 Conclusion 71

7 Single sensor observer **73**
7.1 Practical requirements for the use of one sensor 73
7.2 Single sensor observer hybrid automaton 75
7.3 Single sensor observer equations 77
7.4 Test of the single sensor observer 80
7.5 Conclusion 82

8 Closed loop implementation **83**
8.1 Simulations of closed loop performance 83
8.2 Observer tests on the real system 86

8.3 Conclusion 93

9 Conclusion **95**

9.1 Summary 95

9.2 Methodology 96

9.3 Achievements 97

9.4 Future work 97

Bibliography **98**

Appendix **101**

A Simplified hybrid automaton for the single sensor observer **103**

B Real time implementation **105**

B.1 Simplification of the equations 105

B.2 FSA 110

B.3 Checkmate removal 110

C Results of the closed loop tests of the double sensor observer **113**

Nomenclature **117**

This page is left intentionally blank

INTRODUCTION 1

A Brushless DC Motor (BLDCM) is an electrical motor composed of permanent magnets and windings. Its motion principle is similar to the motion principle of a classical DC motor, or brushed motor. A magnetic field is created by circulating a current through the windings, then the magnetic field created by the magnets aligns to this magnetic field. The alignment of those two magnetic fields is the origin of the motion of the rotor. In the BLDCM the windings are fixed in the motor, while the magnets are fixed on the rotor and therefore can evolve with one degree of freedom. The rotor therefore rotates so that its magnetic field aligns to the fixed magnetic field. Even though the physical principles used to rotate the rotor are similar, the design of a BLDCM is deeply different from the classical DC motor. For the BLDCM the rotating parts are the magnets, while they are the windings in the brushed motor. This results in the absence of a commutator and brushes in the BLDCM, meaning high reliability and longer life time as there is no commutator or brushes erosion. Figure 1.1 shows the physical design of the BLDCM used in this project.

FIGURE 1.1: *Picture of stator and rotor of a BLDCM.*

Compared to the AC machine, which has a similar design, the BLDCM has higher efficiency due to the particular shape of its back-electromotive force (back-EMF). The AC machine receives smooth sinusoidal signals, while the BLDCM receives discontinuous signals shaped by a current inverter. Those discontinuities create ripples in the torque of the BLDCM and they generate vibrations, which make the BLDCM is noisy.

BLDCMs are used for example in PC cooling fans, hard drives, or electric vehicles, where high reliability and extended life time are required. In this report the application

that is considered is the BLDCM of a centrifugal pump, which can be used for instance in waste water treatment or as submersible pump to extract water from sources. In this type of application, it is particularly important to have high reliability as the access to the pump for maintenance is generally restricted. A design robust to mechanical wear is also an important asset knowing that the pump will run constantly at more than 70% of its maximum speed. The tradeoff against this design is the need of an external controller. In the brushed DC motor, the system commutator-brushes act like a mechanical controller, since the rotaton of the commutator changes the brushes to which it is connected, creating the required changes in current flows to move the rotor. As this does not exist on the BLDCM, an external circuit is needed to generate the appropriate currents in the phases. This circuit is called a three-phase inverter.

FIGURE 1.2: *Picture of an immersible pump produced by Grundfos. This is an example of an application, where a BLDCM is used (source Grundfos).*

To control this circuit properly, the angle of the rotor is used to know when the switching has to be done. In many applications, this angle is measured by a position sensor (encoder) on the shaft of the motor (Figure 1.3 on the next page), or by Hall effect sensors measuring the magnetic field created by the Permanent Magnet (PM) to determine the angle, but these elements increase the cost and reduce the reliability of the system, which was one of the main reasons for choosing a BLDCM in the first place. In sensorless applications the angle is generally measured by back-EMF sensing, which is quite efficient,

but has other drawbacks. Those will be pointed out in Section 2.5 on page 15, where the method is described in more details.

FIGURE 1.3: *Picture of a position sensor (encoder) mounted on the shaft (source Quantum Devices, Inc.).*

1.1 MOTIVATION

The motivation of this project is to develop an alternative technique to the back-EMF sensing method for estimating the angle to see if better control of the BLDCM can be achieved. The back-EMF sensing method will be described in details in Section 2.5 on page 15. The method proposed in this report is the use of a hybrid observer for the rotor angle and velocity.

A BLDCM can be studied as a continuous state system using voltages measurements as inputs, but it may also be seen as a system that contains both continuous states, i.e. currents flowing through a coil in a phase, and discrete events whenever a phase is activated or deactivated. The hybrid systems theory is a recent research area developed in order to study systems which have both discrete and continuous characteristics. The use of hybrid systems theory could therefore be highly beneficial to build an observer able to track the angle and the velocity of the rotor precisely, and also to build a hybrid controller for this kind of motor.

It will be shown in Section 2.5 on page 15 that back-EMF sensing does not allow a high precision, it only measures six different positions. The angle is only known at particular times, and therefore the switchings have to be made at those moments. The motivation

of designing an observer is that it would offer a better resolution of the angular position, as the angle estimation would always be available. This would allow advanced control methods to be used in the control of the BLDCM, giving the opportunity to improve the performance of the motor.

The design of a hybrid observer is also motivated by a reduction of the number of sensors used to estimate the angle. The back-EMF sensing method needs three sensors, while the hybrid observer, at least in principle, has the capacity of estimating the angle and the speed on basis of only one sensor, yielding a decrease in the cost and increase of the reliability.

The hybrid observer would be based on measurements of the currents flowing through the windings, meaning that it would be able to work in any situation, while back-EMF sensing requires that one of the winding's current is null. Under certain conditions, it can happen that currents flow all the time in all the windings, in which case the back-EMF sensing method can not be applied.

1.2 BACKGROUND

Previous work showed the benefits from applying hybrid systems theory to the BLDCM. A hybrid model of the BLDCM was derived, and proved to be accurate. The hybrid model used throughout this report was firstly derived in [NP06] on basis of [Han06] and [HB05]. A nonlinear hybrid observer for estimating the rotor angle and velocity was designed on basis of this hybrid model. The parameters of the observer were found by an optimization approach, which has shown to provide good results. The observer showed encouraging accuracy, as it was able to estimate angle of the rotor within $\pm 15^{\circ}$, and the error of the estimate of the angular velocity was within $\pm 12\,[\mathrm{rad} \cdot \mathrm{s}^{-1}]$. This observer was able to handle continuous changes in the angular velocity while keeping the same precision in the estimates.

The hybrid observer was able to estimate angle and speed by using only two currents sensors instead of three. A lot of efforts were made on reducing the computational demand of the observer in order to have a system able to estimate online. Despite large improvements at this level, the observer was still computationally too heavy, and only offline tests have been realized.

1.3 TEST SETUP

The test setup used during the project consisted of a motor connected to a power board with a current inverter and sensors. The power board receives a PWM signal through an optical link generated by a program running on dSpace® . The control of the motor was implemented in MATLAB® using Simulink® models which were compiled to the dSpace® interface to be sent to the target processor. The test setup is shown in Figure 1.4.

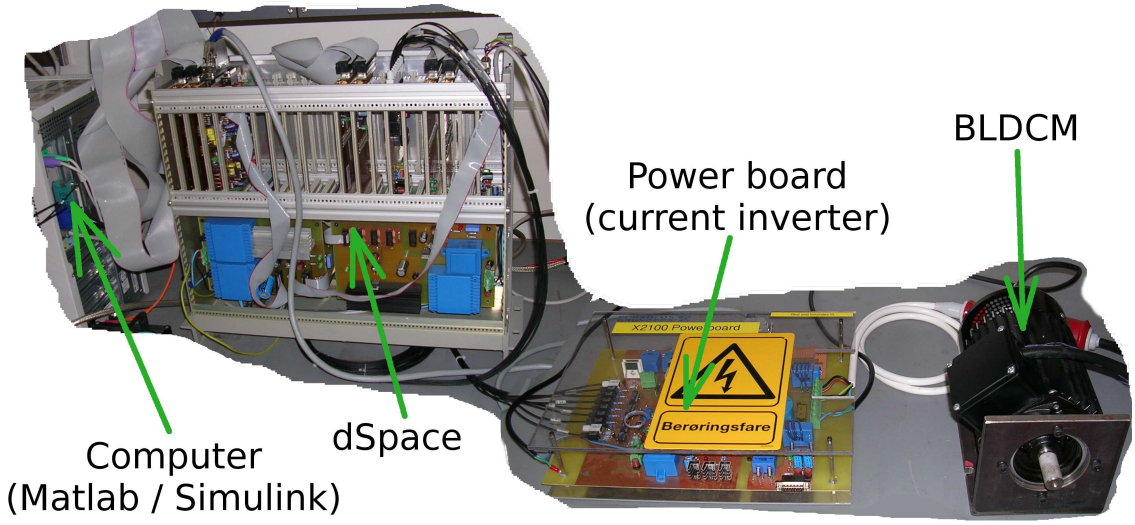

FIGURE 1.4: *Picture of the test setup used in the project.*

The important assumption in the project is that the considered range of speed is $\omega_r \in [500; 1000]$ [rpm]. This can be assumed as the goal of this project is to investigate the possibility of using hybrid observer for controlling the BLDCM in pump application, where the speed does not vary in the full range.

1.4 OBJECTIVES

Previous work has shown that a hybrid observer for the rotor angle and velocity can be designed, and achieve sufficient accuracy. The observer was so far not implemented online due to high computational demands.

In this project there are three main objectives, the first being to continue the work on the hybrid observer. The observer designed in [NP06] has been shown to work correctly, the objective is now to improve the precision of this observer. Firstly the structure of the

previous observer will be modified, i.e. any unused parts will be removed, and some parts will be replaced by others providing a better accuracy of the estimates. Then, several types of Evolutionary Algorithm (EA) will be applied to the optimization problem of finding correct parameters for the observer. EA will be used as they seem to suit well the optimization problem to solve, and therefore they could lead to better results than the optimization procedure used in the previous work.

The second main task is to reduce the number of sensors used by the observer to estimate the angle and the angular velocity. In this report, the use of only one current measurement will be investigated. Tests of this observer will then be run to check that it can work with real measurements.

The final task consists in testing both the single sensor observer and the double sensor observer in a closed loop situation, i.e. when the observers are used to provide the angle to a closed loop controller. This test will allow to check the behaviour of the observers in real conditions, and it will show if the use of an observer is suitable to control a BLDCM. In order to realize this final test, the observers must be able to estimate online on the target processor. The Simulink® implementations of the observers will be optimized so that dSpace® can compile and send them to the target processor. The computational demand of the observers will be reduced in order to be able to estimate the angle and the speed in real time. Then the final tests will be realized, and the results will allow to conclude on the use of a hybrid observer in providing the angle to control a BLDCM.

1.5 REPORT OUTLINE

The report is organized the following way:

Chapter 2: Introduction to the BLDCM
This chapter presents preliminary knowledges to ease the understanding of the report. The main concept of a BLDCM is presented. The current inverter used to control the currents in the BLDCM is then described. The main principles of the Pulse Width Modulation (PWM) modulation are introduced, and the chosen control strategy for the motor is defined. The back-EMF sensing method is presented. The equations for electrical and mechanical dynamics of the BLDCM are derived, and it is shown that only two differential equations are needed to define the electrical dynamics of the motor.

Chapter 3: Hybrid model
Introduces the concept and mathematical formulation of a Hybrid System. A hybrid

automaton for the BLDCM is then derived. The differential equations corresponding to each of the states of the hybrid automaton are expressed based on the differential equations for the BLDCM derived in the previous chapter. The formal description of the hybrid model derived is given. Finally, the results of a test of this model in [NP06] are presented.

Chapter 4: Hybrid observer

This chapter is the description of a novel hybrid observer used in this project. The structure of the observer derived in [NP06] is modified in order to improve it. The new structure is presented, and the equations of the observer are expressed.

Chapter 5: Optimization of observer feedback

The principles of different classes of optimization algorithms suited for the determination of observer's parameters will be presented. The most suitable algorithms for the problem considered will be selected. The different results will be compared and discussed, then the best result of optimization will be kept to be used in the observer.

Chapter 6: Test of the observer

The observer derived in Chapter 4 will be tested using the new feedback parameters found with the optimization methods of Chapter 5. This test will allow to check that the behaviour of the observer is correct, and that its precision has been improved by its new structure and feedback parameters.

Chapter 7: Single sensor observer

This chapter presents the reduction of the number of sensors to one current measurement instead of two. First the two conditions required to be able to observe the BLDCM using only one current sensor will be expressed. Then it will be shown that both of those conditions are fulfilled, and therefore changes will be made to the observer in order for it to use one measurement. A test of this new observer will be realized to check that it remains accurate with one sensor.

Chapter 8: Closed loop test of the observer

First, both observers are tested in Simulink® using the model instead of the real BLDCM. The observers will be used to provide the information of angle of the rotor to the commutator. This test will allow to verify the functionality of the observers in closed loop conditions. Having verified the performance of the observers in simulations, they will be tested in closed loop conditions with the real motor. The results of those closed loop tests will be analysed to determine the efficiency of the system using the observers.

Chapter 9: Conclusion

Results and achievements of the project will be discussed. Then, opportunities for future work will be described.

INTRODUCTION TO THE BLDCM

2

This chapter presents an overview of the BLDCM concept. The drive circuit of the BLDCM, called three phase inverter, is described. The switching method using PWM modulation is defined as well as the control strategy used to rotate the rotor. The back-EMF sensing method is explained and its efficiency is discussed. The mathematical model of the electrical and mechanical dynamics is then described. Those equations correspond to a reduced model for the dynamics in the ab-frame, they were firstly derived in [NP06].

2.1 CONSTRUCTION

The advantages of the brushless design are mostly due to the fact that there is a limited contact between elements inside the motor. This reduces friction, makes the motor more robust to failures, and extends its lifetime. However this comes with a burden of a more difficult control that has to be performed.

A BLDCM is a PM synchronous machine, which has uniformly wounded windings and back-EMF of a trapezoidal shape. A possible configuration of a one pole pair magnet motor is depicted in Figure 2.1 on the following page.

In case there is more than one magnet pole pair in the machine, the electrical angle (θ_e) is not equal to the mechanical angle (θ_r). Electrical angle is the change in the magnetic field, whereas the mechanical angle is the change in the rotor's position. The relation between these angles is given by equation 2.1, where Z_p is a number of magnetic pole pairs. This leads to relation 2.2 for the electrical angular velocity ω_e, which is the time derivative of the angle θ_e.

$$\theta_e = Z_p \theta_r \tag{2.1}$$

$$\omega_e = Z_p \omega_r \tag{2.2}$$

A discontinuous six-step current inverter is used to generate the physical switching between phases. The input signal to this inverter is shaped by a PWM device.

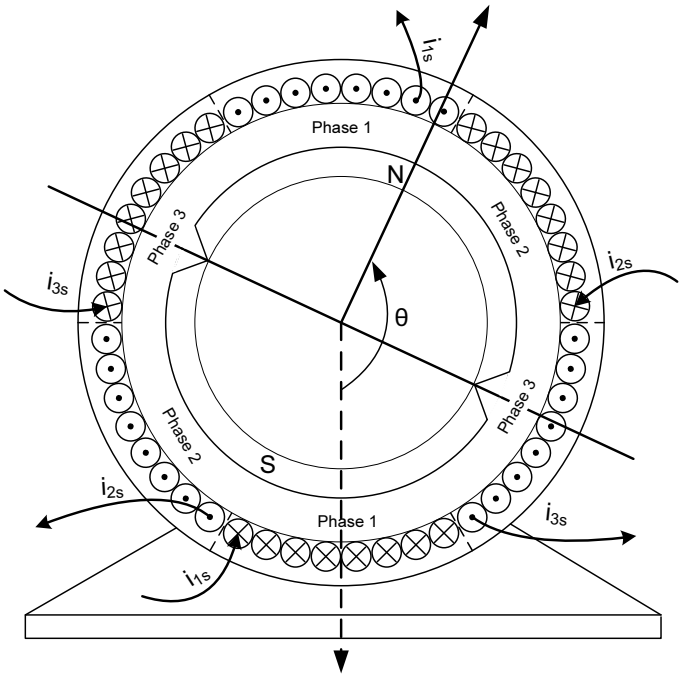

FIGURE 2.1: *Uniform windings of a BLDCM with one magnetic pole pair [Chi05].*

2.2 THREE PHASE INVERTER

The transition between direct current and the alternating current supplied to the motor is carried out by switching MOSFET transistors. The design of such an inverter is depicted in Figure 2.2.

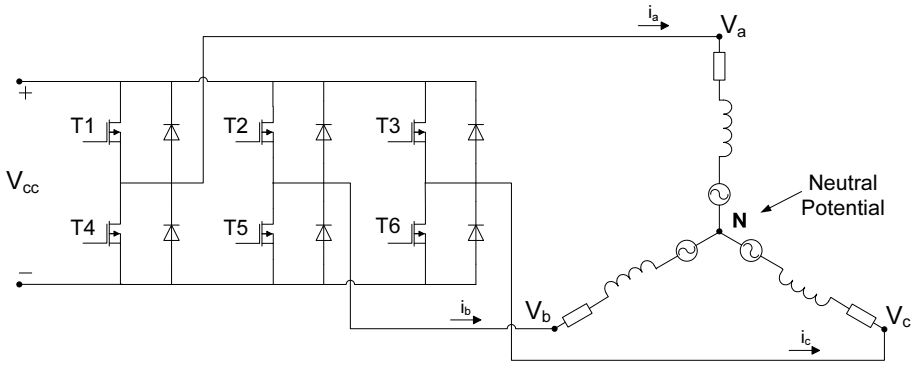

FIGURE 2.2: *Electrical circuit of the* $120°$ *current inverter and a WYE-connected BLDCM.*

The inverter is a six-step current inverter in which one of the phases is eventually open circuited for $120°$ of the cycle. It is connected to the machine such that i_{as}, i_{bs}, i_{cs} are the stator currents. Figure 2.3(a) on the facing page shows the idealized currents applied

to the phases of a machine as a function of time. The EMF, also shown on the figure, can be measured during the tristate periods. It provides a good knowledge about the rotor's position and can be used in sensorless control schemes for a BLDCM, this will be discussed in Section 2.5 on page 15.

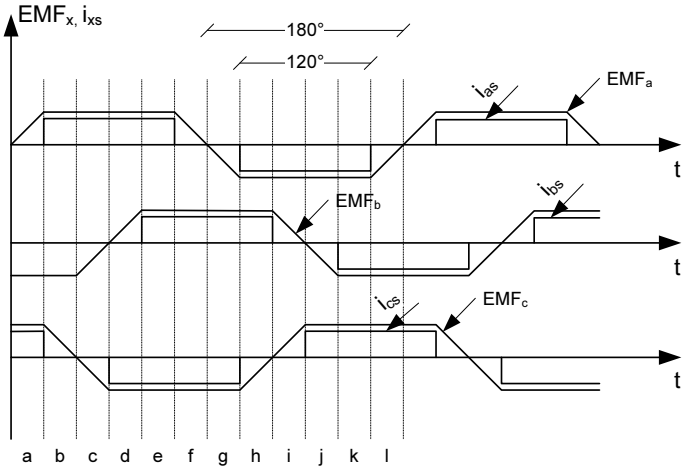

(a) Idealized phase currents applied to the machine. The figure also shows the EMF that can be measured and used in a sensorless methods of control [HB05].

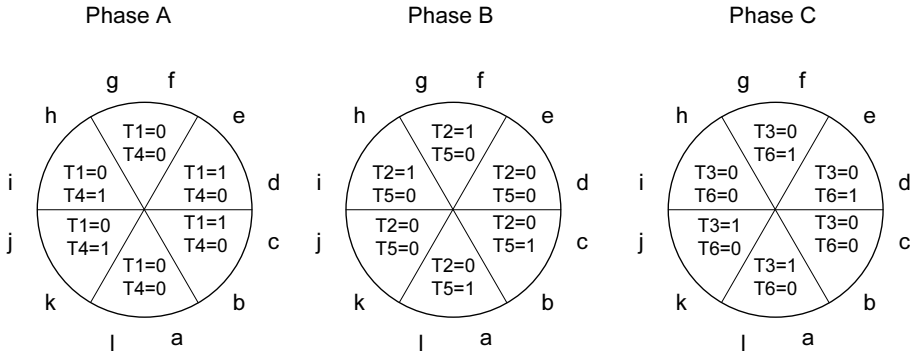

(b) Switching sequence of the MOSFET transistors that converts direct currents into alternating currents [HB05]. Lower case letters $a \ldots l$ correspond to 30° angular intervals shown in (a).

FIGURE 2.3: *Stator currents, EMF of a BLDCM and the switching sequence of the transistors.*

2.3 PULSE WIDTH MODULATION

The power to the BLDCM, and therefore its angular velocity can be controlled by controlling the value of source voltage V_{cc} (shown in Figure 2.2 on the facing page). However, since the control of the current inverter is performed by a digital processor, PWM is a

more efficient way of controlling the motor. The modulation is responsible for switching the transistors so that the amplitudes of the phase voltages have desired values. The principle of the PWM modulation is to constantly switch between the supply voltage and the ground, which explains why it is very suitable with digital processors as it is a binary behaviour. A signal corresponding to a PWM modulation is shown on Figure 2.4.

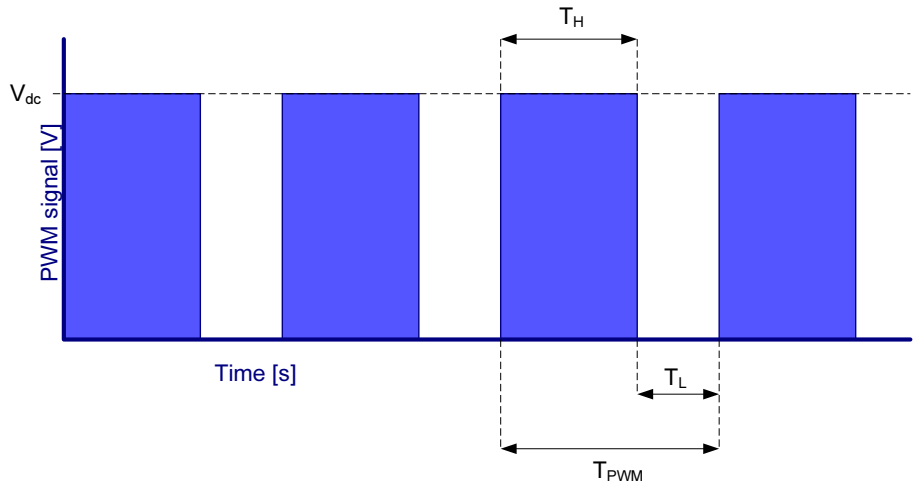

FIGURE 2.4: *Signal representing a PWM modulation.*

V_{dc} is the amplitude of the modulation, T_H is the time at high state, T_L is the time at low state, and T_{PWM} is the period of the PWM signal, with $T_{PWM} = T_H + T_L$. D_{in} is the duty cycle (value between 0 and 1), it defines the width of the impulse as follows:

$$D_{in} = \frac{T_H}{T_H + T_L}$$

A PWM device is usually connected to the machine by a low-pass filter that yields an average of the signal in one processor tact. The frequency chosen for the PWM modulation is $16\,[\text{KHz}]$. The choice of this frequency is important as it will be assumed in the following that the voltages to the phases of the motor are continuous voltages. The potential V_{PWM} created by a PWM modulation will be defined as the mean value of the signal:

$$V_{PWM} = D_{in} \cdot V_{dc} \tag{2.3}$$

This assumption can be made as the motor acts like a low-pass filter, and therefore from its point of view only the mean value matters. The transfer function $H(s)$ from voltage to current of the motor is described by Equation 2.4. This transfer function is written

on basis of Figure 2.2 on page 10, which shows that a phase of the motor is equivalent to an inductance and a resistor connected in serial.

$$H(s) = \frac{\frac{1}{r_s}}{1 + s\frac{L_s}{r_s}} \tag{2.4}$$

With r_s and L_s the resistance and the inductance of a phase respectively. It will be estimated later on that $r_s = 3.8\,[\Omega]$ and $L_s = 0.0135\,[\mathrm{H}]$. The cut-off frequency f_c is defined as $f_c = \frac{r_s}{2\pi L_s} = 44.8\,[\mathrm{Hz}]$. After passing through this filter, the harmonic at $16\,[\mathrm{KHz}]$ undergoes an attenuation of $-46dB$, and thus it is acceptable to consider only the mean value of the PWM signal.

The higher the PWM frequency, the higher the attenuation, however in this case it is not possible to use a frequency larger than $16\,[\mathrm{KHz}]$ for two reasons. Firstly, there is a dead-band time of $1\mu s$. A dead-band time is a short period of time during which the transistors are all switched off before some of them are switched on. This is done as the transistors do not switch off instantaneously, and this time allow them to close completely before the others switch on, avoiding short circuits. In this report, the influence of the dead-band can be neglected, but in case the PWM frequency would be higher, Equation 2.5 would not be a valid approximation for the phase's voltage. The second reason is that the transistors in the three phase inverter are large, so they cannot switch at too high frequency.

As it is represented on Figure 2.2 on page 10, each of the legs of the inverter has two transistors to control the current flow in the phases. The higher D_{in} the bigger voltage drop is created. The duty cycle applied to the higher transistor (T1, T2 or T3) is called D_H and the lower transistor's (T4, T5 or T6) duty cycle is called D_L. The voltage to a phase is due to the superposition of two PWM modulations. Using Equation 2.3 on the facing page, the potential to phase x, V_x is defined as follows:

$$V_x = D_H V_{cc+} + D_L V_{cc-} \tag{2.5}$$

Where V_{cc+} and V_{cc-} are the positive and negative supply potentials respectively. The supply voltage V_{cc} to the current inverter is therefore defined as $V_{cc} = V_{cc+} - V_{cc-}$. The transitors of one leg of the inverter should never be open at the same time, otherwise it would create a short circuit. In order to avoid any short circuit, the transistors are complementary, i.e. when one is open the other one is closed. This means that there is a relation between D_H and D_L: $D_L = 1 - D_H$. Equation 2.5 on the previous page is

rewritten as follows:

$$V_x = D_H V_{cc+} + (1 - D_H) V_{cc-} \tag{2.6}$$

2.4 CONTROL STRATEGY

There are several types of control strategies that can be chosen. Each of them has an effect on the neutral node potential (V_n). In the report, the PWM-PWM-Tristate modulation is used. In this modulation, one phase is off, and the other two phases, x and y, are controlled with a PWM modulation. One phase receives a modulation with D_{in} as duty cycle, and the second receive a modulation with $1 - D_{in}$ as duty cycle. From Equation 2.6, inputs to the active phases x and y at a time are

$$\begin{aligned} v_x &= D_{in} V_{cc+} + (1 - D_{in}) V_{cc-} \\ v_y &= (1 - D_{in}) V_{cc+} + D_{in} V_{cc-} \end{aligned} \tag{2.7}$$

Using Equations 2.7, the voltage drop through the phases is expressed as

$$\begin{aligned} v_x - v_y &= D_{in} V_{cc+} + (1 - D_{in}) V_{cc-} - (1 - D_{in}) V_{cc+} + D_{in} V_{cc-} \\ &= V_{cc+}(2D_{in} - 1) - V_{cc-}(2D_{in} - 1) \\ &= (2D_{in} - 1) V_{cc} \end{aligned} \tag{2.8}$$

As it is shown by Equation 2.8, the advantage of this type of control is that the voltage drop to the phases can vary from $-V_{cc+}$ to V_{cc+}.

Figure 2.5(a) on the next page shows how the magnetic field in the BLDCM is generated by putting currents through proper phases. The following notation is used, "XY" means that phase X is receiving a PWM signal with duty cycle D_{in}, and phase Y with duty cycle $1 - D_{in}$. Based on this figure, the switching sequence for the transistors can be determined. It is presented in Figure 2.5(b) on the facing page. The switching is done so that the torque is maximized, i.e. at a switch the electrical angle between the magnetic field generated by the coils and the magnetic field created by the PM is $90°$.

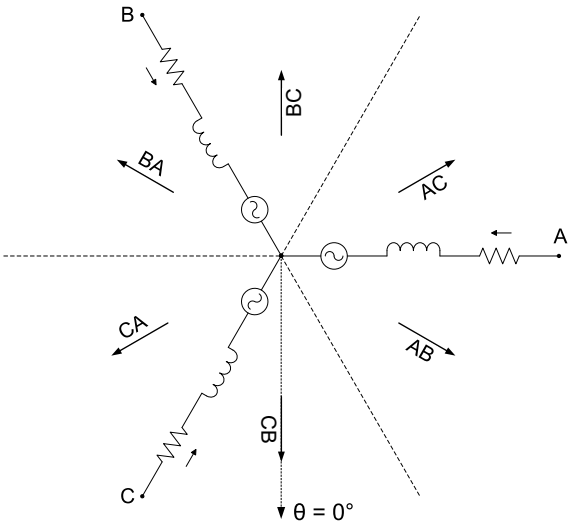

(a) Magnetic field vector directions generated by a current flow in two active phases of the BLDCM at a time. Angle $\theta = 0^\circ$ is chosen that way so that it corresponds to the notation in [KWS95] and the previous reports.

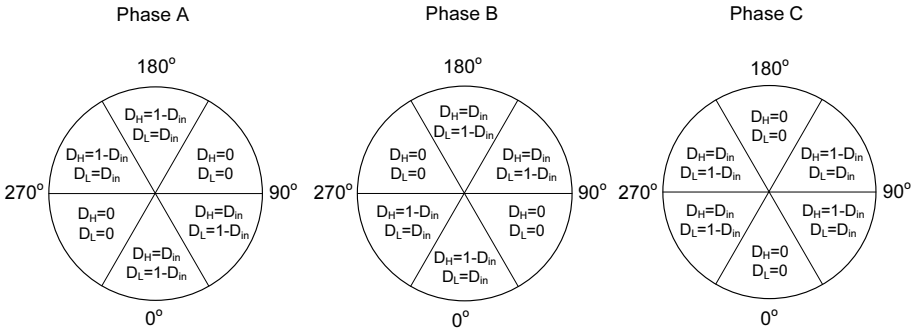

(b) Transistors switching sequence for the DC to AC current conversion. Activation of phases is done such that the torque is maximized at a switch time. The electrical angle, θ_e, is equal to 90° at that moments.

FIGURE 2.5: *Magnetic field generated in a BLDCM and a corresponding phase switching sequence.*

2.5 BACK-EMF SENSING METHOD

Back-EMF sensing method is a technique to estimate the angle of the rotor of a BLDCM, it is used in many applications as it is relatively inexpensive to implement. The principle of this method it to measure the back-EMF of the motor, as it provides an information on the position of the rotor. The back-EMF cannot be measured directly on the motor,

therefore it is sensed through the voltage of the tristated phase [PC05].

In case there is no current in a phase, the inductance and resistor of the phase have no influence on the terminal voltage, and only the back-EMF remains, therefore by measuring the voltage to the tristated phase (assumed to have no current through it) the back-EMF is measured. As shown on Figure 2.3(a) on page 11, the back-EMF has a periodic shape, and it crosses zero when the permanent magnet is aligned to a phase. Zero crossing detection is used to detect those alignments, and when a zero crossing is detected, the correct switchings are made.

This method does not allow advanced control method to be used, as the position of the rotor is only known at certain moments. Better performance could be obtained if the measure of the angle would be always available, for instance torque control techniques could be used to reduce the torque ripples, as it is done in [HLL95].

It is assumed that the current through the tristated phase is null, but the current through a coil does not stop immediately, some current is drained during a certain time after tristating. In certain situations, a drain current can circulate through the phase during the whole tristate period, in that case the back-EMF method is not efficient to estimate the rotor position. This type of situation can happen at high speed, and in that case the coil has very short time to discharge its energy before the phase is switch on again. This can also happen in case the currents are high, which means that the drain current remains longer in the phase.

2.6 DYNAMICS OF THE BLDCM

In order to simplify the dynamical equations of the motor, several assumptions are made. Those are general assumptions that are usually made when modelling a 3-phase balanced machine.

- The BLDCM is balanced, which means that there is 120° (electrical) between the stator windings, and that they have equal ohmic resistance and inductance. The values of the resistance and inductance are assumed constants.
- The influence of the iron is neglected, i.e. the magnetic permeability of the iron is infinite, magnetic fields only exists in the air gap between stator and rotor.
- The rotor is perfectly round and the air gap uniform. The flux lines are radial in the air gap, and the magnetic system is assumed linear.

In the following sections the equations for electrical and mechanical dynamics used in this report are presented. Those equations were derived for the first time in [NP06]. The torque equation uses only two phase currents instead of three. In the previous work voltage equations were transformed to qd-frame where they were simplified and transformed back to the abc-frame. In this report, a new way of deriving the electrical dynamics without transformation is used. Using this description for the dynamics, the system has a form which is easily understandable due to the fact that it uses the input voltages to the phases and the phase currents directly. Those are the inputs and the measurements respectively. No transformation is required inside the MATLAB® /Simulink® model, and only two differential equations are sufficient to describe the dynamics of the motor. Considering that the goal is to implement the observer on-line, and that the observer uses this model, the lighter (in terms of computation) is the model, the lighter is the observer, and therefore the greater is the chance of being able to run the observer on-line.

2.6.1 ELECTRICAL DYNAMICS

The voltage drops across the phases in stator reference frame are described by Equation 2.9, which is written on the basis of Figure 2.2 on page 10. Note that the last term on the right side of the equation corresponds to the back-EMF.

$$\mathbf{v}_{abcs} = \underbrace{\mathbf{L}_s \frac{d}{dt}\mathbf{i}_{abcs}}_{Inductance} + \underbrace{\mathbf{R}_s \mathbf{i}_{abcs}}_{Resistance} + \underbrace{(\frac{d}{d\theta_e}\boldsymbol{\lambda'}_m)\omega_e}_{Back-EMF} \tag{2.9}$$

Where $\mathbf{v}_{abcs} = \begin{bmatrix} v_{as} \\ v_{bs} \\ v_{cs} \end{bmatrix} = \begin{bmatrix} V_{as} - V_n \\ V_{bs} - V_n \\ V_{cs} - V_n \end{bmatrix} = \mathbf{V}_{abcs} - V_n$, V_n being the potential at the neutral node, $\mathbf{V}_{abcs}$ the vector of input voltages, and $\mathbf{i}_{abcs} = \begin{bmatrix} i_{as} & i_{bs} & i_{cs} \end{bmatrix}^T$, the vector of currents trough the phases. Applying Kirchoff's law on the neutral node defines a constraint on these currents:

$$i_{as} + i_{bs} + i_{cs} = 0 \tag{2.10}$$

$\mathbf{L}_s = \begin{bmatrix} L_{ls} + L_{ms} & -\frac{1}{2}L_{ms} & -\frac{1}{2}L_{ms} \\ -\frac{1}{2}L_{ms} & L_{ls} + L_{ms} & -\frac{1}{2}L_{ms} \\ -\frac{1}{2}L_{ms} & -\frac{1}{2}L_{ms} & L_{ls} + L_{ms} \end{bmatrix}$ is the inductance matrix, L_{ls} is the leakage inductance, and L_{ms} is the magnetizing inductance.

The resistance matrix has the form of $\mathbf{R}_s = \begin{bmatrix} r_s & 0 & 0 \\ 0 & r_s & 0 \\ 0 & 0 & r_s \end{bmatrix}$, where r_s is the resistance of a stator winding.

$\boldsymbol{\lambda'}_m$ is the vector of the stator flux linkages created by the permanent magnet, which is a periodic function of the rotor position. A BLDCM is generally designed to have a symmetric trapezoidal back-EMF, therefore $\boldsymbol{\lambda'}_m$ can be decomposed in a series of odd harmonics:

$$\boldsymbol{\lambda'}_m = \lambda'_m \sum_{n=1}^{\infty} N_{2n-1} \begin{bmatrix} \sin((2n-1)\theta_e) \\ \sin((2n-1)(\theta_e - \frac{2\pi}{3})) \\ \sin((2n-1)(\theta_e + \frac{2\pi}{3})) \end{bmatrix} \tag{2.11}$$

With λ'_m being the magnitude of the first harmonic, and N_{2n-1} the magnitude of the n^{th} odd harmonic relative to the fundamental. The comparison between a trapezoidal function and its third order decomposition is shown in Figure 2.6 on the facing page, it is noticed that the first and third harmonics should be enough to describe the flux linkages. In the following, the flux linkages will always be taken as their third order decomposition. More harmonics can be considered if the model becomes inaccurate due to this assumption.

$$\boldsymbol{\lambda'}_m = \lambda'_m \begin{bmatrix} \sin(\theta_e) + N_3 \sin(3\theta_e) \\ \sin(\theta_e - \frac{2\pi}{3}) + N_3 \sin(3\theta_e) \\ \sin(\theta_e + \frac{2\pi}{3}) + N_3 \sin(3\theta_e) \end{bmatrix} \tag{2.12}$$

Using the previous equation, the back-EMF can be expressed:

$$(\frac{d}{d\theta_e}\boldsymbol{\lambda'}_m)\omega_e = \lambda'_m \begin{bmatrix} \cos(\theta_e) + 3N_3 \cos(3\theta_e) \\ \cos(\theta_e - \frac{2\pi}{3}) + 3N_3 \cos(3\theta_e) \\ \cos(\theta_e + \frac{2\pi}{3}) + 3N_3 \cos(3\theta_e) \end{bmatrix} \omega_e \tag{2.13}$$

The constraints on the currents described by Equation 2.10 on the previous page provide an important information. It means that the currents evolve on a two-dimensional manifold, and therefore only two differential equations are needed to describe completely the electrical dynamics of the motor. Equation 2.10 on the preceding page can be rewritten so that i_{cs} is a function of i_{as} and i_{bs}:

$$i_{cs} = -i_{as} - i_{bs} \tag{2.14}$$

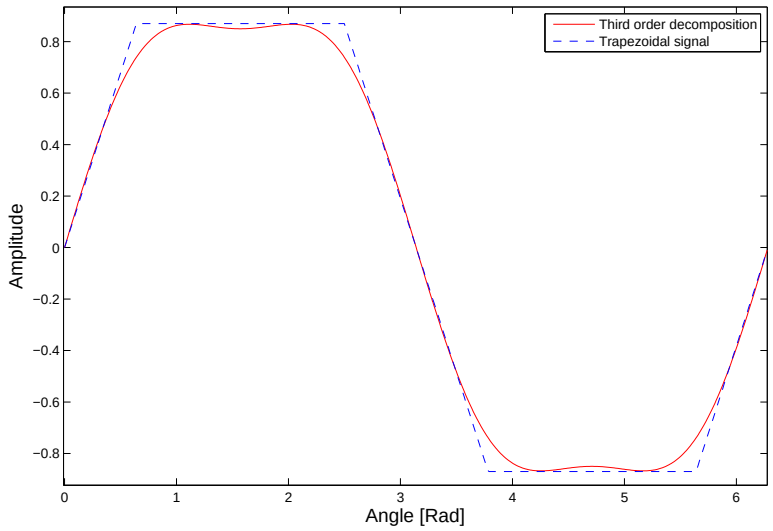

FIGURE 2.6: *Comparison between a trapezoidal function and its third order decomposition.*

As two differential equations are sufficient to describe the dynamics, the equations are composed on basis of Equation 2.9 on page 17. The goal of this manipulation is to get rid of V_N, for which there is no expression. The first equation is the composition of the first row of Equation 2.9 on page 17 minus a half of the two remaining rows; the second equation is the composition of the second row minus a half of the two remaining rows. The new equations are described in Equation 2.15:

$$\begin{aligned}\begin{bmatrix} V_{as} - \frac{1}{2}V_{bs} - \frac{1}{2}V_{cs} \\ V_{bs} - \frac{1}{2}V_{as} - \frac{1}{2}V_{cs} \end{bmatrix} &= \begin{bmatrix} L_{ls} + \frac{3}{2}L_{ms} & -\frac{1}{2}L_{ls} - \frac{3}{4}L_{ms} & -\frac{1}{2}L_{ls} - \frac{3}{4}L_{ms} \\ -\frac{1}{2}L_{ls} - \frac{3}{4}L_{ms} & L_{ls} + \frac{3}{2}L_{ms} & -\frac{1}{2}L_{ls} - \frac{3}{4}L_{ms} \end{bmatrix} \frac{d}{dt}\mathbf{i}_{abcs} \\ &+ \begin{bmatrix} r_s & -\frac{1}{2}r_s & -\frac{1}{2}r_s \\ -\frac{1}{2}r_s & r_s & -\frac{1}{2}r_s \end{bmatrix} \mathbf{i}_{abcs} \\ &+ \lambda'_m \begin{bmatrix} \cos(\theta_e) - \frac{1}{2}\cos(\theta_e - \frac{2\pi}{3}) - \frac{1}{2}\cos(\theta_e + \frac{2\pi}{3}) \\ \cos(\theta_e - \frac{2\pi}{3}) - \frac{1}{2}\cos(\theta_e) - \frac{1}{2}\cos(\theta_e + \frac{2\pi}{3}) \end{bmatrix} \omega_e \end{aligned} \tag{2.15}$$

It is noticed that the third harmonics terms cancel themselves in the previous calculations, this means that this third harmonic has no influence on the dynamics. It is now needed to remove i_{cs} from the equations as just two differential equations are wanted, and differential equations for i_{as} and i_{bs} are chosen. In Equation 2.15 i_{cs} is replaced by its expression in Equation 2.14 on the preceding page. This results in a new set of equations using $\mathbf{i}_{abs} = \begin{bmatrix} i_{as} & i_{bs} \end{bmatrix}^T$ instead of $\mathbf{i}_{abcs}$:

$$\begin{bmatrix} V_{as} - \frac{1}{2}V_{bs} - \frac{1}{2}V_{cs} \\ V_{bs} - \frac{1}{2}V_{as} - \frac{1}{2}V_{cs} \end{bmatrix} = \begin{bmatrix} \frac{3}{2}L_{ls} + \frac{9}{4}L_{ms} & 0 \\ 0 & \frac{3}{2}L_{ls} + \frac{9}{4}L_{ms} \end{bmatrix} \frac{d}{dt}\mathbf{i}_{abs} + \begin{bmatrix} \frac{3}{2}r_s & 0 \\ 0 & \frac{3}{2}r_s \end{bmatrix} \mathbf{i}_{abs} + \lambda'_m \begin{bmatrix} \cos(\theta_e) - \frac{1}{2}\cos(\theta_e - \frac{2\pi}{3}) - \frac{1}{2}\cos(\theta_e + \frac{2\pi}{3}) \\ \cos(\theta_e - \frac{2\pi}{3}) - \frac{1}{2}\cos(\theta_e) - \frac{1}{2}\cos(\theta_e + \frac{2\pi}{3}) \end{bmatrix} \omega_e \quad (2.16)$$

The last term in the previous equation can be simplified by using the trigonometrical property $\cos(a+b) = \cos(a)\cos(b) - \sin(a)\sin(b)$:

$$\begin{bmatrix} \cos(\theta_e) - \frac{1}{2}\cos(\theta_e - \frac{2\pi}{3}) - \frac{1}{2}\cos(\theta_e + \frac{2\pi}{3}) \\ \cos(\theta_e - \frac{2\pi}{3}) - \frac{1}{2}\cos(\theta_e) - \frac{1}{2}\cos(\theta_e + \frac{2\pi}{3}) \end{bmatrix} = \begin{bmatrix} \frac{3}{2}\cos(\theta_e) \\ -\frac{3}{4}\cos(\theta_e) + \frac{3\sqrt{3}}{4}\sin(\theta_e) \end{bmatrix} = \begin{bmatrix} \frac{3}{2} & 0 \\ -\frac{3}{4} & \frac{3\sqrt{3}}{4} \end{bmatrix} \begin{bmatrix} \cos(\theta_e) \\ \sin(\theta_e) \end{bmatrix}$$

The previous expression is used in Equation 2.16 to provide a reduced form of the equations:

$$\begin{bmatrix} V_{as} - \frac{1}{2}V_{bs} - \frac{1}{2}V_{cs} \\ V_{bs} - \frac{1}{2}V_{as} - \frac{1}{2}V_{cs} \end{bmatrix} = \begin{bmatrix} \frac{3}{2}L_{ls} + \frac{9}{4}L_{ms} & 0 \\ 0 & \frac{3}{2}L_{ls} + \frac{9}{4}L_{ms} \end{bmatrix} \frac{d}{dt}\mathbf{i}_{abs} + \begin{bmatrix} \frac{3}{2}r_s & 0 \\ 0 & \frac{3}{2}r_s \end{bmatrix} \mathbf{i}_{abs} + \lambda'_m \begin{bmatrix} \frac{3}{2} & 0 \\ -\frac{3}{4} & \frac{3\sqrt{3}}{4} \end{bmatrix} \begin{bmatrix} \cos(\theta_e) \\ \sin(\theta_e) \end{bmatrix} \omega_e \quad (2.17)$$

Equation 2.17 is then multiplied with $\frac{2}{3}$ and rearranged:

$$\begin{bmatrix} L_s & 0 \\ 0 & L_s \end{bmatrix} \frac{d}{dt}\mathbf{i}_{abs} = -\begin{bmatrix} r_s & 0 \\ 0 & r_s \end{bmatrix} \mathbf{i}_{abs} - \lambda'_m \begin{bmatrix} 1 & 0 \\ -\frac{1}{2} & \frac{\sqrt{3}}{2} \end{bmatrix} \begin{bmatrix} \cos(\theta_e) \\ \sin(\theta_e) \end{bmatrix} \omega_e + \begin{bmatrix} \frac{2}{3} & -\frac{1}{3} & -\frac{1}{3} \\ -\frac{1}{3} & \frac{2}{3} & -\frac{1}{3} \end{bmatrix} \mathbf{V}_{abcs} \quad (2.18)$$

With $L_s = L_{ls} + \frac{3}{2}L_{ms}$ being the equivalent inductance of a phase. Equation 2.18 is rewritten to find the final expression of the electrical dynamics of the BLDCM:

$$\begin{aligned}\frac{d}{dt}\mathbf{i}_{abs} &= -\frac{r_s}{L_s}\mathbf{i}_{abs} - \frac{\lambda'_m}{L_s}\underbrace{\begin{bmatrix} 1 & 0 \\ -\frac{1}{2} & \frac{\sqrt{3}}{2} \end{bmatrix}}_{\mathbf{M''}}\begin{bmatrix} \cos(\theta_e) \\ \sin(\theta_e) \end{bmatrix}\omega_e \\ &+ \frac{1}{L_s}\underbrace{\begin{bmatrix} \frac{2}{3} & -\frac{1}{3} & -\frac{1}{3} \\ -\frac{1}{3} & \frac{2}{3} & -\frac{1}{3} \end{bmatrix}}_{\mathbf{M'}}\mathbf{V}_{abcs} \end{aligned} \tag{2.19}$$

The current i_{cs} is not present in the final electrical dynamics, if it is needed in the implementation it can be easily computed using its expression in Equation 2.14 on page 18.

2.6.2 MECHANICAL DYNAMICS

The equation of the torque produced by the BLDCM is derived from the energy of the magnetic system:

$$T_e = Z_p\left(\frac{d}{d\theta_e}\boldsymbol{\lambda'}_m\right)^T\mathbf{i}_{abcs} \tag{2.20}$$

Replacing i_{cs} by its expression in Equation 2.14 on page 18 and using Equation 2.13 on page 18 leads to a new expression for the torque:

$$T_e = Z_p\lambda'_m\begin{bmatrix} \cos(\theta_e) - \cos(\theta_e + \frac{2\pi}{3}) \\ \cos(\theta_e - \frac{2\pi}{3}) - \cos(\theta_e + \frac{2\pi}{3}) \end{bmatrix}^T\mathbf{i}_{abs} \tag{2.21}$$

Then, using the trigonometric property $\cos(a+b) = \cos(a)\cos(b) - \sin(a)\sin(b)$, the torque is rewritten:

$$T_e = Z_p\lambda'_m\left(\begin{bmatrix} \frac{3}{2} & \frac{\sqrt{3}}{2} \\ 0 & \sqrt{3} \end{bmatrix}\begin{bmatrix} \cos(\theta_e) \\ \sin(\theta_e) \end{bmatrix}\right)^T\mathbf{i}_{abs} \tag{2.22}$$

The motion of the motor is described by the following differential equation:

$$J\frac{d}{dt}\omega_r = T_e - B_m\omega_r + T_L \tag{2.23}$$

Where J is the moment of inertia of the rotor and load, B_m the damping coefficient of the motor, and T_L the torque produced by the load, which can be either positive or negative. Multiplying Equation 2.23 with Z_p allows to find the equation of motion of the BLDCM:

$$J\frac{d}{dt}\omega_e = Z_p T_e - B_m\omega_e + Z_p T_L \tag{2.24}$$

The expression of T_e in Equation 2.22 on the previous page is inserted in Equation 2.24 to find the final description of the mechanical dynamics:

$$J\frac{d}{dt}\omega_e = Z_p^2\lambda'_m \left(\begin{bmatrix} \frac{3}{2} & \frac{\sqrt{3}}{2} \\ 0 & \sqrt{3} \end{bmatrix} \begin{bmatrix} \cos(\theta_e) \\ \sin(\theta_e) \end{bmatrix} \right)^T \mathbf{i}_{abs} - B_m\omega_e + Z_p T_L \tag{2.25}$$

The BLDCM is a nonlinear system as there is are product between variables in the electrical dynamics and the mechanical dynamics.

2.7 CONCLUSION

In this chapter the preliminary knowledge related to the project was presented. This knowledge should allow the reader to understand the concepts presented in the following parts of the report. New mathematical equations describing the physical behaviour of the motor were presented. The qd-transformation is not necessary in this description, which should enhance performance of the model and observer.

HYBRID MODEL 3

This chapter describes the hybrid model used for the BLDCM. Firstly, a recently developed, compact definition of a hybrid system is given. Later, it will be shown how the final hybrid automaton was derived from a general hybrid automaton for the BLDCM, using knowledge of the control strategy in order to reduce the number of states and transitions. The scope of the project is limited to only one rotating direction. This limitation is not very crucial as the BLDCM is used as a centrifugal pump motor. Adding the other rotating direction can easily be done through symmetry. The rotating direction considered here will be $\omega_e > 0$. The continuous time equations corresponding to the states of the hybrid automaton will be expressed on basis of the equations found in the previous chapter. The formal description of the model will be written based on the definition of a hybrid system given in Section 3.1.

3.1 DEFINITION OF A HYBRID SYSTEM

The hybrid systems theory is a relatively new field of research and therefore there is a lot of work in the academic world concentrating on developing its theoretical background. There are several definitions used for describing a hybrid system. In this report the definition proposed in [ALB06] is used.

A hybrid system is a system that encounters abrupt changes in its dynamical behaviour and therefore cannot be described by purely continuous equations of dynamics. The system can be considered as a combination of a continuous system, that is switched by Finite State Automaton (FSA). Figure 3.1 on the following page shows the block diagram and the relations between the continuous and discrete part of the system.

Definition 1
A hybrid system is defined as an 8-tuple:

$$\mathcal{H} = (\mathcal{Q}, X, U, Y, E, \mathcal{F}, \mathcal{G}, \mathcal{T}) \tag{3.1}$$

where

- $\mathcal{Q} = \{1, 2, \ldots, s\} \subset \mathbb{Z}^+$ is the set of location indexes with cardinal number s,
- $X = \{\mathbf{x} | \mathbf{x} \in X_q : q \in Q, X_q \subseteq \mathbb{R}^{n_q}\}$ is the continuous state-space with dimension

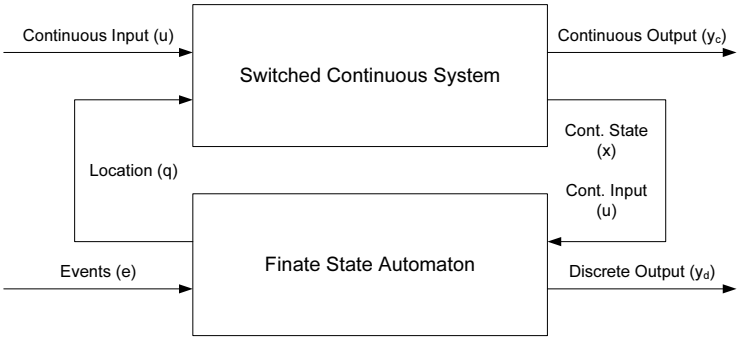

FIGURE 3.1: *Hybrid System can be represented as a combination of Switched Continuous System and Finite State Automaton [EFS02].*

$n_{q\in Q} \in \mathbb{Z}^+$,

- $U = \{\mathbf{u}|\mathbf{u} \in U_q : q \in Q, U_q \subseteq \mathbb{R}^{m_q}\}$ is the continuous input-space with dimension $m_{q\in Q} \in \mathbb{Z}^+$,
- $Y = \{\mathbf{y}|\mathbf{y} \in Y_q : q \in Q, Y_q \subseteq \mathbb{R}^{p_q}\}$ is the continuous output-space with dimension $p_{q\in Q} \in \mathbb{Z}^+$,
- $E = \left\{\mathbf{e}|\mathbf{e} \in 2^{\Sigma}\right\}$ is the set of possible input/output event labels, where Σ is an appropriate set of labels,
- $\mathcal{F} : \mathcal{Q} \times X \times U \to \dot{X}$ is the forcing function on the continuous state-space,
- $\mathcal{G} : \mathcal{Q} \times X \times U \to Y$ is a continuous output map,
- $\mathcal{T} : \mathcal{Q} \times X \times U \times E \to \mathcal{Q} \times X \times E$ is a transition map.

The continuous forcing function $\mathcal{F}$, output mapping $\mathcal{G}$ and discrete transition map $\mathcal{T}$ depend on the discrete location, continues states and inputs, while events e affect only the discrete dynamics.

3.2 HYBRID AUTOMATON

The hybrid automaton for a phase of the BLDCM described in [HB05] has four discrete states depending on the inputs from the inverter and the current that flows through it. This automaton is used as a basis for building the new reduced hybrid automaton for the BLDCM used throughout this report.

- The phase is said to be $passive$ if no current flows trough it.
- The phase is said to be $active$ if one of its two control transistors is conducting. These transistors are in Figure 2.2 on page 10, $T1$ and $T4$ for phase A, $T2$ and $T5$ for phase B, and $T3$ and $T6$ for phase C.
- The phase is said to be in $drain$ state if one of its two free wheel diodes is conducting. There are two cases depending on the sign of the current flowing trough the phase, if the current is positive it is called $positive\ drain$, if it is negative $negative\ drain$.

The hybrid automaton for a phase is shown in Figure 3.2. Each of the events used on this automaton is associated with a boolean expression. The event is immediately triggered when the corresponding boolean expression becomes true.

on_x is the event generated when the controller starts controlling the input voltage to the phase x, meaning that the transistors receive a PWM modulation. The associated boolean expression is $[active_x = 1]$, with $active_x$ being a signal generated by the controller whose value is 1 when the input voltage to phase x is controlled, and 0 otherwise.

$nactive\_pos\_x$ is generated when the controller stops controlling the input voltage to phase x (both transistors are tristated), and the current flowing through this phase, i_{xs}, is positive. The associated boolean expression is $[(active_x = 0) \wedge (i_{xs} > 0)]$.

$nactive\_neg\_x$ is the same as $nactive\_pos\_x$ except it is generated if the current is negative. The boolean expression in this case is $[(active_x = 0) \wedge (i_{xs} < 0)]$.

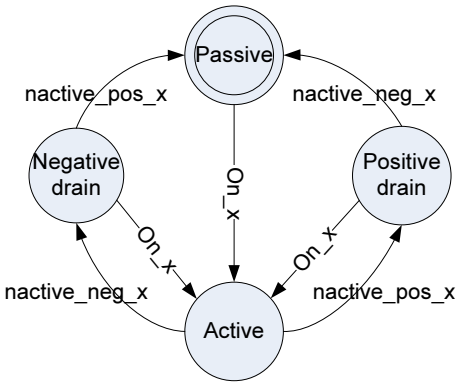

FIGURE 3.2: *Figure of the hybrid automaton for a phase of the BLDCM [HB05].*

In theory, the transitions to go from a $drain$ state to a $passive$ state should be realized when the current through the phase reaches 0, but it can be noticed on Figure 3.2 that

these transitions are realized when the sign of the current changes. In the implementation, the current never reaches exactly zero at any given sample instant, therefore a zero crossing detection is used instead of a zero detection.

The global hybrid automaton for the BLDCM is composed of three phase's automatons in parallel, one for each phase. Each phase's automaton is composed of 4 states, therefore the composition of these three automatons gives an automaton with $4^3 = 64$ states, as derived in [HB05]. Such a large number of discrete states is difficult to consider in practice, and thus the automaton will be reduced in the following.

Knowing the control strategy used, which is described by Figure 2.5(b) on page 15, a large number of the states can be omitted in the final hybrid automaton, as they are not reachable. The states that are in the final automaton must fulfill the following requirements:

- Two phases are active.
- One phase is either $passive$, $positive\ drain$, or $negative\ drain$.

The transitions making the motor turn in the direction $\omega_e < 0$ cannot be realized under the chosen control strategy, as only the rotating direction $\omega_e > 0$ is considered, these transitions are therefore omitted in the final automaton. The final automaton is shown on Figure 3.3 on the facing page, where the value of q is the location index corresponding to the state.

The final hybrid automaton for the BLDCM is composed of 9 different states. There are no deadlocks in this automaton as the events that trigger the transitions are generated outside the automaton. The automaton has a cyclic shape, which is due to the rotating behaviour of the system itself.

It is noticed that the control strategy chosen is included in the automaton. A brief analysis of the automaton allows to find the switching sequence for the phases represented by Figure 2.5(b) on page 15: $ABactive \rightarrow ACactive \rightarrow BCactive \rightarrow ABactive \rightarrow \ldots$ But the automaton is composed of more states than only the ones from the control sequence, there are also the drain states.

Transitions are possible from one drain state directly to another drain state without passing through a state where only two phases are conducting. This happens when one or more of the coils do not have enough time to discharge completely before becoming active again, meaning the currents are too large or the switchings are too fast. Reasons

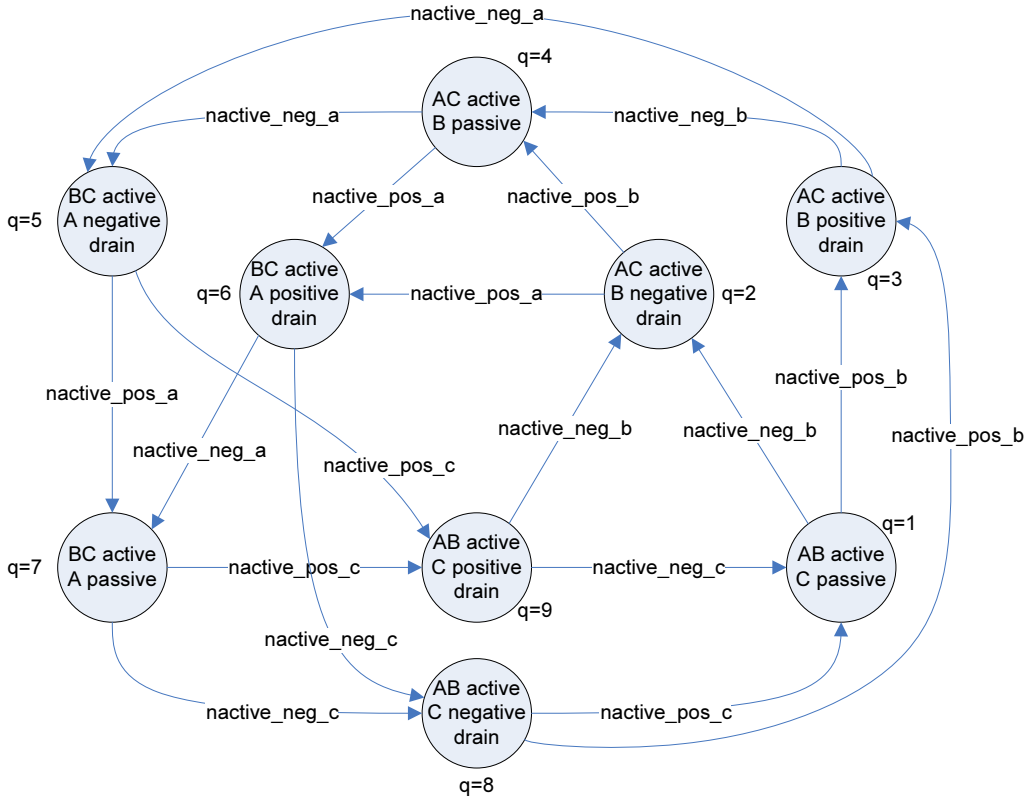

FIGURE 3.3: *Reduced hybrid automaton for the BLDCM.*

for this to happen are a high angular velocity causing fast switchings or a high duty cycle causing large currents in the coils. It is sometimes possible to have periods where the only active states are the drain states.

The final automaton represented in Figure 3.3 does not use the events indicating when a phase of the motor is turned on, on_A, on_B, and on_C. The reason is that it is known from the control strategy that when a phase is switched off, then another one is turned on, therefore those events are redundant and can be disregarded.

It is now needed to find the dynamics of the continuous states corresponding to each of these discrete states, which is done in the following Section.

3.3 CONTINUOUS TIME EQUATIONS

The general equations describing the dynamics of the BLDCM have been described in Section 2.6 on page 16 and it has been shown that the system is nonlinear. In the fol-

lowing section, the model is described as a linear time varying system using state-space representation. The electrical angular velocity, ω_e, is considered to be the time varying parameter. The system is therefore always represented by a set of Equations 3.2.

$$\begin{aligned} \dot{\mathbf{x}} &= (\mathbf{A}_0 + \mathbf{A}_\omega \omega_e)\mathbf{x} + \mathbf{B}\mathbf{V}_{abcs} \\ \mathbf{y} &= \mathbf{C}\mathbf{x} \end{aligned} \tag{3.2}$$

$\mathbf{A}_\omega \omega_\mathbf{e}$ is the time varying term. In the following considerations, the state vector is set to be

$$\mathbf{x} = \begin{bmatrix} i_{as} & i_{bs} & \cos(\theta_e) & \sin(\theta_e) \end{bmatrix}^T \tag{3.3}$$

The measurable outputs are the currents i_{as} and i_{bs}, and thus the output matrix is always $\mathbf{C} = \begin{bmatrix} \mathbf{I}^{2\times 2} & \mathbf{0} \end{bmatrix}$.

It is elaborated when and why the dynamics of the machine change.

NOTE: In the equations derived in the following where only two phases are conducting, i.e $q \in \{1, 4, 7\}$, the state vector could be reduced to three elements only, $\mathbf{x} \in \mathbb{R}^3$. However, from the stability point of view, it would be more convenient to consider systems that have always the same form and size.

3.3.1 THREE PHASES CONDUCTING

As it was previously described, the magnetic field generated in the BLDCM is generated by activating two phases at a time (see Section 2.3 on page 11). The case when three phases are active occurs only when phases are switched. The tristated phase continues to drain the current stored as energy in the coil. Current always has to be continuous and it cannot be stopped instantly.

Consider x being the tristated phase. The input voltage to this phase, V_{xs}, is not controlled, but applied based on the internal structure of the inverter (diodes). It is dependent on the sign of the current i_{xs}. This dependency is expressed as follows:

$$V_{xs} = \begin{cases} V_{cc+} + V_{diode} & \text{if} \quad i_{xs} < 0 \\ V_{cc-} - V_{diode} & \text{if} \quad i_{xs} > 0 \end{cases} \tag{3.4}$$

where V_{diode} is the voltage drop through a conducting diode of the inverter.

When the currents are flowing through all three phases, the electrical dynamics are described by Equation 2.19 on page 21. The system is brought to a linear time varying system representation of the form 3.2 on the preceding page, where the state vector is given in Equation 3.3 on the facing page.

$$\mathbf{A}_0 = \begin{bmatrix} -\frac{r_s}{L_s}\mathbf{I}^{2\times 2} & \mathbf{0} \\ \mathbf{0} & \mathbf{0} \end{bmatrix}, \mathbf{A}_\omega = \begin{bmatrix} \mathbf{0} & -\frac{\lambda'_m}{L_s}\mathbf{M}'' \\ \mathbf{0} & \mathcal{J} \end{bmatrix}, \mathcal{J} = \begin{bmatrix} 0 & -1 \\ 1 & 0 \end{bmatrix} \text{ and } \mathbf{B} = \begin{bmatrix} \frac{1}{L_s}\mathbf{M}' \\ \mathbf{0} \end{bmatrix}$$

and

$$\mathbf{M}' = \begin{bmatrix} \frac{2}{3} & -\frac{1}{3} & -\frac{1}{3} \\ -\frac{1}{3} & \frac{2}{3} & -\frac{1}{3} \end{bmatrix}, \ \mathbf{M}'' = \begin{bmatrix} 1 & 0 \\ -\frac{1}{2} & \frac{\sqrt{3}}{2} \end{bmatrix}$$

The mechanical dynamics are described by Equation 2.24 on page 22, which is used to compute the time-varying parameter ω_e.

3.3.2 TWO PHASES CONDUCTING

This is the default situation from the control point of view. The tristated phase, x, does not drain any current, $i_{xs} = 0$, and the currents through the conducting phases y and z are constrained by $i_{ys} = -i_{zs}$. This corresponds to rewriting of Equation 2.10 on page 17 when one phase current is 0. The equations vary depending on which phase is off, therefore they have to be analyzed separately.

Phase C not conducting The first case to be analysed is when $i_{cs} = 0 \Rightarrow i_{as} = -i_{bs}$. The system can be expressed using only one differential equation. It can be derived from Equation 2.19 on page 21. The voltage in the node that is not controlled, V_c, is governed by internal dynamics of the motor, i.e. the back-EMF voltage inducted by the rotor movement. To remove this voltage from the equation, a small trick is used and the difference $\frac{d}{dt}(i_{as} - i_{bs})$ is analysed.

$$\begin{aligned} \frac{d}{dt}(i_{as} - i_{bs}) = -\frac{r_s}{L_s}(i_{as} - i_{bs}) - \frac{\lambda'_m}{L_s}\begin{bmatrix} \frac{3}{2} & -\frac{\sqrt{3}}{2} \end{bmatrix}\begin{bmatrix} \cos(\theta_e) \\ \sin(\theta_e) \end{bmatrix}\omega_e \\ + \frac{1}{L_s}\begin{bmatrix} 1 & -1 & 0 \end{bmatrix}\mathbf{V}_{abcs} \end{aligned} \tag{3.5}$$

Current i_{bs} is replaced by $-i_{as}$ to find the differential equation for i_{as}:

$$\frac{d}{dt}i_{as} = -\frac{r_s}{L_s}i_{as} - \frac{\lambda'_m}{L_s}\begin{bmatrix} \frac{3}{4} & -\frac{\sqrt{3}}{4} \end{bmatrix}\begin{bmatrix} \cos(\theta_e) \\ \sin(\theta_e) \end{bmatrix}\omega_e + \frac{1}{L_s}\begin{bmatrix} \frac{1}{2} & -\frac{1}{2} & 0 \end{bmatrix}\mathbf{V}_{abcs} \tag{3.6}$$

Using the same state space representation and state vector $\begin{bmatrix} i_{as} & i_{bs} & \cos(\theta_e) & \sin(\theta_e) \end{bmatrix}^T$ as previously, the matrices are:

$$\mathbf{A}_0 = \begin{bmatrix} -\frac{r_s}{L_s}\mathbf{I}^{2\times 2} & \mathbf{0} \\ \mathbf{0} & \mathbf{0} \end{bmatrix}, \mathbf{A}_\omega = \begin{bmatrix} \mathbf{0} & -\frac{\lambda'_m}{L_s}\begin{bmatrix} \frac{3}{4} & -\frac{\sqrt{3}}{4} \\ -\frac{3}{4} & \frac{\sqrt{3}}{4} \end{bmatrix} \\ \mathbf{0} & \mathcal{J} \end{bmatrix} \text{ and } \mathbf{B} = \frac{1}{L_s}\begin{bmatrix} \frac{1}{2} & -\frac{1}{2} & 0 \\ -\frac{1}{2} & \frac{1}{2} & 0 \\ & \mathbf{0} & \end{bmatrix}$$

The mechanical dynamics are also rewritten plugging expression $i_{bs} = -i_{as}$ into Equation 2.24 on page 22.

$$J\frac{d}{dt}\omega_e = Z_p^2\lambda'_m\begin{bmatrix} \frac{3}{2} & -\frac{\sqrt{3}}{2} \end{bmatrix}\begin{bmatrix} \cos(\theta_e) \\ \sin(\theta_e) \end{bmatrix}i_{as} - B_m\omega_e + Z_pT_L \tag{3.7}$$

Phase B not conducting The second case is when $i_{bs} = 0 \Rightarrow i_{as} = -i_{cs}$ The state vector remains the same. The matrices are of a form:

$$\mathbf{A}_0 = \begin{bmatrix} -\frac{r_s}{L_s} & \mathbf{0} \\ \mathbf{0} & \mathbf{0} \\ \mathbf{0} & \mathbf{0} \end{bmatrix}, \mathbf{A}_\omega = \begin{bmatrix} \mathbf{0} & -\frac{\lambda'_m}{L_s}\begin{bmatrix} \frac{3}{4} & \frac{\sqrt{3}}{4} \end{bmatrix} \\ \mathbf{0} & \mathbf{0} \\ \mathbf{0} & \mathcal{J} \end{bmatrix}, \mathbf{B} = \frac{1}{L_s}\begin{bmatrix} \frac{1}{2} & 0 & -\frac{1}{2} \\ & \mathbf{0} & \end{bmatrix}$$

The mechanical dynamics are described by:

$$J\frac{d}{dt}\omega_e = Z_p^2\lambda'_m\begin{bmatrix} \frac{3}{2} & \frac{\sqrt{3}}{2} \end{bmatrix}\begin{bmatrix} \cos(\theta_e) \\ \sin(\theta_e) \end{bmatrix}i_{as} - B_m\omega_e + Z_pT_L \tag{3.8}$$

Phase A not conducting The last case is when $i_{as} = 0 \Rightarrow i_{bs} = -i_{cs}$. Again the state vector remains unchanged. The matrices are:

$$\mathbf{A}_0 = \begin{bmatrix} 0 & 0 & \mathbf{0} \\ 0 & -\frac{r_s}{L_s} & \mathbf{0} \\ \mathbf{0} & \mathbf{0} & \mathbf{0} \end{bmatrix}, \mathbf{A}_\omega = \begin{bmatrix} \mathbf{0} & \mathbf{0} \\ \mathbf{0} & -\frac{\lambda'_m}{L_s}\begin{bmatrix} 0 & \frac{\sqrt{3}}{2} \end{bmatrix} \\ \mathbf{0} & \mathcal{J} \end{bmatrix}, \mathbf{B} = \frac{1}{L_s}\begin{bmatrix} & \mathbf{0} & \\ 0 & \frac{1}{2} & -\frac{1}{2} \\ & \mathbf{0} & \end{bmatrix}$$

The mechanical dynamics are:

$$J\frac{d}{dt}\omega_e = Z_p^2\lambda'_m\begin{bmatrix} 0 & \sqrt{3} \end{bmatrix}\begin{bmatrix} \cos(\theta_e) \\ \sin(\theta_e) \end{bmatrix}i_{bs} - B_m\omega_e + Z_pT_L \tag{3.9}$$

3.4 FORMAL DESCRIPTION OF THE MODEL

Having the hybrid automaton for the BLDCM and the state space description for each of the states of this automata, it is possible to write the formal description of the hybrid model using Definition 1 on page 23.

- With reference to Figure 3.3 on page 27, there are 9 different states in the hybrid automaton, meaning 9 different location indexes:

$$\mathcal{Q} = \{1, 2, 3, 4, 5, 6, 7, 8, 9\}$$

- The continuous state-space systems derived in Section 3.3 on page 27 all have a dimension of 4, $n_q = 4, \forall q \in \mathcal{Q}$, and the state vector remains the same:

$$X = \left\{ \mathbf{x}_q = \begin{bmatrix} i_{as} \\ i_{bs} \\ \cos(\theta_e) \\ \sin(\theta_e) \end{bmatrix} \right\} \subset \mathbb{R}^4, \forall q \in \mathcal{Q}$$

- The continuous inputs to the system do not change depending on the discrete state, they are the 3 input voltages to the phases, $m_q = 3, \forall q \in \mathcal{Q}$:

$$U = \left\{ \mathbf{u}_q = \mathbf{V}_{abcs} = \begin{bmatrix} V_{as} \\ V_{bs} \\ V_{cs} \end{bmatrix} \right\} \subset \mathbb{R}^3, \forall q \in \mathcal{Q}$$

- As the continuous states and inputs, the continuous outputs do not depend on the state of the hybrid automaton. The outputs are the two currents that are measured, i_{as} and i_{bs}, $p_q = 2, \forall q \in \mathcal{Q}$:

$$Y = \left\{ \mathbf{y}_q = \mathbf{i}_{abs} = \begin{bmatrix} i_{as} \\ i_{bs} \end{bmatrix} \right\} \subset \mathbb{R}^2, \forall q \in \mathcal{Q}$$

- In the hybrid automaton for the BLDCM only input events are used:

$$E = \left\{ \begin{array}{ll} nactive\_neg\_a, & nactive\_pos\_a, \\ nactive\_neg\_b, & nactive\_pos\_b, \\ nactive\_neg\_c, & nactive\_pos\_c \end{array} \right\}$$

- The forcing function on the continuous-space is defined using the matrices derived in Section 3.3 on page 27. From the value of the location index q, it is possible to know which phases are conducting by using Figure 3.3 on page 27, so that the correct matrices are used. $\mathcal{F}$ is defined as follows:

$$
\begin{cases}
\underline{\text{For} \quad q \in \{2,3,5,6,8,9\}:} \\
\dot{\mathbf{x}}_q = \left(\begin{bmatrix} -\frac{r_s}{L_s}\mathbf{I}^{2\times 2} & \mathbf{0} \\ \mathbf{0} & \mathbf{0} \end{bmatrix} + \begin{bmatrix} \mathbf{0} & -\frac{\lambda'_m}{L_s}\begin{bmatrix} 1 & 0 \\ -\frac{1}{2} & \frac{\sqrt{3}}{2} \end{bmatrix} \\ \mathbf{0} & \mathcal{J} \end{bmatrix} \omega_e \right) \mathbf{x}_q + \frac{1}{L_s}\begin{bmatrix} \frac{2}{3} & -\frac{1}{3} & -\frac{1}{3} \\ -\frac{1}{3} & \frac{2}{3} & -\frac{1}{3} \\ & \mathbf{0} & \end{bmatrix} \mathbf{u}_q \\
\underline{\text{for} \quad q = 1:} \\
\dot{\mathbf{x}}_q = \left(\begin{bmatrix} -\frac{r_s}{L_s}\mathbf{I}^{2\times 2} & \mathbf{0} \\ \mathbf{0} & \mathbf{0} \end{bmatrix} + \begin{bmatrix} \mathbf{0} & -\frac{\lambda'_m}{L_s}\begin{bmatrix} \frac{3}{4} & -\frac{\sqrt{3}}{4} \\ -\frac{3}{4} & \frac{\sqrt{3}}{4} \end{bmatrix} \\ \mathbf{0} & \mathcal{J} \end{bmatrix} \omega_e \right) \mathbf{x}_q + \frac{1}{L_s}\begin{bmatrix} \frac{1}{2} & -\frac{1}{2} & 0 \\ -\frac{1}{2} & \frac{1}{2} & 0 \\ & \mathbf{0} & \end{bmatrix} \mathbf{u}_q \\
\underline{\text{for} \quad q = 4:} \\
\dot{\mathbf{x}}_q = \left(\begin{bmatrix} -\frac{r_s}{L_s} & \mathbf{0} \\ \mathbf{0} & \mathbf{0} \\ \mathbf{0} & \mathbf{0} \end{bmatrix} + \begin{bmatrix} \mathbf{0} & -\frac{\lambda'_m}{L_s}\begin{bmatrix} \frac{3}{4} & \frac{\sqrt{3}}{4} \end{bmatrix} \\ \mathbf{0} & \mathbf{0} \\ \mathbf{0} & \mathcal{J} \end{bmatrix} \omega_e \right) \mathbf{x}_q + \frac{1}{L_s}\begin{bmatrix} \frac{1}{2} & 0 & -\frac{1}{2} \\ & \mathbf{0} & \end{bmatrix} \mathbf{u}_q \\
\underline{\text{for} \quad q = 7:} \\
\dot{\mathbf{x}}_q = \left(\begin{bmatrix} 0 & 0 & \mathbf{0} \\ 0 & -\frac{r_s}{L_s} & \mathbf{0} \\ \mathbf{0} & \mathbf{0} & \mathbf{0} \end{bmatrix} + \begin{bmatrix} \mathbf{0} & \mathbf{0} \\ \mathbf{0} & -\frac{\lambda'_m}{L_s}\begin{bmatrix} 0 & \frac{\sqrt{3}}{2} \end{bmatrix} \\ \mathbf{0} & \mathcal{J} \end{bmatrix} \omega_e \right) \mathbf{x}_q + \frac{1}{L_s}\begin{bmatrix} & \mathbf{0} & \\ 0 & \frac{1}{2} & -\frac{1}{2} \\ & \mathbf{0} & \end{bmatrix} \mathbf{u}_q
\end{cases}
$$

- The continuous output map is not dependent of the discrete state as the continuous state and output remain the same:

$$\mathcal{G} : \mathbf{y}_q = \underbrace{\begin{bmatrix} \mathbf{I}^{2\times 2} & \mathbf{0} \end{bmatrix}}_{\mathbf{C}} \mathbf{x}_q, \forall q \in \mathcal{Q}$$

- In the hybrid model developed, the transition map $\mathcal{T}$ is just defined using the value of the current discrete state and an event to determine what is the next discrete state, and there is no reset function and no event generated during the transition. Therefore $\mathcal{T}$ is defined as $\mathcal{T} : \mathcal{Q} \times E \rightarrow \mathcal{Q}$. To define $\mathcal{T}$ the following notation will be used : $(q_{current}, e_{received}) \rightarrow q_{new}$, where $q_{current}$ is the current value of the discrete state, $e_{received}$ the event that triggers the transition, and q_{new} the new value of the discrete state.

$$\mathcal{T}: \begin{cases} (1, nactive\_neg\_b) \rightarrow 2 \\ (1, nactive\_pos\_b) \rightarrow 3 \\ (2, nactive\_pos\_b) \rightarrow 4 \\ (2, nactive\_pos\_a) \rightarrow 6 \\ (3, nactive\_neg\_b) \rightarrow 4 \\ (3, nactive\_neg\_a) \rightarrow 5 \\ (4, nactive\_neg\_a) \rightarrow 5 \\ (4, nactive\_pos\_a) \rightarrow 6 \\ (5, nactive\_pos\_a) \rightarrow 7 \\ (5, nactive\_pos\_c) \rightarrow 9 \\ (6, nactive\_neg\_a) \rightarrow 7 \\ (6, nactive\_neg\_c) \rightarrow 8 \\ (7, nactive\_pos\_c) \rightarrow 9 \\ (7, nactive\_neg\_c) \rightarrow 8 \\ (8, nactive\_pos\_c) \rightarrow 1 \\ (8, nactive\_pos\_b) \rightarrow 3 \\ (9, nactive\_neg\_c) \rightarrow 1 \\ (9, nactive\_neg\_b) \rightarrow 2 \end{cases}$$

3.5 TEST OF THE HYBRID MODEL

The hybrid model presented in the previous sections was implemented and tested in [NP06]. The parameters of the motor used for the test were estimated and are given in the following table:

Parameter	Z_p	r_s	L_s	λ'_m	J	B_m
Value	3	$3.8\,[\Omega]$	$0.0135\,[\mathrm{H}]$	$0.2225\,[\frac{\mathrm{V}}{\mathrm{rad}\cdot\mathrm{s}^{-1}}]$	$0.002\,[\mathrm{kg}\cdot\mathrm{m}^2]$	$5\cdot10^{-4}\,[\mathrm{Kg}\cdot\mathrm{m}^2\cdot\mathrm{s}^{-1}]$

Simulations of the hybrid model were made, and the results were compared with measurements taken on the real BLDCM with the same input duty cycle D_{in}. Comparisons were made for different values for D_{in}, but only the results for $D_{in} = 0.59$ are shown as the same comments can be made for all different comparisons. Figure 3.4 on the following page is the comparison of the real and simulated currents of the BLDCM, and Figure 3.5 on the next page is the comparison of the speed. The model has been studied in [NP06] and has shown that the behaviour of the model is close to the real BLDCM.

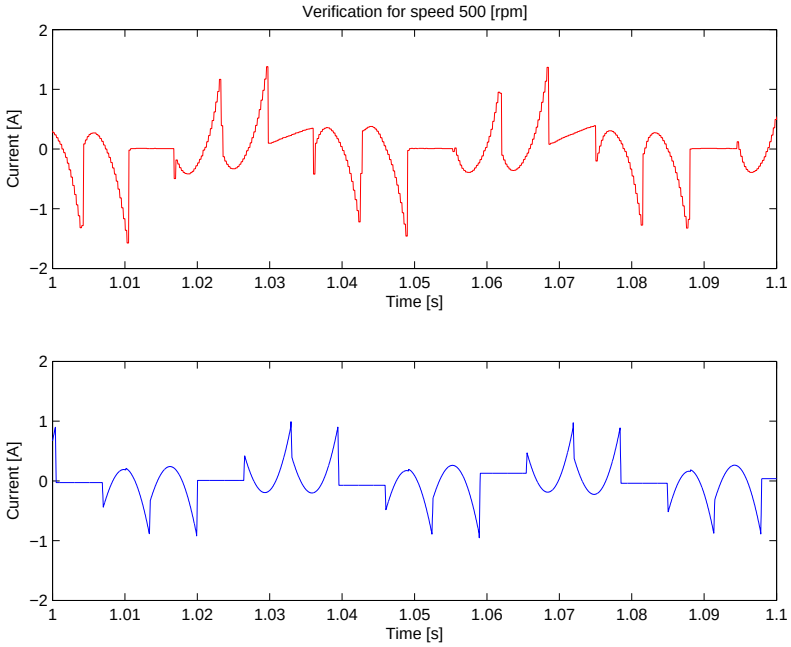

FIGURE 3.4: *Comparison of the simulated and measured currents for $D_{in} = 0.59$. The first graph is the measured current, the second is the simulated current.*

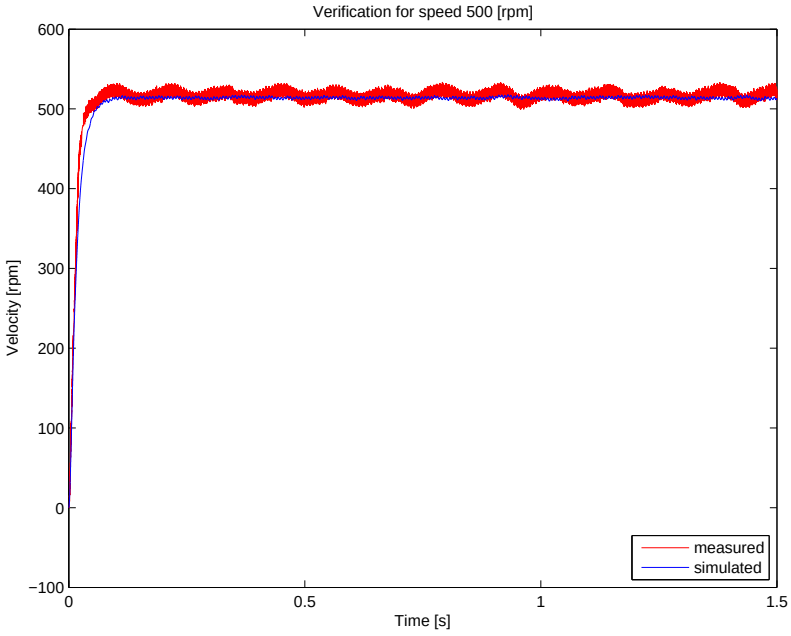

FIGURE 3.5: *Comparison of the simulated and measured angular velocities for $D_{in} = 0.59$.*

3.6 CONCLUSION

In this chapter the hybrid model of the BLDCM has been presented. A construction of the hybrid automaton was shown followed by continuous equations and the formal description of the whole system. Some of the results from the verification of the model has been demonstrated to show that the model is sufficiently close to the real system.

This page is left intentionally blank

HYBRID OBSERVER 4

In this chapter, the new hybrid observer used to estimate the angle and the speed of the rotor is presented. This observer is built based on the observer designed in [NP06]. The core of the observer, i.e. the speed adaptive state estimation will be kept identical as it has shown good capability to estimate the states. However, the structure of the observer is modified. This is done in order to reduce the complexity of the observer and to improve the precision of the estimates.

Firstly, the location automaton is described based on the reduced hybrid automaton that was build in Section 3.2 on page 24. The new structure of the observer is presented, and the new equations for the observer are expressed. Finally, the results of a test of this observer will be presented.

As mentioned earlier, it is assumed that the angular velocity of the rotor is in certain range of values, $\omega_r \in [500; 1000]$ [rpm], that is approximately $\omega_e \in [156; 315]$ [rad/s]. This can be assumed as the speed of the pump is generally not varying in the full range, but operates in a certain region.

4.1 LOCATION AUTOMATON

The hybrid observer consists of two parts: the location automaton and the continuous observer. It is very similar to the definition of the hybrid system, which also consists of those parts and the interactions between them.

Hybrid automaton was proposed in Section 3.2 on page 24, in accordance with certain assumptions that are important based on the scope of the project. It includes the physical behaviour of such a system and the control strategy.

The idea of the location observer is to track the current location of the system and give this knowledge to the continuous part so that the proper set of equations can be chosen. As shown in Figure 4.1 on the following page, the location observer switches based on the estimated states from the continuous part. This prevents erroneous switching based on noisy measurements and is important for the stability of the observer. In the system that is analysed, the exact switching sequence is known. The initial state is also known as there is the startup procedure that aligns the rotor to a known phase. Therefore the location observer is simply a copy of the hybrid automaton.

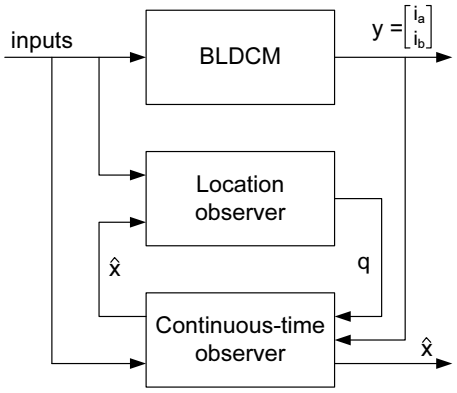

FIGURE 4.1: *The structure and dependencies between the parts of the hybrid observer.*

4.2 STRUCTURE OF THE CONTINUOUS OBSERVER

The observer is designed to deal with ω_e as a time-varying parameter. The structure of the observer is shown in Figure 4.2 on the next page, and the general continuous time equation for it is described by Equation 4.1. The value of θ_e as well as the value of ω_e are computed on basis of the estimated states. The value of ω_e is fed back to the state estimation block, as it is needed to estimate the states.

$$\dot{\hat{\mathbf{x}}} = \underbrace{\left({}^{q}\mathbf{A}_0 + {}^{q}\mathbf{A}_\omega \omega_e\right)}_{{}^{q}\mathbf{A}(\omega_\mathbf{e})} \hat{\mathbf{x}} + {}^{q}\mathbf{B}\mathbf{V}_{abcs} + {}^{q}\mathbf{K}\left(\mathbf{C}\hat{\mathbf{x}} - \mathbf{y}\right) \tag{4.1}$$

The error between the estimated and measured current value is multiplied with the proportional feedback ${}^{q}\mathbf{K}$ and provided to the state estimation part to make the correction on the states. In this project, only proportional correction is used as the previous work has shown very little influence of an integral correction. The correction term of the observer is of the form ${}^{q}\mathbf{K}\left(\mathbf{C}\hat{\mathbf{x}} - \mathbf{i}\right)$, where $\mathbf{C} = \begin{bmatrix} \mathbf{I}^{2\times 2} & \mathbf{0} \end{bmatrix}$ and $\left(\mathbf{C}\hat{\mathbf{x}} - \mathbf{i}\right) = \begin{bmatrix} \hat{i}_{as} - i_{as} \\ \hat{i}_{bs} - i_{bs} \end{bmatrix} = \Delta\mathbf{i}$ is the difference between current estimations ($\hat{i}_{as}$ and $\hat{i}_{bs}$) and measurements (i_{as} and i_{bs}).

In order to improve the quality of the speed estimate, it passes through a low-pass filter. The parameters of this filter were tuned in [NP06] to increase the precision of the estimate without changing its dynamics significantly.

The structure of the continuous observer is derived based on the linear time varying equations described in Section 3.3 on page 27. There are several cases to be analysed, since the equations vary when location, q, changes. In the equations described in Sec-

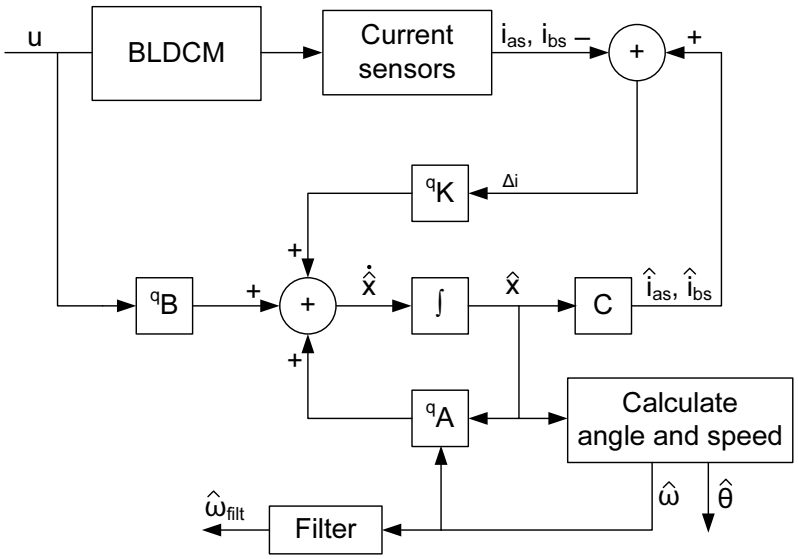

FIGURE 4.2: *Block diagram of the observer structure at a location q.*

tion 3.3 on page 27, the differential equations of the measurable states i_{as} and i_{bs} are dependent on the time varying parameter ω_e, which makes it difficult to design an adaptive observer. The idea is therefore to realize a state transformation in order to decouple ω_e from the measurable states. The new state vector, x, contains the two measurable states i_{as} and i_{bs}, as well as two new states e_α and e_β that are related to the back-EMF. This approach was first presented in [UZ04]. In this work it is extended to fit a different model description. The new parameters are defined as follows:

$$\begin{aligned} e_\alpha &= \omega_e \cos\theta_e \\ e_\beta &= \omega_e \sin\theta_e \end{aligned} \tag{4.2}$$

The derivatives are then of a form:

$$\begin{aligned} \dot{e}_\alpha &= \dot{\omega}_e \cos\theta_e - \omega_e^2 \sin\theta_e = e_\alpha \frac{1}{\omega_e}\dot{\omega}_e - e_\beta \omega_e \\ \dot{e}_\beta &= \dot{\omega}_e \sin\theta_e + \omega_e^2 \cos\theta_e = e_\beta \frac{1}{\omega_e}\dot{\omega}_e + e_\alpha \omega_e \end{aligned} \tag{4.3}$$

The previous equation shows that the acceleration of the rotor $\dot{\omega}_e$ has an influence on the dynamics, but since ω_e is a time-varying parameter, it will be assumed in this project that it is varying slowly compared to the other states, i.e. its derivative is zero, $\dot{\omega}_e = 0$. The acceleration of the rotor was used in the previous work, but it found to

have little influence on the dynamics of the observer (when set to zero there are almost no changes in the estimates), which explains why this assumption can be made. Under this assumption, the derivatives become:

$$\begin{aligned} \dot{e}_\alpha &= -e_\beta \omega_e \\ \dot{e}_\beta &= e_\alpha \omega_e \end{aligned} \tag{4.4}$$

The observer equations may be derived and described for each of the locations, q, where the state vector is of a form Equation 4.5.

$$\hat{\mathbf{x}} = \begin{bmatrix} i_{as} & i_{bs} & e_\alpha & e_\beta \end{bmatrix}^T \tag{4.5}$$

4.3 CALCULATION OF THE ANGLE AND THE SPEED

The states e_α and e_β depend only on the value of the angle and the speed, therefore the estimations of the angle and angular velocity are computed on basis of those states.

The estimation of the angular velocity $\hat{\omega}_e$ is computed using Equation 4.6. This Equation is derived from the expression of e_α and e_β in Equations 4.2 on the preceding page. Since only one direction of the rotation is considered, $\omega_e > 0$, the absolute value can be omitted.

$$\hat{\omega}_e = |\hat{\omega}_e| = \sqrt{e_\alpha^2 + e_\beta^2} \tag{4.6}$$

The estimation of the angle of the rotor $\hat{\theta}_e$ is also computed on basis of the estimated states e_α and e_β. First, $\cos\hat{\theta}_e$ and $\sin\hat{\theta}_e$ are calculated using Equation 4.7, which is derived from Equations 4.2 on the preceding page.

$$\begin{aligned} \cos\hat{\theta}_e &= \frac{e_\alpha}{\hat{\omega}_e} \\ \sin\hat{\theta}_e &= \frac{e_\beta}{\hat{\omega}_e} \end{aligned} \tag{4.7}$$

From the values of $\sin\hat{\theta}_e$ and $\cos\hat{\theta}_e$, the estimation of the angle is found as follows:

$$\hat{\theta}_e = \begin{cases} \arccos\left(\frac{e_\alpha}{\hat{\omega}_e}\right) & \text{for} \quad \sin\hat{\theta}_e \geq 0 \\ 2\pi - \arccos\left(\frac{e_\alpha}{\hat{\omega}_e}\right) & \text{for} \quad \sin\hat{\theta}_e < 0 \end{cases} \tag{4.8}$$

4.4 CONTINUOUS OBSERVER EQUATIONS

The continuous equations for the observer are obtained by using the new state vector described in Equation 4.5 on the preceding page. The derivative of the back-EMF states are expressed in Equation 4.4 on the facing page. The equations are the equations of a simple Luenberger observer, i.e. with proportional feedback (Equation 4.1 on page 38).

The elements of the feedback matrices are set to zero when there is no influence of the state on the corresponding current. For instance, i_{as} has no influence on i_{bs} (this is true $\forall q \in \mathcal{Q}$), therefore there is no correction of the current i_{as} on basis of the error in i_{bs}. In the feedback matrices, the coefficient that maps the error in i_{bs} to the current i_{as} will always be zero.

- **Three phases conducting**

  When all the phases conduct current, i.e. $q \in \{2, 3, 5, 6, 8, 9\}$ the observer equations are as follows:

$$\dot{\hat{\mathbf{x}}}_q = \begin{bmatrix} -\frac{r_s}{L_s}\mathbf{I}^{2\times 2} & -\frac{\lambda'_m}{L_s}\mathbf{M}'' \\ \mathbf{0} & \mathcal{J}\omega_e \end{bmatrix} \hat{\mathbf{x}}_q + \begin{bmatrix} \frac{1}{L_s}\mathbf{M}' \\ \mathbf{0} \end{bmatrix} \mathbf{V}_{abcs} + {}^q\mathbf{K}\Delta\mathbf{i} \tag{4.9}$$

  where

$$\mathbf{M}' = \begin{bmatrix} \frac{2}{3} & -\frac{1}{3} & -\frac{1}{3} \\ -\frac{1}{3} & \frac{2}{3} & -\frac{1}{3} \end{bmatrix}, \mathbf{M}'' = \begin{bmatrix} 1 & 0 \\ -\frac{1}{2} & \frac{\sqrt{3}}{2} \end{bmatrix}, \mathcal{J} = \begin{bmatrix} 0 & -1 \\ 1 & 0 \end{bmatrix}.$$

  The feedback matrix is of a form 4.10.

$${}^q\mathbf{K} = \begin{bmatrix} k_1 & 0 \\ 0 & k_2 \\ k_3 & k_4 \\ 0 & k_5 \end{bmatrix} \tag{4.10}$$

- **C phase passive**

When phase C is passive, i.e. $q = 1$, the observer's equations are as follows:

$$\dot{\hat{\mathbf{x}}}_1 = \begin{bmatrix} -\frac{r_s}{L_s}\mathbf{I}^{2\times 2} & -\frac{\lambda'_m}{L_s}{}^1\mathbf{M}'' \\ \mathbf{0} & \mathcal{J}\omega_e \end{bmatrix} \hat{\mathbf{x}}_1 + \begin{bmatrix} \frac{1}{L_s}{}^1\mathbf{M}' \\ \mathbf{0} \end{bmatrix} \mathbf{V}_{abcs} + {}^1\mathbf{K}\Delta\mathbf{i} \tag{4.11}$$

where

$${}^1\mathbf{M}' = \begin{bmatrix} \frac{1}{2} & -\frac{1}{2} & 0 \\ -\frac{1}{2} & \frac{1}{2} & 0 \end{bmatrix}, {}^1\mathbf{M}'' = \begin{bmatrix} \frac{3}{4} & -\frac{\sqrt{3}}{4} \\ -\frac{3}{4} & \frac{\sqrt{3}}{4} \end{bmatrix}.$$

The feedback matrix is of a form 4.12.

$${}^1\mathbf{K} = \begin{bmatrix} k_6 & 0 \\ 0 & k_7 \\ k_8 & 0 \\ k_9 & 0 \end{bmatrix} \tag{4.12}$$

- **B phase passive**

When phase B is passive, i.e. $q = 4$, the observer's equations are as follows:

$$\dot{\hat{\mathbf{x}}}_4 = \begin{bmatrix} \begin{bmatrix} -\frac{r_s}{L_s} & 0 \\ 0 & 0 \end{bmatrix} & -\frac{\lambda'_m}{L_s}{}^4\mathbf{M}'' \\ \mathbf{0} & \mathcal{J}\omega_e \end{bmatrix} \hat{\mathbf{x}}_4 + \begin{bmatrix} \frac{1}{L_s}{}^4\mathbf{M}' \\ \mathbf{0} \end{bmatrix} \mathbf{V}_{abcs} + {}^4\mathbf{K}\Delta\mathbf{i} \tag{4.13}$$

where

$${}^4\mathbf{M}' = \begin{bmatrix} \frac{1}{2} & 0 & -\frac{1}{2} \\ 0 & 0 & 0 \end{bmatrix}, {}^4\mathbf{M}'' = \begin{bmatrix} \frac{3}{4} & \frac{\sqrt{3}}{4} \\ 0 & 0 \end{bmatrix}.$$

The feedback matrix is of a form 4.14.

$${}^4\mathbf{K} = \begin{bmatrix} k_{10} & 0 \\ 0 & 0 \\ k_{11} & 0 \\ k_{12} & 0 \end{bmatrix} \tag{4.14}$$

- **A phase passive**

When phase A is passive, i.e. $q = 7$, the observer's equations are as follows:

$$\dot{\hat{\mathbf{x}}}_7 = \begin{bmatrix} \begin{bmatrix} 0 & 0 \\ 0 & -\frac{r_s}{L_s} \end{bmatrix} & -\frac{\lambda'_m}{L_s}{}^7\mathbf{M}'' \\ \mathbf{0} & \mathcal{J}\omega_e \end{bmatrix} \hat{\mathbf{x}}_7 + \begin{bmatrix} \frac{1}{L_s}{}^7\mathbf{M}' \\ \mathbf{0} \end{bmatrix} \mathbf{V}_{abcs} + {}^7\mathbf{K}\Delta\mathbf{i} \tag{4.15}$$

where

$${}^7\mathbf{M}' = \begin{bmatrix} 0 & 0 & 0 \\ 0 & \frac{1}{2} & -\frac{1}{2} \end{bmatrix}, {}^7\mathbf{M}'' = \begin{bmatrix} 0 & 0 \\ 0 & \frac{\sqrt{3}}{2} \end{bmatrix}.$$

The feedback matrix is of a form 4.16.

$${}^7\mathbf{K} = \begin{bmatrix} 0 & 0 \\ 0 & k_{13} \\ 0 & 0 \\ 0 & k_{14} \end{bmatrix} \tag{4.16}$$

4.5 CONCLUSION

A new structure for the observer was build in this chapter, which has reduced complexity and better precision. In the next chapter, the optimization approach for finding new feedback coefficients will be described. Optimization algorithms will be verified to check whether the accuracy of the observer can be improved by finding better correction coefficients.

This page is left intentionally blank

OPTIMIZATION OF OBSERVER FEEDBACK

5

The core part of the design of the observer is the optimization of the feedback parameters, as it is very difficult if not impossible to explicitly find the coefficients subject to the constraints imposed in the previous chapters. This chapter describes the problem of the feedback design from an optimization point of view. It gives an overview of some of the existing methods that could be applied to this problem. The most suitable methods are then implemented, and applied to the problem.

5.1 PROBLEM OVERVIEW

The problem of the observer design lies in finding correct values of the feedback matrices ${}^{q}\mathbf{K}$, such that the error of estimation converges to zero. In order to achieve this, a cost function is introduced. The cost function Q is defined as follows[1]:

$$Q = \underbrace{\left| \int_{t}^{t+\tau} e_\theta(t)dt \right|}_{Mean} + \underbrace{\int_{t}^{t+\tau} e_\theta^2(t)dt}_{Variance} \tag{5.1}$$

The value $e_\theta(t)$ is a difference between the electrical angle estimated by the observer, $\hat{\theta}_e$, and the measured electrical angle, θ_e. $[t; t+\tau]$ is the time range for which the cost function is calculated. The choice of the value of τ is a trade-off between the time of computation of the cost function and the quantity of information included in the cost function, in this project τ will be $0.5\,[\mathrm{s}]$. The cost function will be calculated on a set of data corresponding to a step in the angular velocity from 0 to $500\,[\mathrm{rpm}]$, which means that the coefficients will be optimized for this speed. A step in the angular velocity is chosen as it allows to optimize the convergence time of the observer as well as its steady state performance.

The cost function described by Equation 5.1 was chosen so that it represents the sum of the variance (when mean is zero) and the absolute value of the mean of the estimation error. Those are the two values to be minimized in order to have a good estimation of the

[1] It can be noticed in Equation 5.1 that the mean value is already included in the term that represents the variance (which explains why this term represents the variance only when the mean is zero). However, from the practical point of view, the cost function of this type has shown to be more efficient than the cost function without mean value term.

angle of the rotor.

Optimization limitations

There are a several key assumptions and important features of the problem, that should be taken into consideration before choosing a suitable optimization strategy. The optimization is run off-line, based on measurements taken from a real system. It requires input signals to the system and corresponding measurements of the currents, rotor angle and velocity. The goal is to tune the feedback parameters so that the observer follows the hybrid trajectory of the real system as closely as it is possible.

Overall there are 14 feedback parameters k in the matrices ${}^{q}\mathbf{K}$ that need to be determined. Due to the system complexity it is very difficult if not impossible to calculate the gradient of the performance function with respect to the feedback gains. The problem is highly non-linear and multidimensional. The optimization is done through very computational demanding simulations. Because of this, the number of potential methods that could be applied is limited.

The results of an optimized observer trajectory must be compared to the real system. This however implies that for each set of values k, the system must be simulated and its output must be stored for comparison purposes. The problem lies in the duration and complexity of the simulation of such a system, while using Simulink® software. It takes several seconds, to simulate 0.5 [s] of the system's performance, i.e. the cost function. The cost function must be evaluated many times, thus it is important to minimize the computational demands of the system, by writing an efficient code. This problem is deliberated in Appendix B on page 105, where unnecessary computations in the previously established model are removed. Nonetheless, the time of computation of one iteration plays a key role when choosing the optimization strategy.

Due to the complexity of the problem and other limitations, conventional optimization techniques cannot be used in the optimization problem of finding feedback coefficients for the non-linear hybrid observer. Other techniques must be adapted to this problem.

5.2 RANDOM SEARCH METHODS

Random Weight Change (RWC) algorithm is an example of a random search algorithm that can be used in Artificial Neural Networks (ANN) training. It is a probabilistic

method that is opposed to deterministic methods like backpropagation. During each of the cycles, the set of parameters is perturbed randomly with a magnitude δ. The cost is calculated and compared with the cost using previous set of parameters. If the value is smaller, then the new set of parameters replaces the previous values. One of the biggest advantages of such an approach is the simplicity of this algorithm. It can be easily implemented and more importantly it is fast [KHB+98].

In the previous work [NP06], RWC has shown good performance for finding an optimization region. Acquiring very precise values was not a goal for this algorithm, the goal was rather to find a good initial point for another optimization strategy.

5.3 Particle Swarm Optimization

Particle Swarm Optimization (PSO) belongs to a new research area of Swarm Intelligence (SI). It bases its strategy on the analogy to a swarm of birds or school of fish. The population, called swarm, is a potential set of solutions. It then tries to iteratively explore the whole search area in analogy to a search for food. During this process, the particles, that is the individuals of the swarm, exchange the informations among each other. All the particles benefit from this strategy [WQ05].

According to [WQ05], *PSO exhibits good performance in solving hard optimization problems and engineering applications, and compares favourably to other optimization algorithms*. Nonlinear Simplex Search (NSS) is a Hybrid PSO algorithm, that has shown some advantages over other optimization techniques, like Evolutionary Algorithms or Tabu Search [WQ05].

In the case of the optimization of k parameters, NSS was used for fine tuning the values in [NP06]. The initial point for this algorithm was determined by RWC.

5.4 Evolutionary Computation

This class of algorithms uses Darwinian evolution theory as a method for determining an optimum point. It is inspired by mechanisms found in nature, namely selection and adaptation. *The problems dealt with by such computational systems are usually highly nonlinear and contain inaccurate and noisy data* [SMY03, p. 27]. This is exactly the case with the observer optimization.

The Evolutionary Computation (EC) tries to mimic the nature by accommodating the advantages of the evolution theory, where only the best (the one that fit the environment best) survive. This allows species to adapt to changes in their environment, because the next generation consists of a population that is better suited. Natural selection eliminates the weakest individuals and gives a chance for the strongest to reproduce and spread their genes. However, the offspring is usually not a pure copy of the parents' genes. Some of the genes mutate (change) and can either make the fitness better or worse. The requirement for the algorithm to be implemented is that there must be a way to evaluate the fitness of each individual. Without it, there would not be a possibility to choose the best members, that would cross and give next generation.

A particular approach for optimization using multidimensional individuals, represented as vectors, was developed at the Technical University of Berlin, by two students Hans-Georg Beyer and Hans-Paul Schwefel. They have used it for an automatic design and analysis of experiments for adjusting parameters that were difficult to calculate. An example of this kind of optimization is designing a shape of a slender 3D body in a wind tunnel, so that it has a minimal drag per volume. It was demonstrated, that a simple randomized heuristic outperformed univariate and gradient strategies adopted from numerical strategies. This approach was found to be efficient under noisy and obviously multimodal conditions. *The new strategy showed up to be effective and sufficiently efficient to be used for a couple of other experimental optimization tasks, e.g., the design of a 3D convergent-divergent hot water flashing nozzle* [BS02]. This optimization approach seems to be very well suited for the purpose of optimization of the observer's parameters.

5.4.1 CLASSICAL EVOLUTIONARY ALGORITHM

Classical Evolutionary Algorithm (EA) bases its operation on genetic modifications of individuals in a population. Each of the individuals is represented as a set of genes. The easiest is to imagine those genes as a set of binary numbers that represent each value on a numerical machine. Those sets undergo each of the stages of the EA, that is evaluation of the fitness, selection, reproduction (crossover or recombination) and mutation.

Figure 5.1 on the facing page shows how each of these steps depend on each other.

The general structure of EA should be as follows:

- Create a random population (initial step).

- Evaluate fitness of each individual.

- Reproduce and mutate - individuals with high fitness value are more likely to reproduce. Reproduction is a combination of parents' genes. The offspring can mutate after reproduction.

- Next generation - if the solution is not good enough, perform the previous steps again.

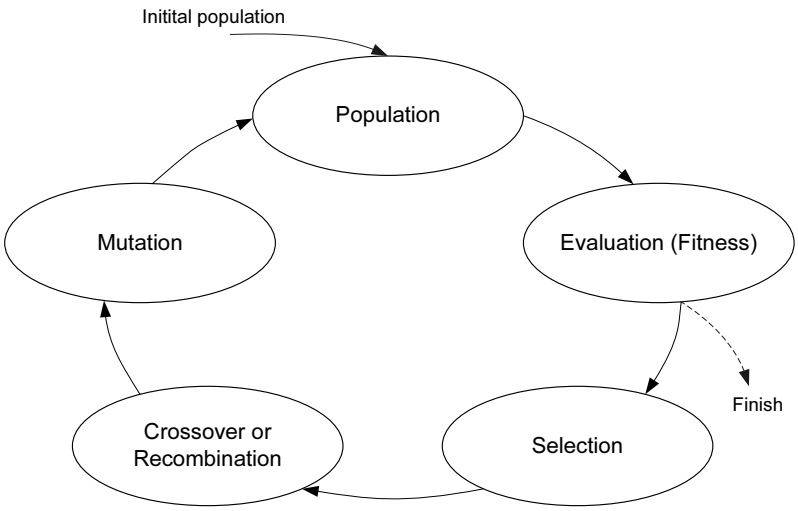

FIGURE 5.1: *The structure of the Evolutionary Algorithm (EA) presenting the dependencies between parts of the algorithm.*

Fitness

The evaluation of the fitness is a necessary condition for implementing EA. The fitness function represents how well the corresponding individual fits its environment. Without knowledge of this fitness, it would be impossible to determine which of the individuals suits the environment best, and consequently it would not be possible to evolve in the direction of better individuals.

For the optimization problem of the observer, there is no fitness function defined but a cost function. The cost function represents how bad the observer works. The fitness function in the case of the observer will therefore be taken as the inverse of the cost function: $Fitness = \frac{1}{Q}$.

Selection

In nature, the individuals that are better adapted to the environment, have better chances to find food, survive and reproduce. This principle is also used in the algorithm implementation. There are several methods of choosing the best individuals. Best members of the population should have larger chance to reproduce and create next generation, but sometimes also the weaker ones are allowed to cross. This allows to keep a genetic diversity, which is important as weaker individuals could carry good genes.

Among the methods of selecting the candidates for reproduction, are a proportional method (roulette selection or stochastic universal sampling), tournament method or truncation method. Those methods are described below and presented in Figures 5.2 on the next page to 5.4 on the facing page [Ped05].

- **Proportionate selection** - Each of the individuals has an area of the circle whose size is proportional to its fitness. The better the individual is, the larger is the corresponding area, meaning that better individuals have higher probability to be chosen. Roulette selection places randomly an arrow on the circle, the individual for which the arrow is in its area is chosen as a parent. This operation is repeated μ times until the population of parents is filled. Stochastic Universal Sampling (SUS) uses the same method as roulette selection except that it places μ equispaced arrows to choose the parents instead of randomly chosen arrows.

- **Tournament selection** - It compares n random individuals at a time and chooses the best one among them.

- **Truncation selection** - This is a deterministic method in which, the top most fit individuals are selected and copied to fill the next generation.

There are two most commonly used schemes for selecting the new population, (λ, μ) and $(\lambda + \mu)$. In the *comma* scheme, the offspring population, λ, completely replaces the parent population. This strategy is based on birth surplus, that is $\lambda > \mu$. In the *plus* scheme the best parents and children are selected among the population. According to [Ped05], lately, the elitist *plus* scheme is used more and more often in the algorithms.

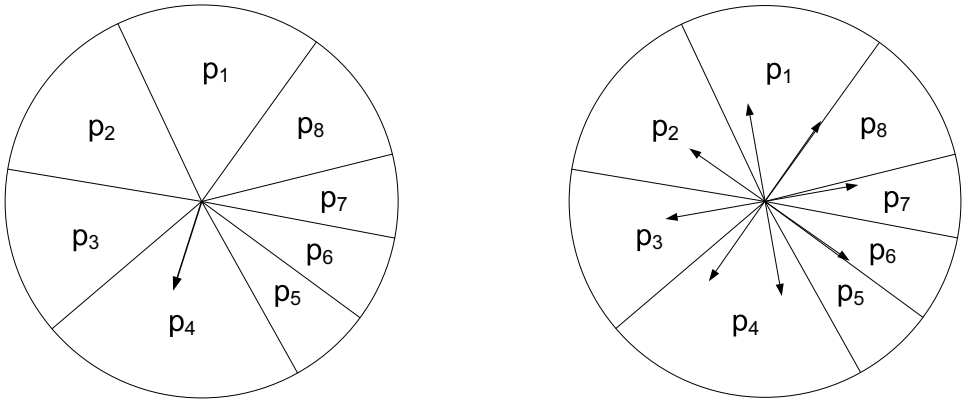

(a) Roulette selection

(b) Stochastic Universal Sampling (SUS)

FIGURE 5.2: *Proportionate selection of individuals [Ped05].*

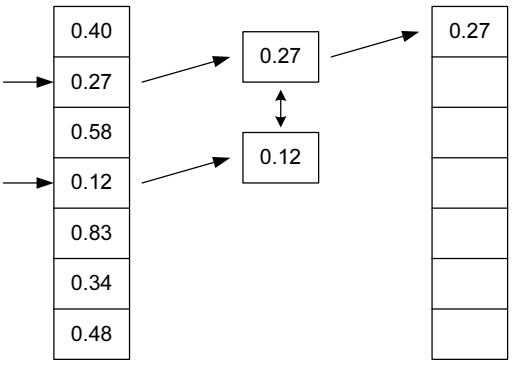

FIGURE 5.3: *Tournament selection with size 2 [Ped05]. The values represent the fitness of the individuals.*

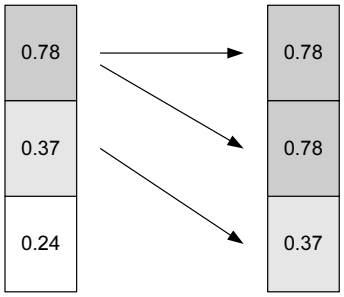

FIGURE 5.4: *Truncation selection. The values represent the fitness of the individuals.*

Reproduction

- **Crossover**

  The individuals selected as parents, are crossed to create offspring, which should

hopefully improve the fitness of the population.

Crossover is a genetic operator that is inspired by the reproduction of the highest species in the nature. This operator can be implemented in several ways.

The simplest and most common is the single point crossover. Having two binary strings, that represent two real number, a random point in the string is chosen. The strings are then swapped. This is illustrated in Figure 5.5. Similarly, there might also be n-point crossover which is also illustrated in the same figure. This operator can be considered as random shuffle.

There also exist methods for using real valued numbers in crossing. There are two widely used methods to do so, blended crossover (BLX) and simulated binary crossover (SBX). Those methods are not further discussed as they are not further used. To find more details about them, please refer to [Ped05].

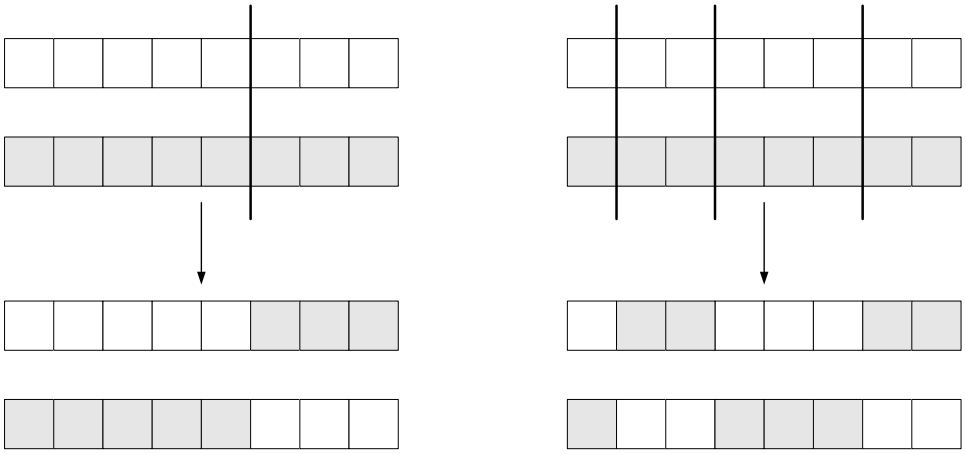

(a) Single point (b) Triple point

FIGURE 5.5: *Example of a crossover for a binary string [Ped05].*

- **Recombination**

  There exist many widely used methods for the recombination. Among the most common is an intermediate recombination. The procedure is done according to the formula:

  $$x_i^o = \alpha \cdot x_i^{p1} + (1 - \alpha) \cdot x_i^{p2}$$

  where x is the set of optimization parameters, α is randomly chosen parameter from a uniform distribution with interval $[0, 1]$, superscript o corresponds to *offspring* and p corresponds to *parent*. When $\alpha = 0.5$, the value of offspring is simply the mean value of its parents. This is illustrated in Figure 5.6 on the facing page.

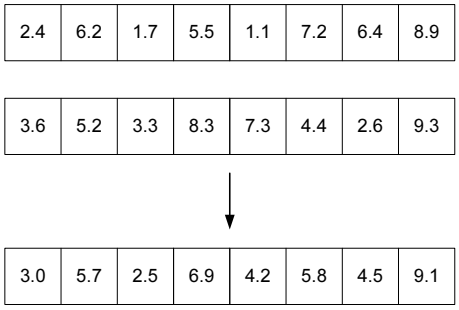

FIGURE 5.6: *Intermediate recombination for multidimensional members, where* $\alpha = 0.5$ *[Ped05].*

Mutation

Mutation is called an asexual operator, whereas crossover is called a sexual operator. This is due to the fact that the mutation operator requires one individual only, which undergoes the mutation. The crossover operator requires at least two parents, but sometimes more than two can be used as well.

In nature, due to various reasons like pollution or radiation, some of the genes are sometimes randomly changed. This very often can cause that the individual is no longer suitable for the environment, but it may also happen that such a change will positively influence the fitness. In the case of optimization, this would allow to find the optimum point faster.

It is a good idea to use annealing of the mutation factor as the number of iterations increases. The mutation should decrease as the solution becomes more suitable (optimal). However, finding a good annealing function for a particular problem can be very difficult and it is not considered in this project.

In early implementations, the mutation was performed with a predefined step, however, recently it is done according to a Gaussian distribution. This makes the mutations more flexible and thus better to adopt to the problem environment.

Parameters of the EA

The choice of EA parameters like initial population size, mutation probability, and others, can be very crucial to the performance of the algorithm. According to [BB03], *The choice of an adequate parameter setting, or EA design, can be based on expert knowledge. But in many cases there is no such knowledge available*. The real-world problems are usually computationally

demanding, therefore it is important to have a good initial population. There is no explicit way of finding the parameters, therefore there exist other methods to determine them. An example could be design of experiment (DOE) techniques presented in [BB03]. There are also techniques that allow self-tuning of such algorithms, in order to optimize the algorithm parameters on-line, while it is executed [BS02].

The evolutionary techniques of optimization can be very sensitive to those internal parameters. An *evolutionary window* is a term to describe the range of parameters for which an EA performs well. If some of them are chosen wrongly, the algorithm will not work.

5.4.2 DIFFERENTIAL EVOLUTION

Differential Evolution (DE) is an optimization algorithm which uses the idea of the gradient algorithm, i.e. it uses differences in the value of the cost function of the individuals to create better individuals. In the DE, the idea of the gradient algorithm is combined with the classical EA [UV03]. This algorithm is of $(\lambda + \mu)$ type, which means that only the best individuals are kept. The general structure of the DE is as follows:

1. Create a random population and evaluate fitness of each individual (initial step).
2. For each individual x_i^p in the population, **create an offspring** x_i^o .
3. Evaluate the offspring x_i^o.
4. If x_i^o is better than the parent x_i^p, copy it in the next population, otherwise copy x_i^p in the next population.
5. Next generation - if the solution is not good enough, perform the previous steps again with the new population.

The core part of this algorithm is the way of creating the offspring x_i^o. Several variants for creating the new candidate have been proposed. The offspring is generally built by first creating an intermediate offspring $x_i^{o\prime}$.

- In [UV03], in order to create $x_i^{o\prime}$, three extra parents of the current population x_i^{p1}, x_i^{p2}, and x_i^{p3} different from the current parent x_i^p are randomly chosen. Equation 5.2 on the next page represents how $x_i^{o\prime}$ is built, with F being a scaling factor, and $Q(x)$

is the fitness of the individual x.

$$x_i^{o\prime} = \begin{cases} x_i^{p1} + F \cdot (x_i^{p2} - x_i^{p3}) & \text{if } Q(x_i^{p3}) > Q(x_i^{p2}) \\ x_i^{p1} + F \cdot (x_i^{p3} - x_i^{p2}) & \text{if } Q(x_i^{p2}) > Q(x_i^{p3}) \end{cases} \tag{5.2}$$

It is noticed in Equation 5.2 that the intermediate offspring depends on the values of the cost function for the randomly chosen parents; this is because it is needed to go in the correct direction, i.e. in the direction of decreasing values for the cost function as a minimum needs to be found.

- Another approach for creating $x_i^{o\prime}$ is used in [SP95]. In that case, the best individual of the current population, x_i^{pbest}, is also used as a parent. The formula for $x_i^{o\prime}$ is as follows:

$$x_i^{o\prime} = \begin{cases} x_i^{p} + \lambda \cdot (x_i^{pbest} - x_i^{p}) + F \cdot (x_i^{p2} - x_i^{p3}) & \text{if } Q(x_i^{p3}) > Q(x_i^{p2}) \\ x_i^{p} + \lambda \cdot (x_i^{pbest} - x_i^{p}) + F \cdot (x_i^{p3} - x_i^{p2}) & \text{if } Q(x_i^{p2}) > Q(x_i^{p3}) \end{cases} \tag{5.3}$$

Where λ and F are scaling parameters. The idea behind Equation 5.3 is to add the direction of the best individual so that it would increase the speed of convergence of the algorithm. However, the tradeoff against this method is that it adds an extra parameter to the algorithm.

The final offspring x_i^o is created by combining the intermediate offspring $x_i^{o\prime}$ and the current parent x_i^p with a multi-point crossover. Figure 5.7 shows how the final offspring is created in the two dimensional case, using Equation 5.2 to create $x_i^{o\prime}$, and assuming that the cost of x_i^{p3} is larger than the cost of x_i^{p2}.

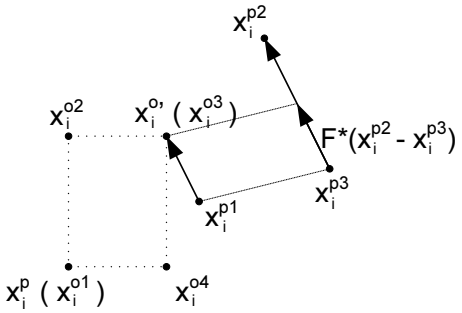

FIGURE 5.7: *Creation of the offspring x_i^o for the DE algorithm using Equation 5.2 [UV03]. x_i^{o1}, x_i^{o2}, x_i^{o3}, and x_i^{o4} are the four possible offsprings depending on the result of the crossover.*

The advantage of the DE compared to the classical EA is that it requires less parameters and is more straightforward to implement.

In the next section, the different optimization algorithms presented will be implemented and applied to the problem. This study should allow to come up with a general approach for finding the feedback parameters of the observer, so that the optimization method could be re-used with an observer for a BLDCM with different electrical parameters.

5.5 IMPLEMENTATION AND VERIFICATION

This section describes the implementation of the most beneficial algorithms suitable for the problem. The NSS algorithm was already used and tested previously in [NP06]. It has shown rather good performance, however, new optimization approaches are verified in order to choose the most suitable solution. Therefore implementation of NSS is not described nor verified in this chapter.

The optimization of feedback gains is run off-line in MATLAB®/Simulink®.

RWC

A very important parameter for many optimization algorithms is an initial population or a starting point. Very often the optimization is preceded by an analysis of the problem that establishes a starting point. For the optimization of the observer's feedback matrices the RWC algorithm is used to find the starting point. This algorithm is very fast, as it only requires one run of the simulation per epoch, which makes it suitable for scanning the optimization area.

The algorithm's flow chart is presented in Figure 5.8 on the facing page. The algorithm, perturbs the optimization coefficients with a random variable δ with distribution $\mathcal{N}(0, \sigma^2)$. The perturbed coefficients are defined as follows (where j is the index of the coefficient):

$$k_{perturbed,j} = k_{previous,j} + \delta \cdot \sqrt{k_{previous,j}}\,, \quad 1 \leq j \leq 14$$

The advantage of this formula is that the variance of the perturbation adapts to the value of the corresponding coefficient, the variance of the perturbation is $\sigma^2 \cdot k_{previous,j}$. When the perturbed coefficients are more suitable than the previous coefficients, that is the cost function is smaller, they are saved and the perturbation occurs from this point again.

The performance of a few random runs is depicted in Figure 5.9 on the next page. As

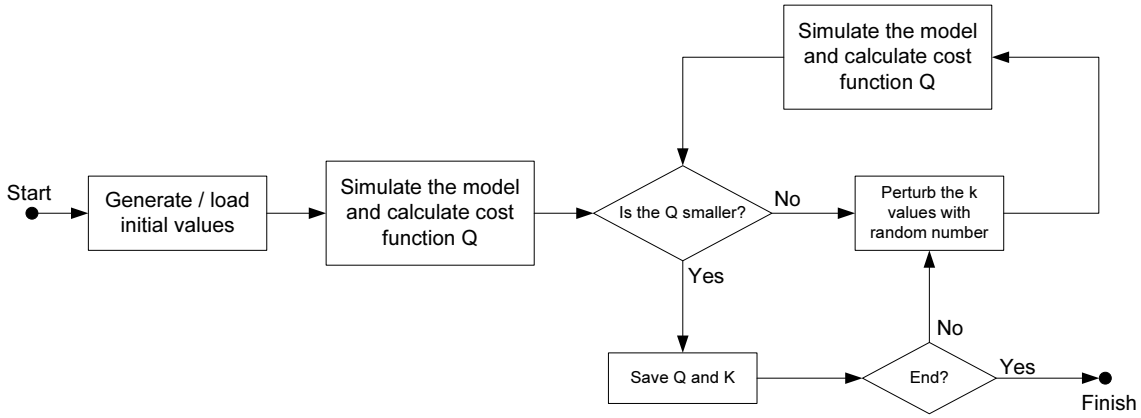

FIGURE 5.8: *Flow chart of the RWC algorithm implementation.*

can be seen, the algorithm starts at random point and can quickly find coefficients that correspond to cost function of around 5000.

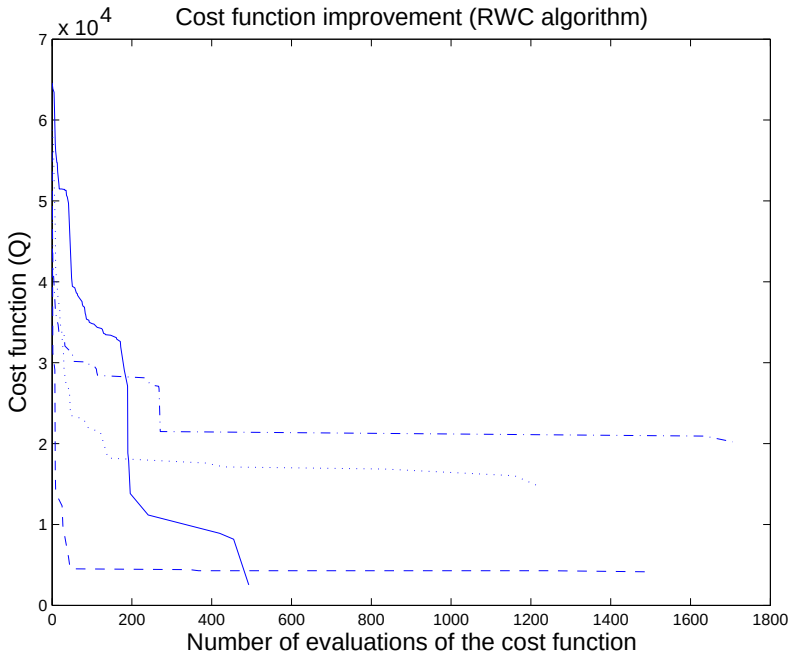

FIGURE 5.9: *Results of finding a good optimization region using an RWC algorithm.*

Textbook example of EA

The implemented EA has a structure that was described previously in Section 5.4 on page 47. There are many possible implementation for the EA. A "textbook" example is

implemented first, where the parts of the algorithm are realized as follows:

- **Fitness** - calculation of the cost function Q as stated in Section 5.1 on page 45.
- **Selection** - a proportionate selection method (roulette) is chosen. The **comma** selection is chosen, that is all the parents are replaced by the offspring. The only exception is for the best individual that is always kept, which prevents losing the best parameters.
- **Crossover** - single point crossover is chosen. The point of crossover is found randomly according to a uniform distribution. Two individuals are created from two parents by swapping the values.
- **Mutation** - occurs for one gene at a time. The probability of mutation is equal to 4.4%, corresponding to the probablility mass outside $\pm 2\sigma$ in a normal distribution. Mutation strength depends on the current value of a gene that is undergoing the procedure. A value φx_i^0 is added to the mutated gene. φ is a random variable with a distribution $\mathcal{N}(0, 0.1)$.

The implementation of the algorithm is described in Pseudo-code 5.1 on the facing page.

The starting point for this algorithm was found using RWC. The corresponding cost is 1203.67. The population for this algorithm is determined by finding random individuals around the starting point. The population was containing 40 individuals, which is a trade-off between a large size of population that is necessary for EAs and the computational demands of simulations, which are very high.

As it can be seen in Figure 5.10 on page 60, the cost is reduced by around 50% of the initial value. This is achieved in less than 20 iterations, meaning that the simulation was performed less than 800 times. This level of cost function value is suitable for use in the observer. Further optimization does not improve the performance noticably. At this level the optimization tries to fit the function to reproduce the noise in the measurements. Therefore the procedure may be stopped at this point.

This "textbook" example is easy to implement, however it is not very suitable for the problem that is faced in this optimization. There are a several reasons for this.

Roulette selection is not a very good method for such defined cost functions. The values of Q are very large and therefore small improvements are likely to be neglected. For

N population size, n number of genes, x^o offspring, x^p parent, ψ random variable $\mathcal{N}(0, 0.1)$.
Initialize the population with random individuals around the starting point.
1. Simulate the observer with given set of feedback parameters and calculate cost functions Q for all the individuals in the population
2. Calculate probabilities for each individual i to be chosen as a parent

$$P_i = \frac{\frac{1}{Q_i}}{\sum_{i=1}^{\mu} \frac{1}{Q_i}}$$

3. Choose N parents using roulette selection.
4. Generate random crossover point c and cross the parents according to the formula (using Matlab-like notation)

$$\begin{cases} x_i^{o1} = \left[x_i^{p1}(1:c) \;\; x_i^{p2}(c+1:n) \right] \\ x_i^{o2} = \left[x_i^{p2}(1:c) \;\; x_i^{p1}(c+1:n) \right] \end{cases}$$

5. Mutate random elements.
For each offspring x_i^o
for each element j
if `randn` > `mutation_threshold`

$$x_i^o(j) = x_i^o(j) + \psi \cdot \sqrt{x_i^o(j)}$$

end for
end for
6. Replace the first offspring x_1^o with the best individual from the previous population.
7. Replace previous population by offspring.
Next iteration

PSEUDO-CODE 5.1: *Description of the "textbook" EA used in finding feedback coefficients.*

example, if in a population consisting of three individuals, the cost values are $Q_1 = 5000$, $Q_2 = 5050$ and $Q_3 = 5060$, the probability of selecting the best individual is almost the same as choosing the worst one.

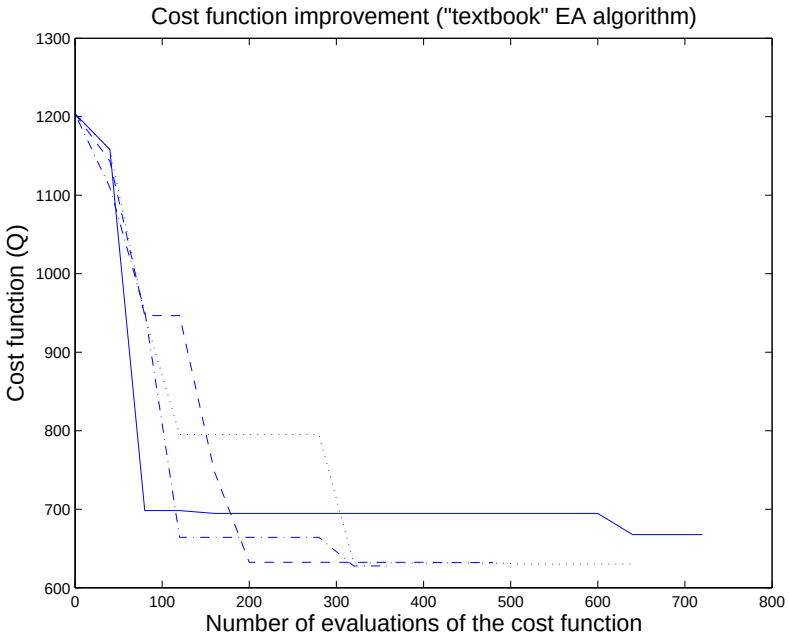

FIGURE 5.10: *Results of an optimization using "textbook" EA.*

Single point crossover is not very well suited when some of the feedback coefficients are related or dependent on each other. For example, when k_1 and k_{14} are related and must be changed in the same manner, single point crossover would not allow. Therefore a multi-point crossover or recombination should be used to avoid this problem.

EA with tournament selection and recombination

A more suitable version of classical EA used for the optimization utilises tournament selection and intermediate recombination methods. It is realized as follows:

- **Fitness** - calculation of the cost function Q as stated in Section 5.1 on page 45.
- **Selection** - a tournament method of selection is chosen, where 2 random individuals are compared at a time. The selection is performed according to *comma* strategy, but the best individual is always kept.
- **Recombination** - intermediate recombination is chosen.
- **Mutation** - is realized the same way as in the "textbook" EA implementation, using the same parameters.

The implementation of the EA with tournament selection and intermediate recombination is described in Pseudo-code 5.2. The starting point and the population size for this algorithm were the same as previously in "textbook" EA.

N population size, x^o offspring, x^p parent, ψ random variable $\mathcal{N}(0, 0.1)$, α random number with uniform distribution in $[0; 1]$.
Initialize the population with random individuals around the starting point.
1. Simulate the observer with given set of feedback parameters and calculate cost functions Q for all the individuals in the population
2. Select N parents using tournament selection comparing two individuals at a time.
3. Find offspring using intermediate recombination, according to:

$$x_i^o = \alpha \cdot x_i^{p1} + (1 - \alpha) \cdot x_i^{p2}$$

4. Mutate random elements.
  For each offspring x_i^o
    for each element j
    if `randn` > `mutation_threshold`

$$x_i^o(j) = x_i^o(j) + \psi \cdot \sqrt{x_i^o(j)}$$

    end for
  end for
5. Replace the first offspring x_1^o with the best individual from the previous population.
6. Replace previous population by offspring.
Next iteration

PSEUDO-CODE 5.2: *Description of the "improved" EA.*

As it can be seen from Figure 5.11 on the following page, the number of iterations to achieve a half of initial cost value is larger than in case of "textbook" EA. However, this does not necessarily imply that this approach is worse than the previous one. The performance of EAs depends significantly on the evolutionary window, but this is not going to be investigated in this report.

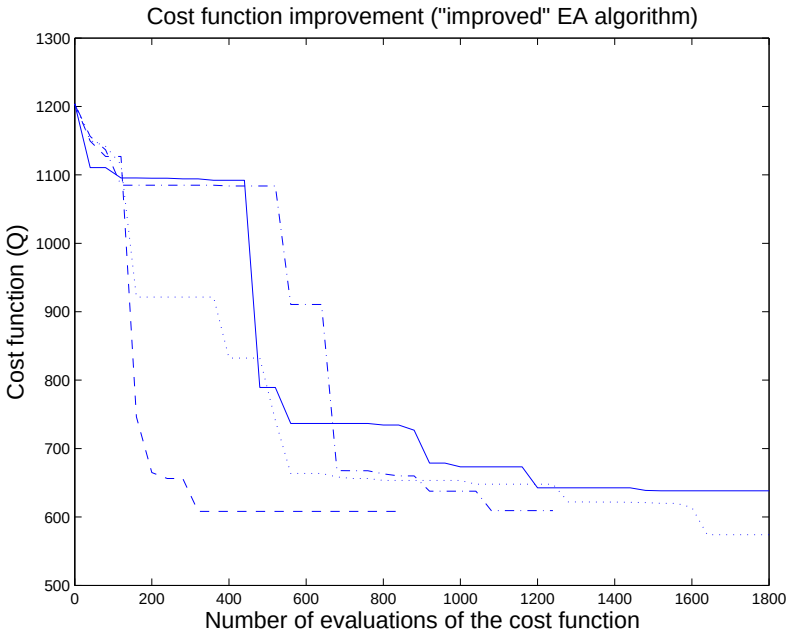

FIGURE 5.11: *Results of an optimization using EA algorithm with tournament selection and intermediate recombination.*

DE

The variant of the DE algorithm that is implemented is the one presented in [UV03]. Pseudo-code 5.3 on the next page shows the implementation of this algorithm. A population of $N = 10$ individuals is chosen as the DE does not require a large population to work correctly. The scaling factor is set to $F = 0.35$, and the threshold for the crossover is set to $P_c = 0.2$. Those values chosen for the parameters P_c and F have proven to work correctly on a wide range of problems [Urs05].

Using the same starting point as for the classical EA, the results of several runs of the DE algorithm are shown on Figure 5.12 on page 64.

Figure 5.12 on page 64 shows that DE has good performance for finding the feedback parameters. It takes less than 600 iterations to reduce the value of the cost function to a half. Compared to the classical EAs implemented before, it can be noticed that the trajectories of the cost function are smoother and closer to each other, which shows that this algorithm is less random.

x^o offspring, x^p parent, α random number with uniform distribution in $[0; 1]$.
Initialize the population with random individuals around the starting point and evaluate cost.
For each element, x_i^p, in the current population.

1. Randomly select 3 individuals different from x_i^p in the current population, x_i^{p1}, x_i^{p2}, x_i^{p3}.
2. Build intermediate offspring $x_i^{o\prime}$, according to:

$$x_i^{o\prime} = \begin{cases} x_i^{p1} + F \cdot (x_i^{p2} - x_i^{p3}) & \text{if } Q(x_i^{p3}) > S(x_i^{p2}) \\ x_i^{p1} + F \cdot (x_i^{p3} - x_i^{p2}) & \text{if } Q(x_i^{p2}) > Q(x_i^{p3}) \end{cases}$$

3. Build the offspring x_i^o by crossover of $x_i^{o\prime}$ and x_i^p:
   for each element j

$$x_i^o[j] = \begin{cases} x_i^{o\prime}[j] & \text{if } \alpha < P_c \\ x_i^p[j] & \text{otherwise} \end{cases}$$

   end for
4. Evaluate cost of the offspring x_i^o
5. if $Q(x_i^o) > Q(x_i^p)$
   Copy the x_i^p in the new population
   else
   Copy the x_i^o in the new population

end for
Next iteration, with new population

PSEUDO-CODE 5.3: *Description of the DE algorithm implementation.*

5.6 CONCLUSION

In this chapter, different methods for solving non-convex optimization problems were described. The main effort was put on selecting the best algorithm to obtain the feedback parameters. The problem is very computational demanding and high-dimensional ($\mathbb{R}^{14}$). The set of feedback matrices is not pre-calculated and therefore the starting point is not known.

A good method of resolving this problem is to determine the starting point first with an RWC algorithm. This is a fast method of finding good optimization region when a

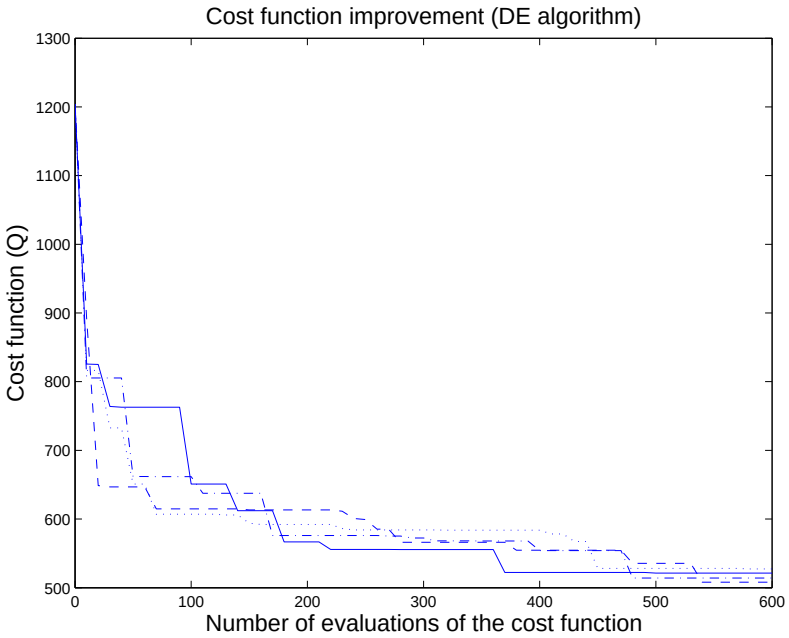

FIGURE 5.12: *Results of an optimization using DE.*

starting point is not known. Not all of the runs may lead to the good region, however, it is very likely to find it after running the algorithm for a few times.

Once the good region of optimization is found Evolutionary Algorithm (EA)s can be used to determine an optimal value of the coefficients. All the different EA implemented previously are suitable for this purpose. However, the DE algorithm has less internal parameters than the classical approaches of EAs, and it seems to be less random and work faster. Therefore, the RWC plus DE algorithm is the most appropriate method for finding optimal feedback parameters for the observer.

VERIFICATION OF THE OBSERVER

6

The purpose of this chapter is to test the new hybrid observer developed throughout this report against real measurements. The observer as described in Chapter 4 on page 37 will be first tested. It will be then shown that the accuracy of the estimates may be increased by adding an extra correction. A test of the observer with this extra correction will be run, and the results will be discussed.

6.1 TEST SETUP

The observer is implemented in Simulink® , as shown in Figure 6.1. It can be noticed that there is an extra block called "proportional correction", it is to improve the precision of the estimates, it will be described later on. The sampling period used for the system is chosen to be the same as the PWM period, i.e. $T_s = T_{PWM} = 6.25 \cdot 10^{-5}$ [s]. The observer is now using the feedback matrices found in the previous chapter. The optimization allowed to reduce a lot the cost function, and therefore the new coefficients should be more efficient than the coefficients used in previous work.

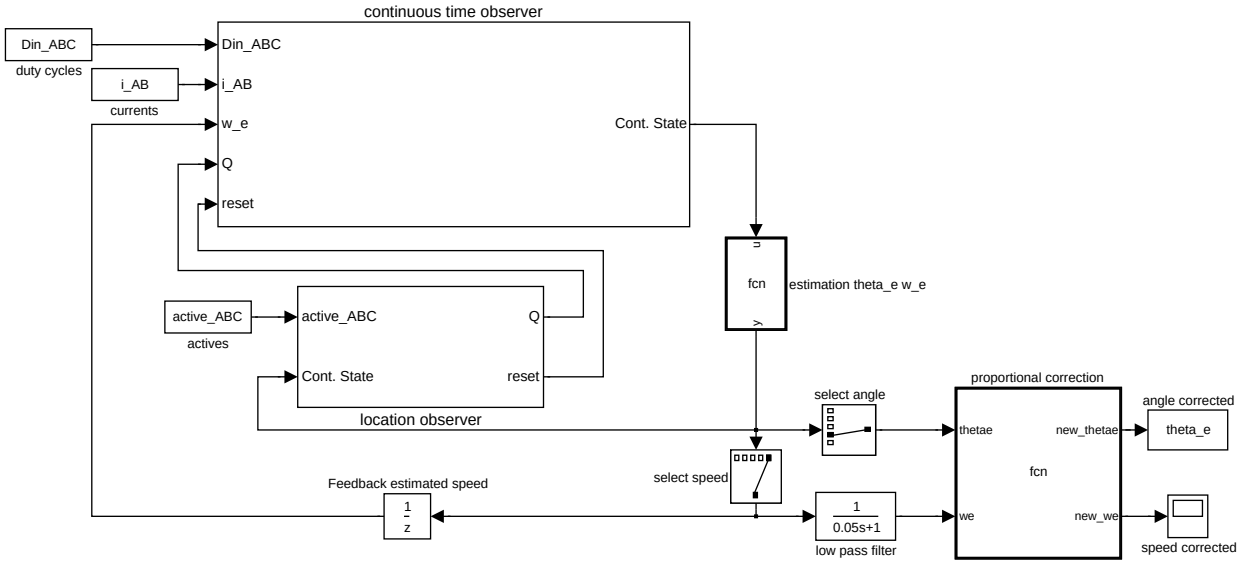

FIGURE 6.1: *Simulink implementation of the new hybrid observer.*

A test scenario is defined in order to check the behaviour in the whole range of speed considered ($\omega_r \in [500; 1000]$ [rpm]). This test scenario also allows to see how the observer handles continuous change in the angular velocity. Under no load conditions (which is

the case here), the speed of the motor can be considered proportional to the input duty cycle D_{in}. For this test, D_{in}, which represents the speed, is depicted in Figure 6.2.

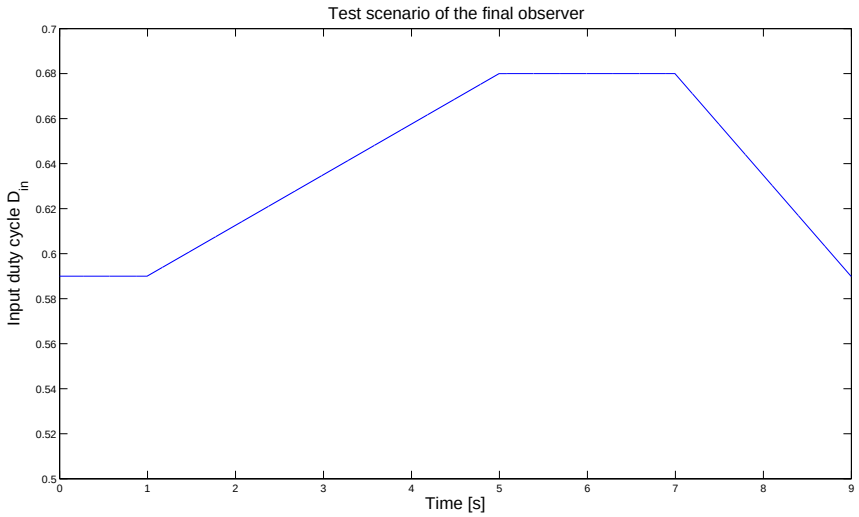

FIGURE 6.2: *Evolution of the input duty cycle during the test of the observer.*

The test is run off-line, the measurements are taken from the real BLDCM, and then fed to the Simulink® implementation of the observer.

6.2 TEST RESULTS

The observer that was derived in Chapter 4 on page 37 (without the proportional correction) is tested against real measurements, Figures 6.3 on the facing page and 6.4 on the next page represent the accuracy of the estimates of the new observer.

A brief study of Figure 6.3 on the facing page and Figure 6.4 on the next page allows to notice that there is a strong correlation between the mean value of the errors and the current value of the angular velocity. This is because the feedback coefficients k_1 to k_{14} and the parameters of the model are very dependent on the speed and are found for an angular velocity around $500\,[\mathrm{rpm}]$. Therefore it is needed to have an additional correction of the estimates if the speed is different from $500\,[\mathrm{rpm}]$.

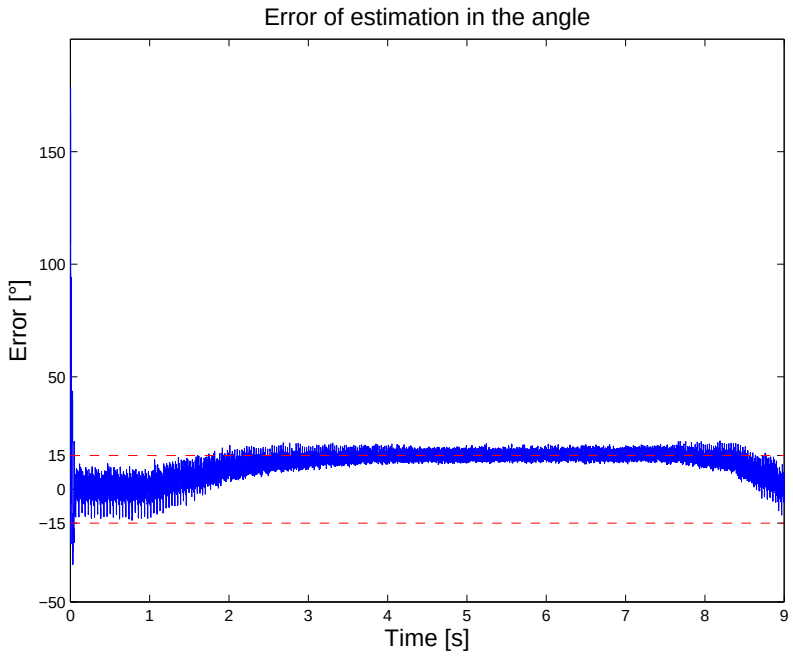

FIGURE 6.3: *Accuracy of the angle without proportional correction*

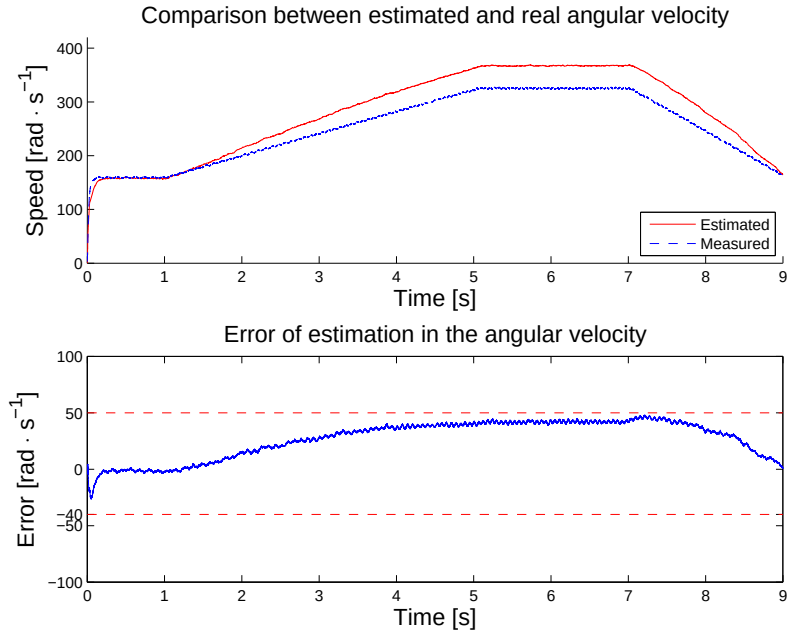

FIGURE 6.4: *Accuracy of the speed without proportional correction*

6.3 PROPORTIONAL CORRECTION OF THE ESTIMATES

The accuracy of the estimates may be increased by a proportional correction of $\hat{\omega_e}$ and $\hat{\theta_e}$. The purpose is to compensate for the changes in the time varying parameter ω_e. The mean values of the errors are proportional to the current speed, therefore the corrected estimates $\hat{\omega_c}$ and $\hat{\theta_c}$ are defined as follows:

$$\begin{aligned} \hat{\omega}_c &= \hat{\omega}_e - \alpha(\hat{\omega}_e - 160) \\ \hat{\theta}_c &= \hat{\theta}_e - \beta(\hat{\omega}_e - 160) \end{aligned} \tag{6.1}$$

$\omega_e = 160\,[\mathrm{rad} \cdot \mathrm{s}^{-1}]$ is the reference speed, it is equivalent to $\omega_r = 500\,[\mathrm{rpm}]$, at this speed no correction is needed. The correction applied depends on how far the current speed is from the reference speed. The parameters α and β are calculated on basis of Figure 6.3 on the preceding page and 6.4 on the previous page as they are the slope of the error as a function of the speed. It is calculated $\alpha = 0.24\,[]$ and $\beta = 0.0015\,[\frac{\mathrm{rad}}{\mathrm{rad/s}}]$.

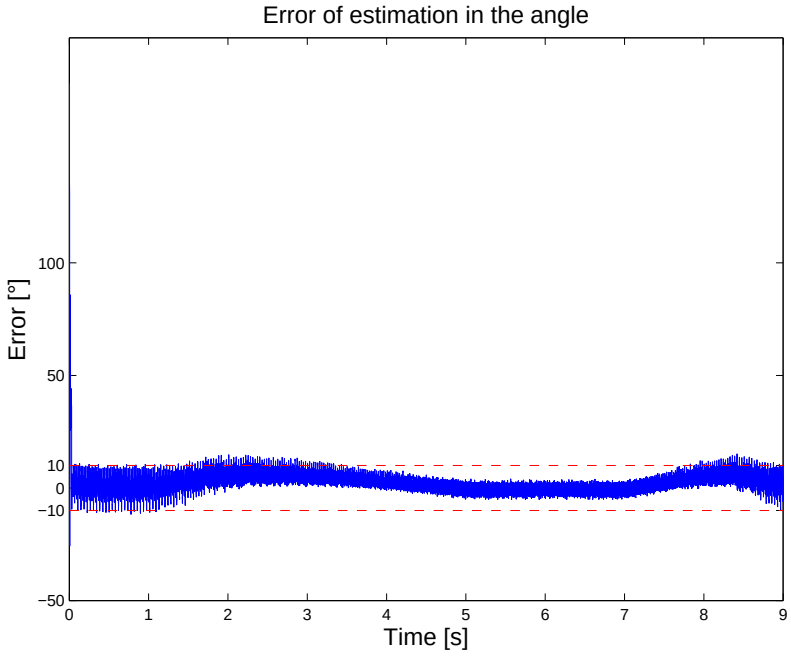

FIGURE 6.5: *Error of estimation in the rotor angle.*

The advantage of this type of correction is that it is easy to implement, and it requires a reduced the number of calculations. Another advantage of this correction is that it is very easy to tune, as there is only one coefficient per estimate, which can be changed to

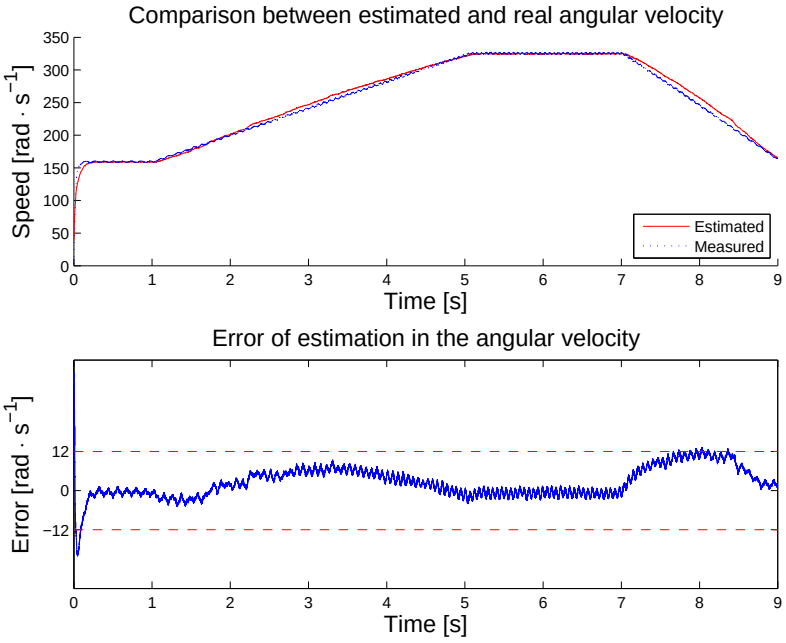

FIGURE 6.6: *Comparison between real and estimated angular velocity.*

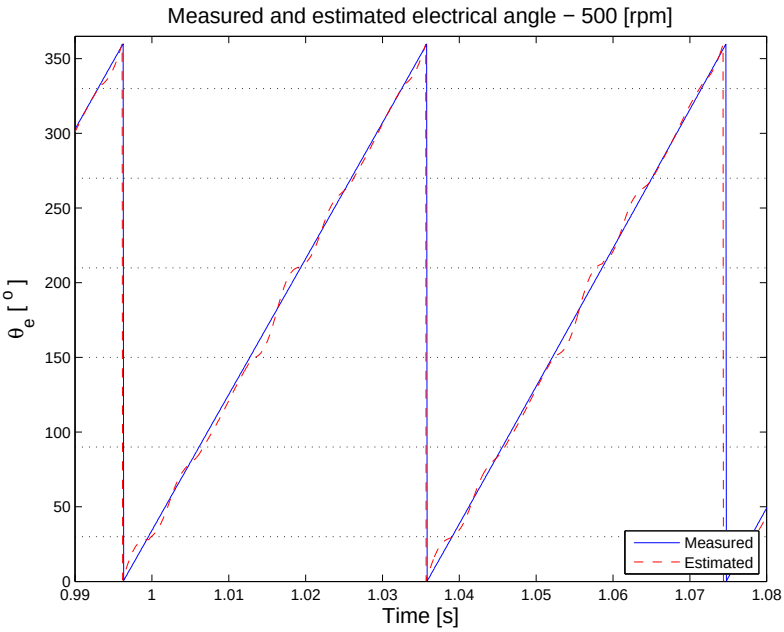

FIGURE 6.7: *Measured and estimated electrical angle at* $\omega_r = 500\,[\mathrm{rpm}]$.

bring the mean value of the error to zero.

The test of the observer is ran with the proportional correction, Figure 6.5 on the facing

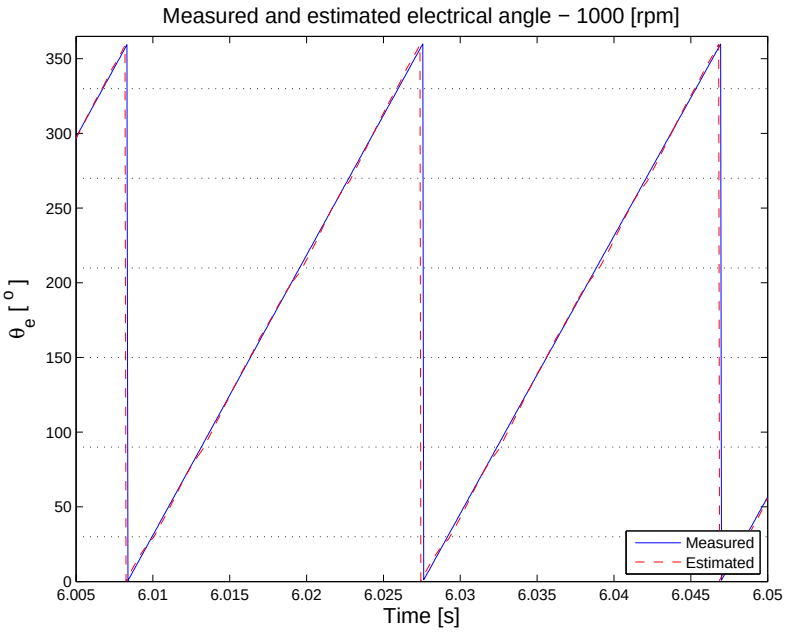

FIGURE 6.8: *Measured and estimated electrical angle at* $\omega_r = 1000\,[\mathrm{rpm}]$.

page shows the estimation error in the angle, and Figure 6.6 on the previous page is the comparison of the real and estimated speed together with the estimation error in the speed.

The estimates converge to their correct values in less than $0.2\,[\mathrm{s}]$, and the observer is able to keep a certain precision even during speed changes. The precision of the estimation of the angle is within $\pm 10°$, which means that this observer is better than the one derived in [NP06]. Figures 6.7 and 6.8 show the comparison between the measured and estimated electrical angle respectively for 500 and $1000\,[\mathrm{rpm}]$. The new structure of the observer together with new feedback coefficients allowed to gain $5°$ in the precision of the angle. The best precision in the angle estimation is at $\omega_r = 1000\,[\mathrm{rpm}]$, where the precision is within $\pm 3°$. The precision of the speed estimation is $\pm 12\,[\mathrm{rad} \cdot \mathrm{s}^{-1}]$, and when the speed is constant the precision of the estimation is much better, the error is within $\pm 4\,[\mathrm{rad} \cdot \mathrm{s}^{-1}]$.

It can be noticed that the precision of the estimates decreases when the speed is varying, this is due to the fact that the acceleration of the rotor is assumed to be zero in the observer's equations. The results of the test show that the offset correction of the estimates is working well, as the mean value of the estimation errors is very close to zero when the speed is constant.

6.4 CONCLUSION

The observer has been tested against real measurements, those results allowed to improve the quality of the estimates by adding an extra correction. The observer is now more precise and less complex, which is one step toward a real time implementation of the observer, and a test in closed loop situation. The observer uses two current sensors to estimate the speed and the angle. In the next chapter a new observer using one current sensor to estimate the angle and the speed will be derived.

This page is left intentionally blank

SINGLE SENSOR OBSERVER 7

The hybrid observer derived in the previous chapters requires the use of two current sensors, i.e. the measures of i_{as} and i_{bs}. In this chapter, the previous observer will be modified in order to be able to estimate using only one current measurement. The advantage of the use of a single sensor to estimate angle and speed is that the cost is reduced, and the reliability of the system is improved as there are less elements likely to fail. If more sensors are available, they can be used for fault detection purposes.

Two practical conditions for being able to estimate with a single sensor will be expressed. It will be shown that the first condition can be realized by the system that is considered in this report. For the second condition to be realized however, a new hybrid automaton for the observer will be derived. Then, the corresponding equations for the observer will be expressed. Finally, the observer will be tested against real measurements to check that it is still able to estimate correctly the angle and the speed of the rotor.

7.1 PRACTICAL REQUIREMENTS FOR THE USE OF ONE SENSOR

To reduce the number of sensors used, the system and the observer should meet two requirements:

- As the goal is to use one current measurement, there cannot be cases where the observer needs two different measurements.
- There must be a measurable current from which value it is possible to express the currents i_{as} and i_{bs} in all discrete states where they are needed.

It can be noticed in Equation 4.9 on page 41 that the first requirement is not fulfilled by the double sensor observer. When all three phases are conducting (drain states), it needs measures of i_{as} and i_{bs}, which can only be provided by two different current sensors. The drain states are usually short (in terms of time), therefore they don't have much influence on the dynamics of the observer. In order to meet the first requirement, the idea is to have only predictive behaviour of the observer during the drain states. To verify that it is possible to have only predictive behaviour during drain states, the double sensor is tested with the feedback parameters k_1, k_2, k_3, k_4, and k_5 in Equation 4.10 on page 41 set to 0. The performance is found to be satisfactory, despite a slight loss in precision.

Having verified that an observer can work using one current measurement at a time, it is needed to verify the second requirement. Figure 7.1 represents the different measurable currents that are available on the inverter used in the project.

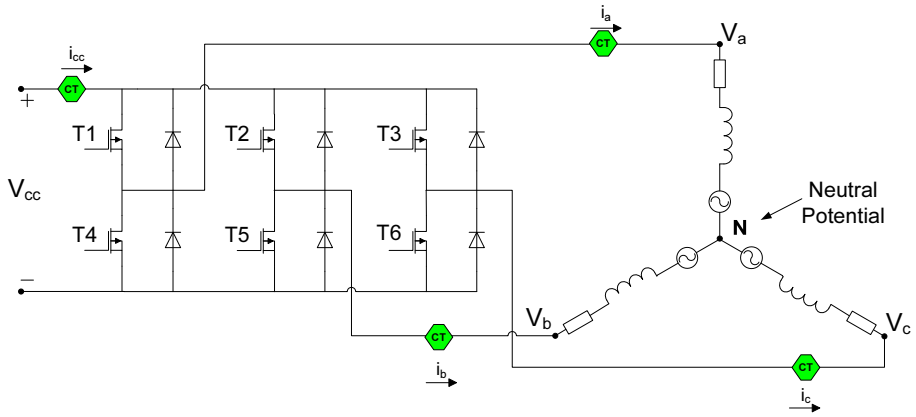

FIGURE 7.1: *Current sensors available on the inverter.*

Four current measurements are available on the electronic board. There are the phase currents i_{as}, i_{bs}, and i_{cs}, which have already been used. The last sensor measures the supply current to the inverter i_{cc}. There is no current from which value it is possible to express the value of the currents i_{as} and i_{bs} in the locations where they are needed, i.e. $q = 1$, $q = 4$, or $q = 7$.

However, it is noticed that it would be possible to process the value of i_{cc} to be able to estimate i_{as} and i_{bs}. If X is the phase that is receiving the PWM modulation with duty cycle D_{in}, during the time $D_{in}T_{PWM}$ the high transistor of phase X (T1, T2, or T3) is conducting and $i_{cc} = i_{xs}$. During the remaining time, $(1 - D_{in})T_{PWM}$, the current is looping in the inverter and it is not passing through the power supply, therefore $i_{cc} = 0$. This means that when sampling the current i_{cc}, its value will be either 0 or the value of the current in phase X. In order to have a measurement that is usable, the value of i_{cc} is low pass filtered before it is sampled. A simple RC filter is used whose cut-off frequency is $2.6\,[\text{KHz}]$. This means that the value of i_{cc} measured can be assumed to be the mean value of a PWM modulation whose duty cycle is D_{in}, and whose amplitude is i_{xs}: $i_{cc} = D_{in} \cdot i_{xs}$. The value of the current through the phase X that receives the PWM modulation with duty cycle D_{in} can be estimated using the following equation:

$$i_{xs} = \frac{i_{cc}}{D_{in}} \tag{7.1}$$

Therefore, if it was known which one of the phases receives the input duty cycle D_{in}, the currents could be estimated as follows:

- For $q = 1$, which corresponds to the AB case ($i_{bs} = -i_{as}$):

$$i_{as} = \begin{cases} \frac{i_{cc}}{Din} & \text{if phase A receives } D_{in} \\ -\frac{i_{cc}}{Din} & \text{if phase B receives } D_{in} \end{cases} \tag{7.2}$$

- For $q = 4$, which corresponds to the AC case ($i_{bs} = 0$):

$$i_{as} = \begin{cases} \frac{i_{cc}}{Din} & \text{if phase A receives } D_{in} \\ -\frac{i_{cc}}{Din} & \text{if phase C receives } D_{in} \end{cases} \tag{7.3}$$

- For $q = 1$, which corresponds to the BC case ($i_{as} = 0$):

$$i_{bs} = \begin{cases} \frac{i_{cc}}{Din} & \text{if phase B receives } D_{in} \\ -\frac{i_{cc}}{Din} & \text{if phase C receives } D_{in} \end{cases} \tag{7.4}$$

This means that the locations $q = 1$, $q = 4$, and $q = 7$ need to be refined so it would be possible to know which phase receives the PWM modulation with D_{in}. In the next section, a new hybrid automaton is derived in order to make this distinction.

7.2 SINGLE SENSOR OBSERVER HYBRID AUTOMATON

The new hybrid automaton derived is built on basis of hybrid automaton depicted in Figure 3.3 on page 27. The states where only two phases are conducting are replaced with two new states. The following notation is used, "XY" means that phase X is receiving a PWM signal with duty cycle D_{in}, and phase Y with duty cycle $1 - D_{in}$. The new hybrid automaton derived is presented in Figure 7.2 on the following page[1].

It is noticed that from a state where the passive phase has no current through it (XY state), when the next switching occurs it is possible to go either to the negative drain or the positive drain of the phase that has just been deactivated. This is because in XY case, even if $V_{xs} > V_{ys}$, it is possible that the current flows from X to Y or from Y to X. For instance, this can happen when there is no load on the motor ($T_L = 0$, which is the case

[1]In case there would be a load on the motor, and this load would be large enough such that the BLDCM could not behave like a generator, the hybrid automaton in Figure 7.2 on the next page can be simplified as some of the transitions can never be realized. This simplified hybrid automaton can be found in Appendix A on page 103.

here), during short periods the BLDCM behaves like a generator and reverses the current through the active phases. This also means that it is not possible from the knowledge of the current drain state to determine the next reachable discrete state, and additional information is required. To determine the correct discrete state after a drain state, the new hybrid automaton uses the values of the duty cycles of the PWM modulations to the phases: D_A is the duty cycle to phase A and D_B is the duty cycle to phase B.

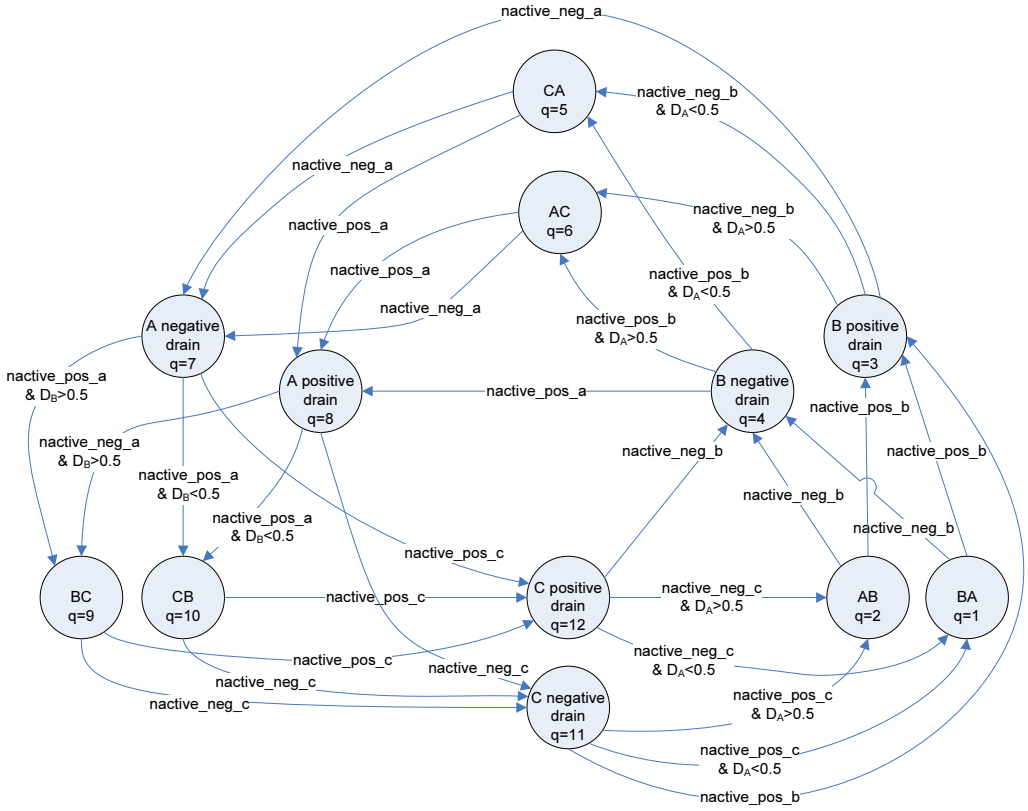

FIGURE 7.2: *New hybrid automaton for the single sensor observer.*

The hybrid automaton on Figure 7.2 is composed of 12 discrete states. The reduction of the number of sensors used to estimate the angle and the speed consists in adding more discrete states. This new hybrid automaton will be used as location automaton for the single sensor observer. In the next section, the new equations for the hybrid observer are derived.

7.3 SINGLE SENSOR OBSERVER EQUATIONS

The equations for the single sensor observer are very similar to the equations of the two sensors observer described in Section 4.4 on page 41. The differences are that there is no feedback in ABC case, and that the measurement of i_{cc} is used instead of the measurements of i_{as} and i_{bs}.

It is recalled from Chapter 4 that $\Delta\mathbf{i} = \begin{bmatrix} \hat{i}_{as} - i_{as} \\ \hat{i}_{bs} - i_{bs} \end{bmatrix}$. As the measurements of i_{as} and i_{bs} are not available, there is: $\Delta\mathbf{i} = \begin{bmatrix} \hat{i}_{as} - {}^{q}f_1(i_{cc}) \\ \hat{i}_{bs} - {}^{q}f_2(i_{cc}) \end{bmatrix}$, where ${}^{q}f_1(i_{cc})$ and ${}^{q}f_2(i_{cc})$ are the expressions of i_{as} and i_{bs} as functions of i_{cc}, depending on the discrete state. ${}^{q}f_1(i_{cc})$ and ${}^{q}f_2(i_{cc})$ are defined by Equations 7.2, 7.3, and 7.4 on page 75. The new observer's equations are as follows:

- **Drain cases**

  When all the phases conduct current, i.e. $q \in \{3, 4, 7, 8, 11, 12\}$ the observer equations are run in open-loop, i.e. without feedback correction:

$$\dot{\hat{\mathbf{x}}}_q = \begin{bmatrix} -\frac{r_s}{L_s}\mathbf{I}^{2\times 2} & -\frac{\lambda'_m}{L_s}\mathbf{M''} \\ \mathbf{0} & \mathcal{J}\omega_e \end{bmatrix} \hat{\mathbf{x}}_q + \begin{bmatrix} \frac{1}{L_s}\mathbf{M'} \\ \mathbf{0} \end{bmatrix} \mathbf{V}_{abcs} \tag{7.5}$$

  where

$$\mathbf{M'} = \begin{bmatrix} \frac{2}{3} & -\frac{1}{3} & -\frac{1}{3} \\ -\frac{1}{3} & \frac{2}{3} & -\frac{1}{3} \end{bmatrix}, \mathbf{M''} = \begin{bmatrix} 1 & 0 \\ -\frac{1}{2} & \frac{\sqrt{3}}{2} \end{bmatrix}, \mathcal{J} = \begin{bmatrix} 0 & -1 \\ 1 & 0 \end{bmatrix}.$$

- **BA case**

  This is the case when phase C is passive and phase B receives D_{in}, i.e. $q = 1$. In that case, $i_{as} = -\frac{i_{cc}}{Din}$ and $i_{bs} = \frac{i_{cc}}{Din}$, replacing the value of the measurements in $\Delta\mathbf{i}$, leads to the new observer's equation:

$$\dot{\hat{\mathbf{x}}}_1 = \begin{bmatrix} -\frac{r_s}{L_s}\mathbf{I}^{2\times 2} & -\frac{\lambda'_m}{L_s}{}^{1}\mathbf{M''} \\ \mathbf{0} & \mathcal{J}\omega_e \end{bmatrix} \hat{\mathbf{x}}_1 + \begin{bmatrix} \frac{1}{L_s}{}^{1}\mathbf{M'} \\ \mathbf{0} \end{bmatrix} \mathbf{V}_{abcs} + {}^{1}\mathbf{K} \begin{bmatrix} \hat{i}_{as} + \frac{i_{cc}}{Din} \\ \hat{i}_{bs} - \frac{i_{cc}}{Din} \end{bmatrix} \tag{7.6}$$

  where

$$ {}^1\mathbf{M}' = \begin{bmatrix} \frac{1}{2} & -\frac{1}{2} & 0 \\ -\frac{1}{2} & \frac{1}{2} & 0 \end{bmatrix}, {}^1\mathbf{M}'' = \begin{bmatrix} \frac{3}{4} & -\frac{\sqrt{3}}{4} \\ -\frac{3}{4} & \frac{\sqrt{3}}{4} \end{bmatrix}, {}^1\mathbf{K} = \begin{bmatrix} k_6 & 0 \\ 0 & k_7 \\ k_8 & 0 \\ k_9 & 0 \end{bmatrix}. $$

- **AB case**

  This is the case when phase C is passive and phase A receives D_{in}, i.e. $q = 2$. In that case, $i_{as} = \frac{i_{cc}}{Din}$ and $i_{bs} = -\frac{i_{cc}}{Din}$, replacing the value of the measurements in $\Delta\mathbf{i}$, leads to the new observer's equation:

$$ \dot{\hat{\mathbf{x}}}_1 = \begin{bmatrix} -\frac{r_s}{L_s}\mathbf{I}^{2\times 2} & -\frac{\lambda'_m}{L_s}{}^1\mathbf{M}'' \\ \mathbf{0} & \mathcal{J}\omega_e \end{bmatrix} \hat{\mathbf{x}}_1 + \begin{bmatrix} \frac{1}{L_s}{}^1\mathbf{M}' \\ \mathbf{0} \end{bmatrix} \mathbf{V}_{abcs} + {}^1\mathbf{K} \begin{bmatrix} \hat{i}_{as} - \frac{i_{cc}}{Din} \\ \hat{i}_{bs} + \frac{i_{cc}}{Din} \end{bmatrix} \quad (7.7) $$

  where

$$ {}^1\mathbf{M}' = \begin{bmatrix} \frac{1}{2} & -\frac{1}{2} & 0 \\ -\frac{1}{2} & \frac{1}{2} & 0 \end{bmatrix}, {}^1\mathbf{M}'' = \begin{bmatrix} \frac{3}{4} & -\frac{\sqrt{3}}{4} \\ -\frac{3}{4} & \frac{\sqrt{3}}{4} \end{bmatrix}, {}^1\mathbf{K} = \begin{bmatrix} k_6 & 0 \\ 0 & k_7 \\ k_8 & 0 \\ k_9 & 0 \end{bmatrix}. $$

- **CA case**

  When phase B is passive and phase C receives D_{in}, i.e. $q = 5$, $i_{as} = -\frac{i_{cc}}{Din}$ and $i_{bs} = 0$. Since the current i_{bs} is zero, it is not used in the feedback correction. The observer's equation is as follows:

$$ \dot{\hat{\mathbf{x}}}_4 = \begin{bmatrix} \begin{bmatrix} -\frac{r_s}{L_s} & 0 \\ 0 & 0 \end{bmatrix} & -\frac{\lambda'_m}{L_s}{}^4\mathbf{M}'' \\ \mathbf{0} & \mathcal{J}\omega_e \end{bmatrix} \hat{\mathbf{x}}_4 + \begin{bmatrix} \frac{1}{L_s}{}^4\mathbf{M}' \\ \mathbf{0} \end{bmatrix} \mathbf{V}_{abcs} + {}^4\mathbf{K} \begin{bmatrix} \hat{i}_{as} + \frac{i_{cc}}{Din} \\ 0 \end{bmatrix} \quad (7.8) $$

  where

$$ {}^4\mathbf{M}' = \begin{bmatrix} \frac{1}{2} & 0 & -\frac{1}{2} \\ 0 & 0 & 0 \end{bmatrix}, {}^4\mathbf{M}'' = \begin{bmatrix} \frac{3}{4} & \frac{\sqrt{3}}{4} \\ 0 & 0 \end{bmatrix}, {}^4\mathbf{K} = \begin{bmatrix} k_{10} & 0 \\ 0 & 0 \\ k_{11} & 0 \\ k_{12} & 0 \end{bmatrix}. $$

- **AC case**

Phase B is passive and phase A receives D_{in}, i.e. $q = 6$. In that case $i_{as} = \frac{i_{cc}}{Din}$ and $i_{bs} = 0$. The observer's equation is as follows:

$$\dot{\hat{\mathbf{x}}}_4 = \begin{bmatrix} \begin{bmatrix} -\frac{r_s}{L_s} & 0 \\ 0 & 0 \end{bmatrix} & -\frac{\lambda'_m}{L_s}{}^4\mathbf{M}'' \\ \mathbf{0} & \mathcal{J}\omega_e \end{bmatrix} \hat{\mathbf{x}}_4 + \begin{bmatrix} \frac{1}{L_s}{}^4\mathbf{M}' \\ \mathbf{0} \end{bmatrix} \mathbf{V}_{abcs} + {}^4\mathbf{K} \begin{bmatrix} \hat{i}_{as} - \frac{i_{cc}}{Din} \\ 0 \end{bmatrix} \quad (7.9)$$

where

$${}^4\mathbf{M}' = \begin{bmatrix} \frac{1}{2} & 0 & -\frac{1}{2} \\ 0 & 0 & 0 \end{bmatrix}, {}^4\mathbf{M}'' = \begin{bmatrix} \frac{3}{4} & \frac{\sqrt{3}}{4} \\ 0 & 0 \end{bmatrix}, {}^4\mathbf{K} = \begin{bmatrix} k_{10} & 0 \\ 0 & 0 \\ k_{11} & 0 \\ k_{12} & 0 \end{bmatrix}.$$

- **BC case**

In that case, phase A is passive and phase B receives D_{in}, i.e. $q = 9$. $i_{as} = 0$, therefore there is no correction on its basis, and $i_{bs} = \frac{i_{cc}}{Din}$. The observer's equation is as follows:

$$\dot{\hat{\mathbf{x}}}_7 = \begin{bmatrix} \begin{bmatrix} 0 & 0 \\ 0 & -\frac{r_s}{L_s} \end{bmatrix} & -\frac{\lambda'_m}{L_s}{}^7\mathbf{M}'' \\ \mathbf{0} & \mathcal{J}\omega_e \end{bmatrix} \hat{\mathbf{x}}_7 + \begin{bmatrix} \frac{1}{L_s}{}^7\mathbf{M}' \\ \mathbf{0} \end{bmatrix} \mathbf{V}_{abcs} + {}^7\mathbf{K} \begin{bmatrix} 0 \\ \hat{i}_{bs} - \frac{i_{cc}}{Din} \end{bmatrix} \quad (7.10)$$

where

$${}^7\mathbf{M}' = \begin{bmatrix} 0 & 0 & 0 \\ 0 & \frac{1}{2} & -\frac{1}{2} \end{bmatrix}, {}^7\mathbf{M}'' = \begin{bmatrix} 0 & 0 \\ 0 & \frac{\sqrt{3}}{2} \end{bmatrix}, {}^7\mathbf{K} = \begin{bmatrix} 0 & 0 \\ 0 & k_{13} \\ 0 & 0 \\ 0 & k_{14} \end{bmatrix}.$$

- **CB case**

In that case, phase A is passive and phase C receives D_{in}, i.e. $q = 10$. $i_{as} = 0$ and $i_{bs} = -\frac{i_{cc}}{Din}$. The observer's equation is as follows:

$$\dot{\hat{\mathbf{x}}}_7 = \begin{bmatrix} \begin{bmatrix} 0 & 0 \\ 0 & -\frac{r_s}{L_s} \end{bmatrix} & -\frac{\lambda'_m}{L_s}{}^7\mathbf{M}'' \\ \mathbf{0} & \mathcal{J}\omega_e \end{bmatrix} \hat{\mathbf{x}}_7 + \begin{bmatrix} \frac{1}{L_s}{}^7\mathbf{M}' \\ \mathbf{0} \end{bmatrix} \mathbf{V}_{abcs} + {}^7\mathbf{K} \begin{bmatrix} 0 \\ \hat{i}_{bs} + \frac{i_{cc}}{Din} \end{bmatrix} \quad (7.11)$$

where

$${}^7\mathbf{M}' = \begin{bmatrix} 0 & 0 & 0 \\ 0 & \frac{1}{2} & -\frac{1}{2} \end{bmatrix}, {}^7\mathbf{M}'' = \begin{bmatrix} 0 & 0 \\ 0 & \frac{\sqrt{3}}{2} \end{bmatrix}, {}^7\mathbf{K} = \begin{bmatrix} 0 & 0 \\ 0 & k_{13} \\ 0 & 0 \\ 0 & k_{14} \end{bmatrix}.$$

Having the location automaton and the continuous time equations, the single sensor observer will be tested against real measurements in the next section.

7.4 TEST OF THE SINGLE SENSOR OBSERVER

The single sensor observer is implemented in Simulink®, as it was done for the previous observer. In order to test this new observer, it is needed to take new measurements on the real BLDCM as the value of i_{cc} is needed instead of i_{as} and i_{bs}. As the structure of the single sensor observer is different from the structure of the double sensor observer, the feedback gains are re-optimized using the feedback parameters of the double sensor observer as a starting point. The optimization problem is in $\mathbb{R}^9$ while it was in $\mathbb{R}^{14}$ for the optimization of the feedback parameters of the double sensor observer. This is due to the fact that the five feedback coefficients for the drain states are not used in the single sensor observer. Three additional dimensions are introduced without increasing the complexity of the problem compared to the optimization of the double sensor observer, the problem is now in $\mathbb{R}^{12}$. Those three new dimensions correspond to the electrical parameters of the model (r_s, L_s, λ'_m), which means that they are also optimized. The advantage is that the electrical parameters will be optimized instead of being estimated, which should provide better results.

The test setup used for the test of the single sensor observer is the same as the test of the regular observer in Chapter 6 on page 65, i.e. an acceleration and then a deceleration of the motor through the whole range of speed considered in this project. Figure 7.3 on the next page represents the estimation error in the angle during the test, and Figure 7.4

on the facing page is the comparison of the real and estimated speed together with the estimation error in the speed.

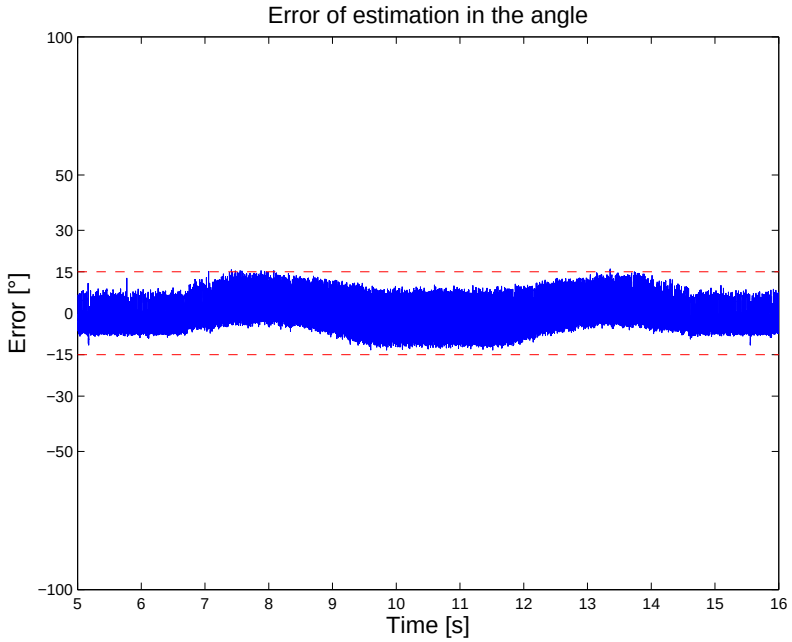

FIGURE 7.3: *Error of estimation in the rotor angle when only one current sensor is used.*

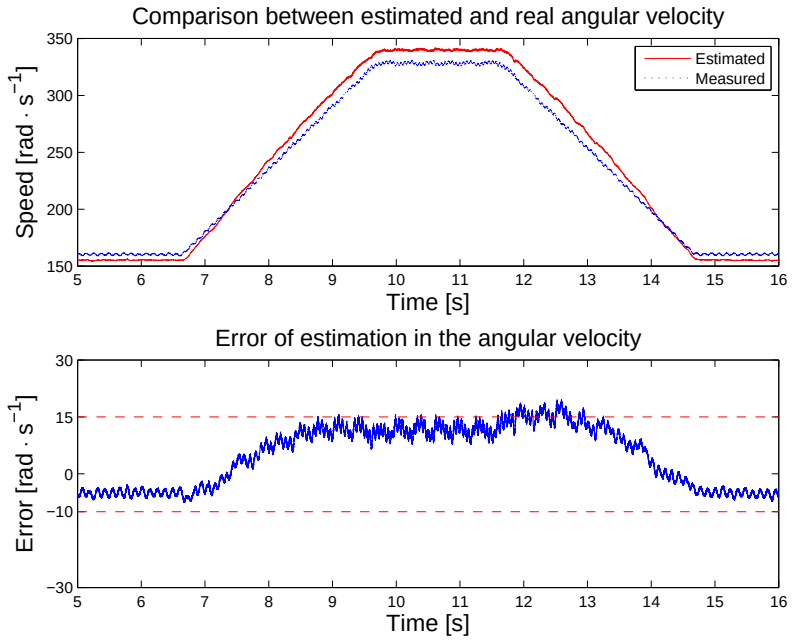

FIGURE 7.4: *Real and estimated angular velocity when only one current sensor is used.*

As shown on Figure 7.3 on the previous page, the precision of the angle estimation has decreased compared to the double sensor observer; it is within $\pm 15^\circ$ for the single sensor observer. The precision of the estimated angular velocity is $\pm 15\,[\mathrm{rad} \cdot \mathrm{s}^{-1}]$, which is also worse than the double sensor observer. This was to be expected, as the observer has less information to estimate the angle and the speed. Another reason for the loss in precision of the estimates is the poor quality of the measurement of i_{cc}. Figure 7.5 depicts the measurement of i_{cc}. It can be noticed that the resolution of the measurement is $50\,[\mathrm{mA}]$ and that there is an important quantification noise.

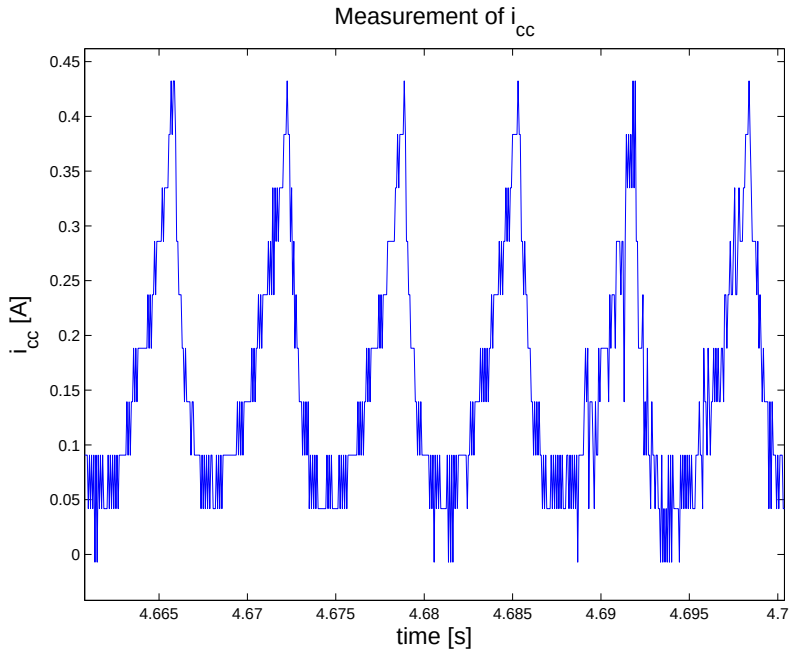

FIGURE 7.5: *Measurement of i_{cc}. It is noticed that there is an important quantification noise and a low resolution of the measurement.*

7.5 CONCLUSION

An observer using only one current measurement to estimate the rotor angle and speed was designed throughout this chapter. New hybrid automaton and the new continuous time equations for the observer were derived. The parameters of the observer were then optimized. The observer was tested against real measurements, and has shown satisfactory performance despite the low resolution of the current sensor used. Having both observers working with real measurements, they can be tested in closed-loop conditions.

CLOSED LOOP IMPLEMENTATION

8

In this chapter, the observers are tested under closed loop conditions and their usability is asserted. Those tests determine the possible applications of the observers, for instance control of a BLDCM, or fault detection applications.

Before the observers are tested in closed loop, they are reworked so that they can estimate online. The reduction of the computational complexity of the observers is described in Appendix B on page 105.

8.1 SIMULATIONS OF CLOSED LOOP PERFORMANCE

Before testing the observers on the real BLDCM, it is verified that they are able to work in closed loop in simulations. Those simulations should reveal whether the observers behave stable in closed loop and if there is a chance to use them on a real motor.

The simulations are conducted as shown in Figure 8.1. Since the observers cannot run from the initial point, where the angular velocity is zero, there must be an initialization procedure. In the case of simulations, the motor model is used as it would have feedback from a position encoder. After $0.5\,[\mathrm{s}]$ the feedback is switched and from that moment, the estimated angle is used to control the motor.

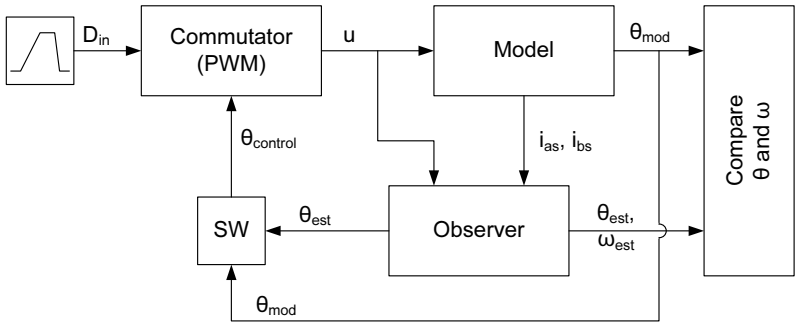

FIGURE 8.1: *Block diagram of simulation procedure to verify the closed loop performance. Switch SW is activated after* $0.5\,[\mathrm{s}]$ *to feed the estimated angle to the commutator instead of the modelled angle.*

In the simulations, the same test signal as in the verification of the observer is used, i.e. an acceleration to the maximum speed ($1000\,[\mathrm{rpm}]$), and a deceleration to the minimum speed ($500\,[\mathrm{rpm}]$). Since the scenario tests the whole range of speeds, it verifies in which regions of speed the observers can work in closed loop.

8.1.1 OBSERVER WITH PHASE CURRENTS MEASUREMENTS

As described earlier, this observer uses the knowledge of two phase currents while estimating angle and speed of the rotor. Figure 8.2 depicts the results of the simulation of the observer observing the model of the BLDCM in closed loop conditions.

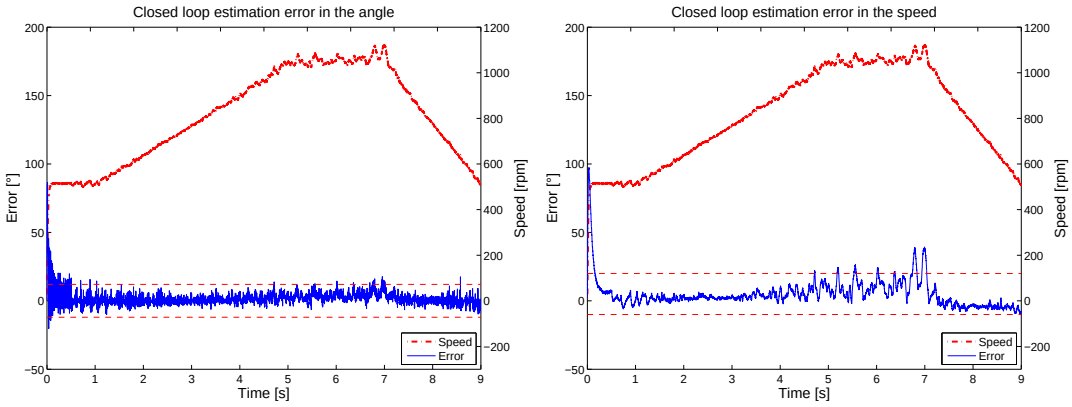

FIGURE 8.2: *Error in the angle estimation while using the observer in closed loop.*

This test shows that the observer can be used to control the model of the BLDCM on the whole region of speed considered, i.e. $\omega_r \in [500; 1000]\,[\mathrm{rpm}]$. This means that in theory the observer should be able to control the BLDCM. However, this is the idealized case as there is no noise and no difference between the parameters of the model and those of the observer. The parameters of the model are therefore changed to introduce some difference between the model and the observer. Similar differences occur between the observer and the real BLDCM. The model parameters that were changed are shown in Table 8.1.

Parameter	Original value	Changed value
r_s	$3.8\,[\Omega]$	$3.9\,[\Omega]$
L_s	$0.0135\,[\mathrm{H}]$	$0.0133\,[\mathrm{H}]$
λ'_m	$0.2225\,[\mathrm{V}\cdot\mathrm{s/rad}]$	$0.22\,[\mathrm{V}\cdot\mathrm{s/rad}]$

TABLE 8.1: *Alternated parameters of the model that were used for simulating closed loop performance of the observer.*

Figure 8.3 on the next page represents the performance of the observer while observing the model with changed parameters in open loop. After the parameter changes made to the model, it is noticed that the observer is less precise than it was when using measurements from the real BLDCM.

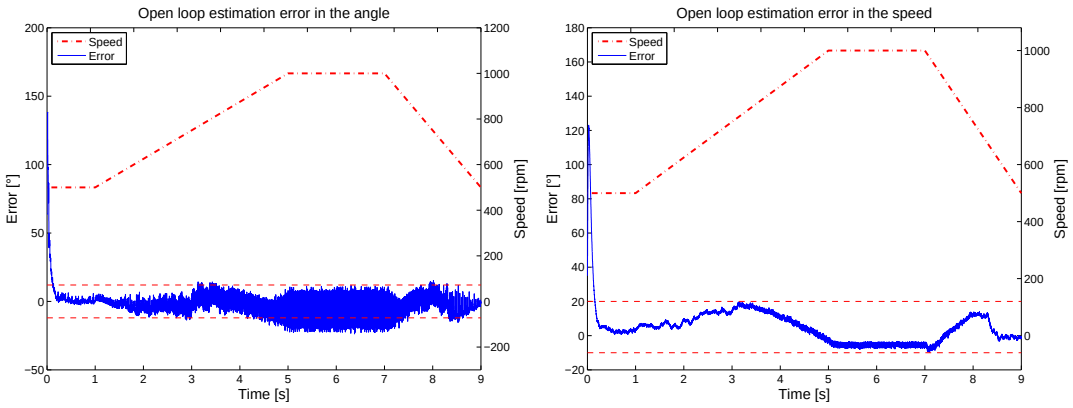

FIGURE 8.3: *Error in the angle and speed estimation while using the observer on the model of the BLDCM with changed parameters in open loop.*

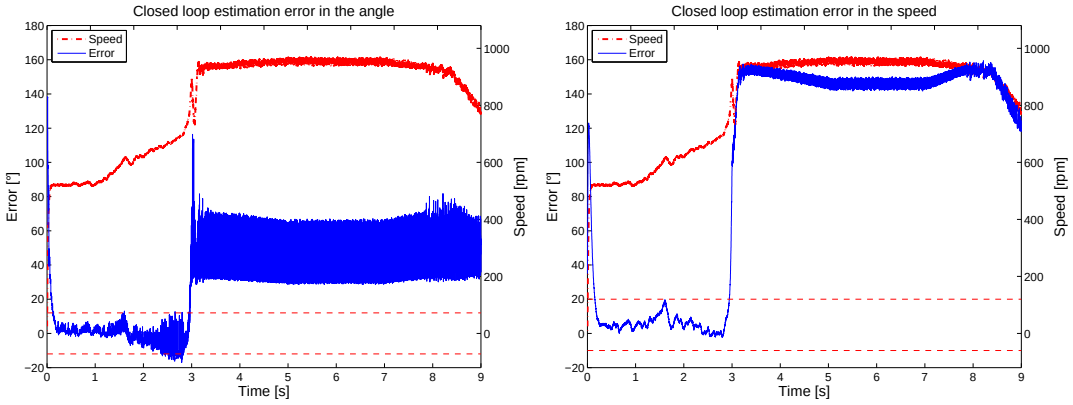

FIGURE 8.4: *Error in the angle estimation while using the observer in closed loop when parameters of the model are changed. The observer estimates well around* $500\,[\mathrm{rpm}]$*, however the results are poor when the speed is too high.*

The simulation in closed loop is run, and the results of this simulation are depicted on Figure 8.4. As it can be seen, the observer in closed loop works properly from $0.5\,[\mathrm{s}]$ to approximately $2\,[\mathrm{s}]$, i.e. when the angular velocity is in the range of $[500; 600]\,[\mathrm{rpm}]$. When the speed is higher than $600\,[\mathrm{rpm}]$, the observer provides wrong switching angle, which creates very high currents ($i_{as}, i_{bs} > 20\,[\mathrm{A}]$) in the phases.

This closed loop simulation showed that there is a possibility for the observer to control the motor with angular velocities around $500\,[\mathrm{rpm}]$. If the angular velocity diverges to far from $500\,[\mathrm{rpm}]$, the observer loses track of the angle. This is because the feedback coefficients were optimized for this angular velocity, and therefore the observer works well around this speed. This test shows that proportional correction might not be the

best way to handle large changes in the angular velocity when operating in closed loop. The range of speed where the observer works properly ($[500; 600]$ [rpm]) is reduced compared to the range of speed that was considered in this project ($[500; 1000]$ [rpm]).

Better results are expected during the closed loop test with the real motor since the introduced parameter perturbations are likely to be to large. Particularly, the range of speed where the observer can run in closed loop should be larger, and the precision of the angle estimate should increase.

8.1.2 SINGLE SENSOR OBSERVER

This observer uses only one current sensor (i_{cc} current) to estimate the angle and the speed of the rotor. The particularity of this observer is that there is no feedback correction in the three phase cases (drain states). For the purpose of the simulation, the current i_{cc} is computed on basis of the two phase currents i_{as} and i_{bs} that are the outputs of the model. This value is then fed to the single sensor observer, and its behaviour under closed loop conditions is tested in the same way as for the classical observer.

The results of the simulations of the single sensor observer is that it is not able to estimate correctly the angle of the rotor in closed loop conditions. However, the observer was not tuned to work with the model but with the real motor, therefore better results might be obtained during the closed loop test with the real BLDCM.

8.2 OBSERVER TESTS ON THE REAL SYSTEM

The simulations of the observers in closed loop have shown that the two sensors observer could be used to provide the information of the angle to replace the encoder for the control of the real BLDCM. The single sensor observer, however, has not shown good performance in closed loop operation in simulations. The double sensor observer will be tested first. Having shown that the double sensor observer works in closed loop, the single sensor observer will be tested to verify the results obtained during closed loop simulations. The test setup for the closed loop tests with the real motor is shown on Figure 8.5 on the next page. It is the same setup as for the simulations only the model is replaced with the real motor and the outputs are measured with sensors.

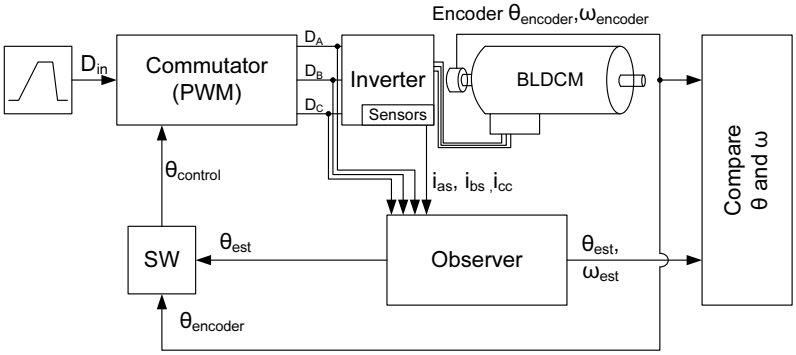

FIGURE 8.5: *Test setup for the closed loop performance with the real BLDCM. SW chooses which angle is fed to the commutator, it is controlled manually during the test.*

8.2.1 TEST OF THE OBSERVER USING TWO CURRENT MEASUREMENTS

First it needs to be verified that the observer works properly in closed loop with constant speed of $500\,[\mathrm{rpm}]$, which is the speed where the optimization was made, and therefore where it is most probable to work. Then, the observer will be tested with smooth changes in the speed. This will allow to determine whether it can work properly when the angular velocity varies, and in which range of speed.

Figure 8.6 on the following page, Figure 8.7 on the next page, and Figure 8.8 on page 89 depict the results of the closed-loop test with constant angular velocity. The observer works properly at $500\,[\mathrm{rpm}]$, the error in the angle estimate is within $\pm 15^\circ$, and the error in the speed estimate is approximately constant. Figure 8.6 on the next page shows that there is a correlation between the estimate error in the angle and the fact that the observer is used for the control. When it is used there is a slight decrease of the precision. It is shown on Figure 8.8 on page 89 that there is also a link between the amplitude of the currents and the fact that the observer is used for the control. The amplitude of the currents increase when operating with the observer. This is because the switching angle is not precisely 90° but $90 \pm 15^\circ$, which changes the amplitude of the currents. As it can be noticed on Figure 8.7 on the next page, the consequence of this change in the amplitude of the currents is that there are irregular ripples in the angular velocity of the BLDCM.

Having verified that the observer works in real conditions with constant angular velocity, it can now be tested with smooth changes in speed. The test scenario is, from $500\,[\mathrm{rpm}]$ an acceleration to a higher speed, then a steady state at this speed, and finally a deceleration to $500\,[\mathrm{rpm}]$. Several tests will be run with different values for the maximum

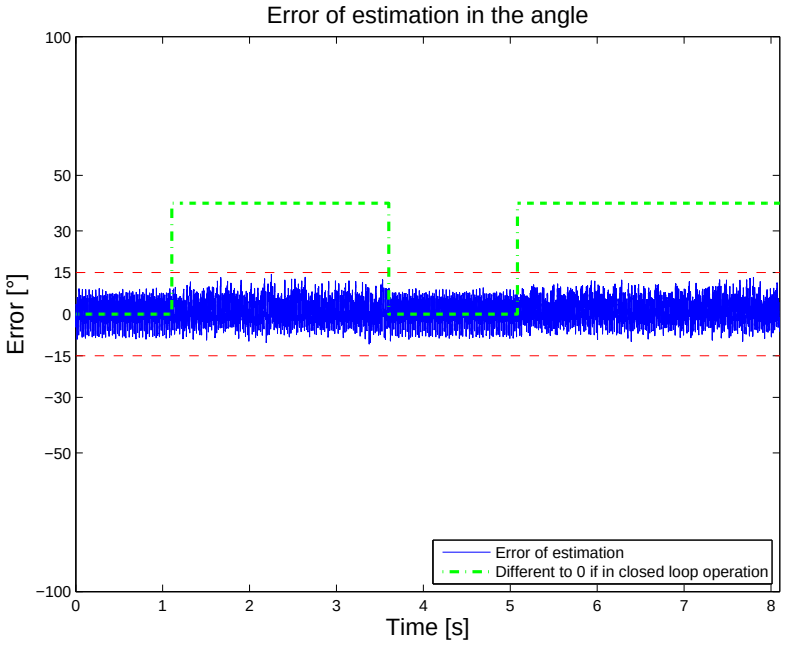

FIGURE 8.6: *Angle estimation during the closed loop test with constant angular velocity.*

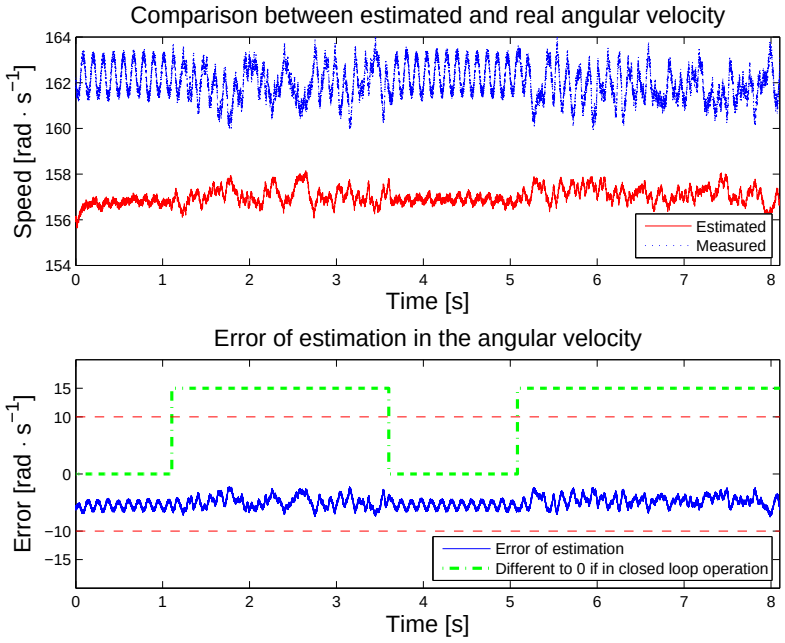

FIGURE 8.7: *Error of estimation in the angular velocity during the closed loop test with constant angular velocity.*

value of the angular velocity. This maximum angular velocity will be increased step by step until the control with the observer will not be satisfactory. Figure 8.9 on page 90 and

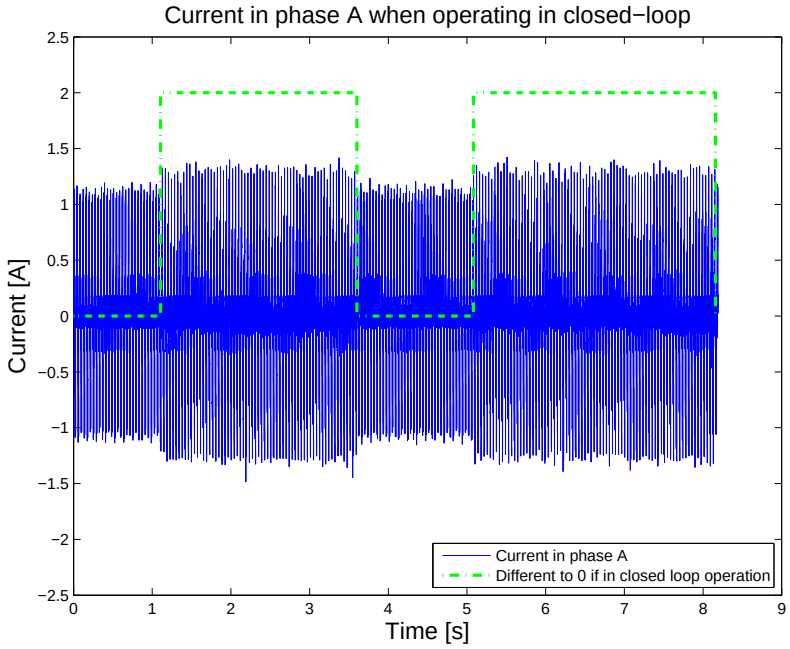

FIGURE 8.8: *Current in phase A during the closed loop test with constant angular velocity.*

Figure 8.10 on the next page are the results of the closed loop test where the maximum value for the angular velocity is $640\,[\mathrm{rpm}]$. Figure 8.11 on page 91 and Figure 8.12 on page 91 are the results for the test where the maximum angular velocity is $875\,[\mathrm{rpm}]$, i.e. the highest value tested. The results of the tests with different values of the maximum speed can be found in Appendix C on page 113.

An analysis of the results presented on Figure 8.9 on the next page and Figure 8.10 on the following page allows to verify that the observer is working properly. As it was expected from the simulations, the observer is able to handle changes in the angular velocity while operating in closed loop in the region of speed around $500\,[\mathrm{rpm}]$. The estimates remain relatively precise, $\pm 15°$ for the angle and $\pm 10\,[\mathrm{rad}\cdot\mathrm{s}^{-1}]$ for the speed. The same general comments as for the previous test with the constant angular velocity can be made, when using the observer in the control loop the precision of the estimates decreases, and the amplitude of the currents changes creating speed ripples.

Results presented in Figures 8.11 on page 91 and 8.12 on page 91 show that the error in the estimates increase together with the speed. For angular velocities above $750\,[\mathrm{rpm}]$, the accuracy of the angle estimation is worse than $\pm 15°$. For those speeds, the observer can still be used to provide the angle to the commutator, but it provides a poor control, large peaks of currents can be observed as well as significant speed ripples. Speed above

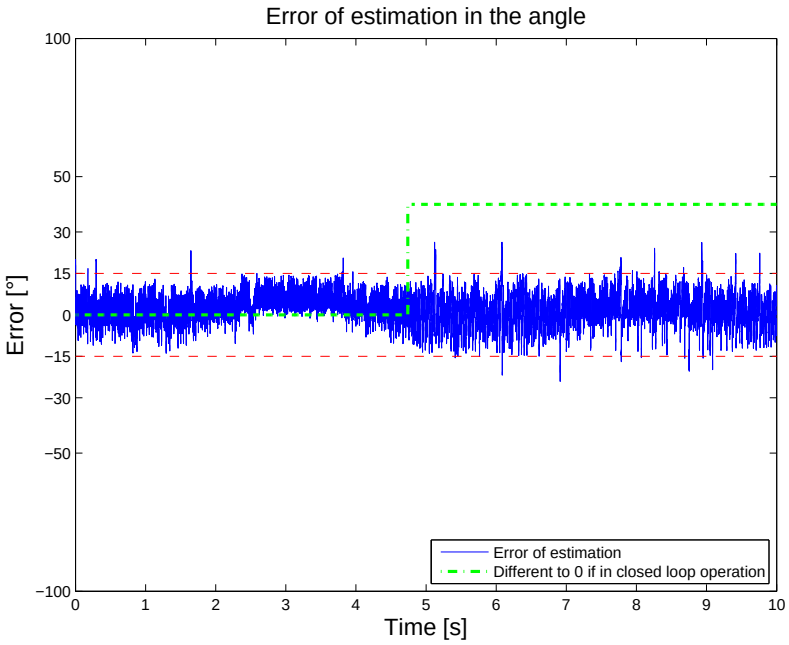

FIGURE 8.9: *Angle estimation during the closed loop test of the double sensor observer with smooth changes in angular velocity.*

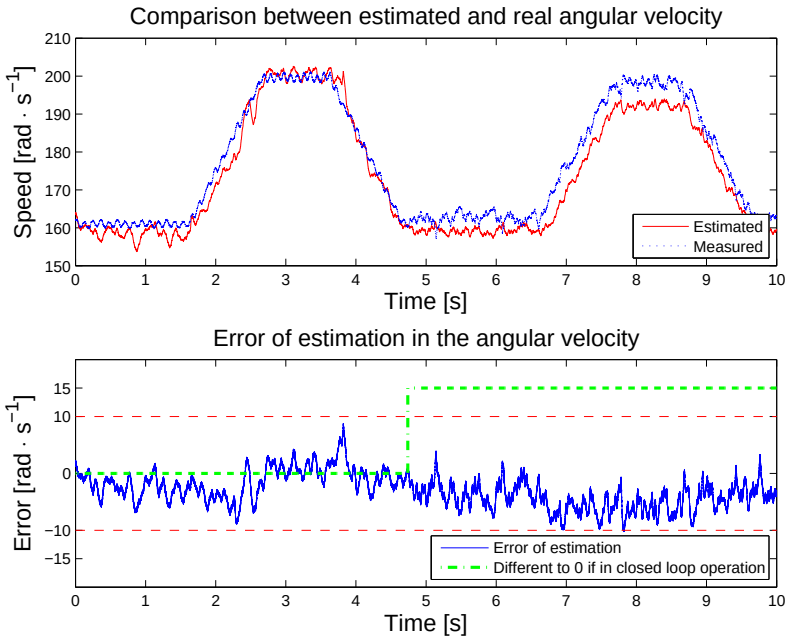

FIGURE 8.10: *Speed estimation during the closed loop test of the double sensor observer with smooth changes in angular velocity.*

875 [rpm] have not been tested as they would create currents that the hardware could not handle. The performance of the observer is considered satisfactory for speeds in range of

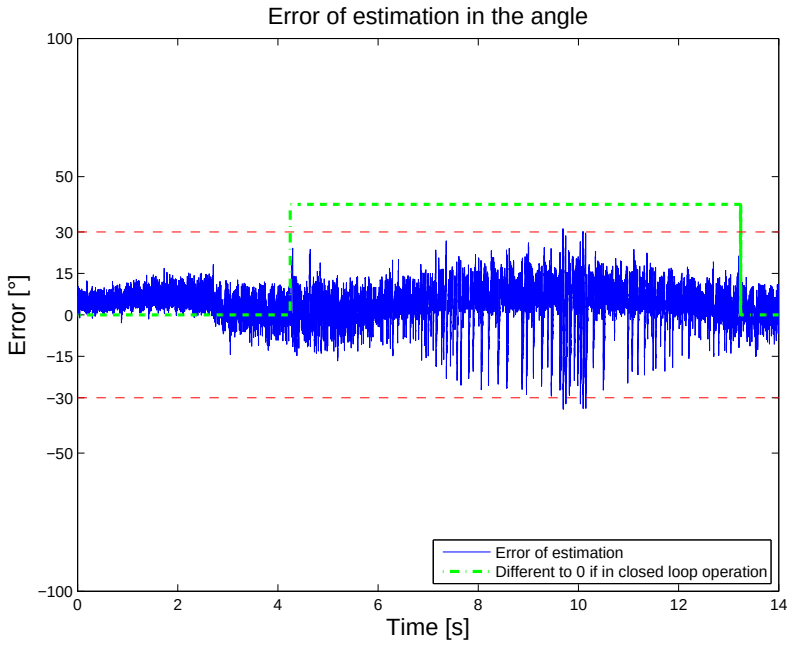

FIGURE 8.11: *Error of estimation in the angle with maximum speed* $\omega_e = 275\,[\mathrm{rad}\cdot\mathrm{s}^{-1}]$ *(*$\omega_r = 875\,[\mathrm{rpm}]$*).*

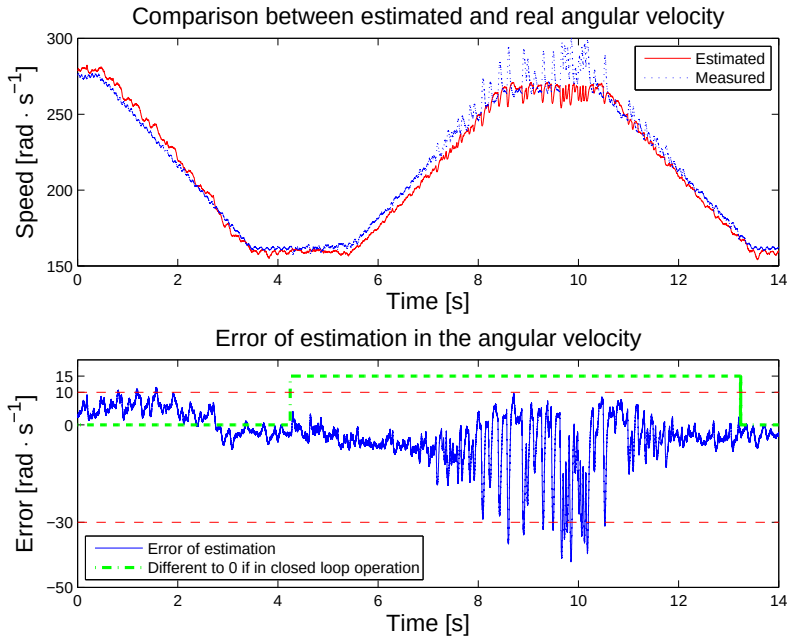

FIGURE 8.12: *Speed estimation with maximum speed* $\omega_e = 275\,[\mathrm{rad}\cdot\mathrm{s}^{-1}]$ *(*$\omega_r = 875\,[\mathrm{rpm}]$*).*

$[500; 750]\,[\mathrm{rpm}]$.

The observer is working properly on half the range of speed that was considered orig-

inally ($[500; 1000]\,[\mathrm{rpm}]$). However it works on a bigger range than in simulation since it was tuned to work with the real motor. Those are encouraging results for testing the single sensor observer in real conditions, which will be done in the next subsection.

8.2.2 TEST OF THE SINGLE SENSOR OBSERVER

The single sensor observer is tested in closed loop with constant angular velocity, $\omega_e = 160\,[\mathrm{rad} \cdot \mathrm{s}^{-1}]$, and the results of this test are shown on Figure 8.13 and Figure 8.14 on the facing page.

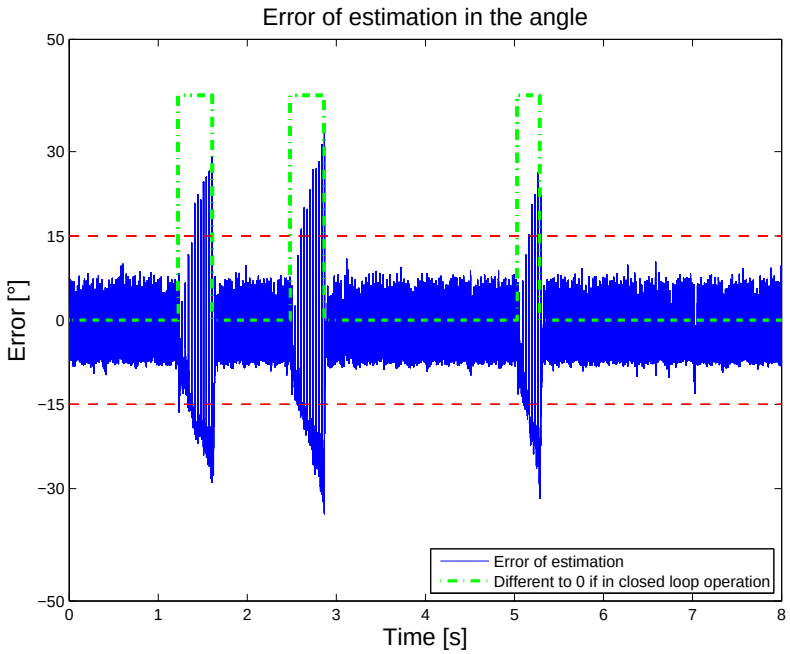

FIGURE 8.13: *Error of estimation in the angle during the closed loop test of the single sensor observer with constant angular velocity.*

The error of estimation in the angle on Figure 8.13 is rapidly increasing when the single sensor observer is operating in closed loop, and it is noticed on Figure 8.14 on the facing page that it also creates an increase in the angular velocity of the BLDCM. Those results show that the single sensor observer is not able to operate in closed loop, as it was expected from the simulations. This means that reducing the number of sensors removes crucial information for the estimation in closed loop, the feedback correction during drain states seems to be essential for a correct behaviour of the observer in closed loop.

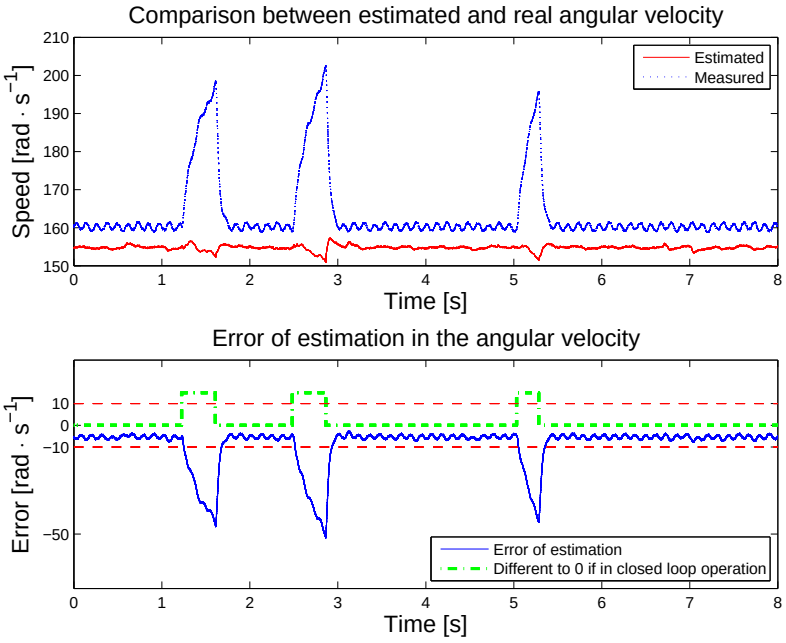

FIGURE 8.14: *Speed estimation during the closed loop test of the single sensor observer with constant angular velocity.*

8.3 CONCLUSION

This chapter has allowed to check the functionality of both observers under closed loop conditions. It has allowed to verify if the control of the BLDCM could be done with a hybrid observer. It has been shown that the double sensor can be used for controlling the motor in a reduced range of speed, $[500; 750]\,[\mathrm{rpm}]$. The single sensor observer has shown poor performance under closed loop conditions, as it is not possible to use it for controlling the motor. However, this observer could be used in other types of applications, for instance fault detection purposes, as it has correct precision in open loop, and only requires one current measurement. Even though the results obtained are only partly successful, they opened a wide range of possible applications for using hybrid observers in the control of the BLDCM.

This page is left intentionally blank

CONCLUSION 9

This chapter concludes the work done during the project. It presents the achievements and compares them with the project requirements stated in the introduction. The most important results and possible applications of the developed observer are gathered and discussed. Future work possibilities are presented.

9.1 SUMMARY

This project was a continuation of previously conducted work on modelling and state estimation for brushless DC motors using hybrid theory ([HB05], [Han06] and [NP06]). It mostly relies on the development of a novel hybrid model and observer presented in [NP06], where it was shown that there is a possibility of constructing a hybrid adaptive observer that would estimate the rotor angle and speed based on two current measurements. The goal stated in this project was to further improve the observer and verify its usability in a real application. Such an observer could be potentially used in a various of applications replacing some of the already known BLDCM control techniques.

It was shown in [NP06], that the observer tracks the rotor angle and speed very well, but at that point it was not possible to verify it on a real system. The observer needed to be optimized in a variety of ways.

Since it was very difficult to find the observer's feedback coefficients, it was needed to improve the optimization technique used for this purpose. Various techniques were compared and it was found that the optimization should be done in two stages. First stage would determine the region where the feedback coefficients are sufficiently close to the optimal values. For this purpose the RWC algorithm was found to be very suitable. In the second stage, the DE algorithm would be employed to find correct values of the feedback gains. This algorithm benefits from gradient and evolutionary techniques and requires a very limited number of internal parameters. Those parameters are easy to find and they are not very crucial for the optimization.

The observer was very computational demanding the way it was implemented previously. Therefore, to ensure real time computation, it was necessary to lower the demands. This was done by simplifying the equations (removing zero multiplications), removing necessity of using Checkmate and Stateflow toolboxes. In the end, the computational demands were lowered significantly and it was possible to run the observer on the dSpace®

platform in real time.

An alternative version of the observer was also developed. In this observer the angular position and speed were estimated using only one current measurement (DC current). A novel hybrid automaton and novel equations were derived for this purpose.

The observers were tested against real measurements in open loop conditions and have shown satisfactory performance. The double sensor observer has a precision of $\pm 10^{\circ}$ in the angle and a precision of $\pm 12\,[\mathrm{rad}\cdot\mathrm{s}^{-1}]$ in the speed, while the single sensor observer has a precision of $\pm 15^{\circ}$ in the angle and a precision of $\pm 15\,[\mathrm{rad}\cdot\mathrm{s}^{-1}]$ in the speed.

Both of the observers were then verified on the real system in closed loop. This was preceded by series of simulations, that have shown that there is a possibility to use the double sensor observer in the closed loop on the real motor. The one sensor observer has shown poor performance in the simulations and real application. The double sensor observer works well in closed loop, however the operating region is smaller than it was expected. The functionality is sufficient between 500 and $750\,[\mathrm{rpm}]$ with a precision of $\pm 15^{\circ}$ and $\pm 10\,[\mathrm{rad}\cdot\mathrm{s}^{-1}]$.

Possible applications of the observers include fault detection, tolerant control and advanced control to remove the torque ripples. The observer may replace the encoder in case of a fault or can be used to determine whether the fault has occurred. Further improvements of the hybrid adaptive observers may allow the control based on the estimation instead of the back-EMF sensing.

9.2 METHODOLOGY

The method of developing the hybrid adaptive observer for a BLDCM presented in this report consists of the following procedures:

1. Determine the internal parameters of the motor.
2. Implement the observer equations and hybrid automaton.
3. Acquire measurements from the BLDCM (speed step response) – two phase currents, rotor's angle and inputs.
4. Use the measurements for the optimization of the feedback coefficients – find optimization region with RWC algorithm and tune the coefficients with DE algorithm.

5. Extend the performance of the observer on the operating region by one of the following methods:

   (a) Determine the proportional correction coefficients.

   (b) Repeat the optimization procedure for different rotation speeds in the operating region. Verify the dependencies between coefficients at various rotation speeds and interpolate them on the whole operating region. This methods requires more online and offline calculations.

9.3 ACHIEVEMENTS

The goal of the project, to verify the usability of the observer in the real application, was achieved. The determination of the feedback coefficients through optimization was analysed and improved. An observer that uses only one current sensor to estimate the angular position and velocity of the rotor was developed.

The observers were tested in closed loop where the position encoder was replaced by the estimate in order to determine the switching sequence of the transistors. Single sensor observer has shown poor performance in closed loop and therefore its application possibilities are limited compared to the double sensor observer. The double sensor observer can be used to control the BLDCM with a precision of $\pm 15^{\circ}$ in a reduced range of speed $\omega_r \in [500; 750]\,[\mathrm{rpm}]$. The quality of the control using the double sensor observer is slightly worse than when using the encoder (the amplitude of the currents increases and the speed has larger ripples). The potential applications of such observers in the control of a BLDCM are very broad.

9.4 FUTURE WORK

The estimation method using hybrid theory was verified and gave successfully results. It was shown that the observer is suitable to operate in closed loop. However, the operating region should be extended as it was smaller than the range of speed considered originally. The influence of the motor load should be verified. It is expected that the observer would perform better when the motor is running with a load. This is due to the fact that the currents would be larger and easier to observe.

An observer that assumes both rotating directions should be implemented, so that the

motor can be controlled with positive or negative angular velocities. Additional feedback correction could be used to verify if the accuracy of the observers can be improved by using integral feedback correction in addition to the proportional feedback. The parameters of the model could be considered as time-varying parameters and estimated online. This could improve the performance of the observers, as those parameters are dependent on the angular velocity.

Advanced control methods should be used together with the observer, for instance to reduce the torque ripples of the BLDCM. This study would allow to verify whether the observer provides sufficient precision for those techniques.

A startup procedure should be designed in case the encoder would be completely replaced by the observer. The motor could be running in an open loop and the loop would be closed when the observer has converged.

The observer could be tested under various conditions to verify whether it can be implemented in commercial applications. There are limited academic research tasks to be done in order to improve it. The future work would concentrate on implementing the observer for being used in real applications.

BIBLIOGRAPHY

[ALB06] Lars Almind, Karl Kaas Laursen, and Jan Dimon Bendtsen.
A Reusable Software Architecture for Small Satellite AOCS Systems.
Small Satellite Systems and Services Conference, Greece, 2006.

[BB03] Thomas Bartz-Beielstein.
Experimental Analysis of Evolution Strategies - Overview and Comprehensive Introduction.
Technical report, Universtität Dortmund, 2003.

[BS02] Hans-Georg Beyer and Hans-Paul Schwefel.
Evolution strategies. a comprehensive introduction.
Natural Computing, 1(1), 2002.

[Chi05] John Chiasson.
Modeling and High-Performance Control of Electric Machines.
John Wiley & Sons, Incorporated, 2005.

[EFS02] Sebastiaan Engell, Goran Frehse, and Eckehard Schnieder.
Modelling, Analysis, and Design of Hybrid Systems.
Springer-Verlag Berlin Heidelberg New York, 2002.

[Han06] Hans Brink Hansen.
Hybrid Adaptive Observer for a Brushless DC Motor.
Technical report, Institute of Electronic Systems - Aalborg University, 2006.

[HB05] Hans Brink Hansen and Simon Børresen.
Hybrid Model of a Brushless DC Motor.
Technical report, Institute of Electronic Systems - Aalborg University, 2005.

[HLL95] Uk-Youl Huh, Je-Hie Lee, and Tae-Gyoo Lee.
A torque control strategy of brushless dc motor with low resolution encoder.
Proceedings of 1995 International Conference on Power Electronics and Drive Systems, 1, 1995.

[KHB+98] Farrukh Kamran, Ronald G. Harley, Bruce Burton, Thomas G. Habetler, and Martin A. Brooke.
A fast on-line neural-network training algorithm for a rectifier regulator.
IEEE TRANSACTIONS ON POWER ELECTRONICS, 13, 1998.

[KWS95] Paul C. Krause, Oleg Wasynchuk, and Scott D. Sudhoff.
Analysis of Electric Machinery.
IEEE PRESS, 1995.

[NP06] Piotr Niemczyk and Thomas Porchez.
Nonlinear hybrid observer for a BLDCM.
Technical report, Institute of Electronic Systems - Aalborg University, 2006.

[PC05] Libor Prokop and Leos Chalupa.
3-Phase BLDC Motor Control with Sensorless Back EMF Zero Crossing Detection Using 56F80x.
Technical report, Freescale Semiconductor, 2005.

[Ped05] Gerulf K. M. Pedersen.
Towards Automatic Controller Design using Multi-Objective Evolutionary Algorithms.
PhD thesis, Department of Control Engineering - Aalborg University, 2005.

[SMY03] Ruhul Sarker, Masoud Mohammadian, and Xin Yao.
Evolutionary Optimization.
Kluwer Academic Publishers, 2003.

[SP95] Rainer Storn and Kenneth Price.
Differential Evolution - A simple and efficient adaptive scheme for global optimization over continuous spaces.
Technical Report TR-95-012, International Computer Science Institute - Berkley, march 1995.

[Urs05] Rasmus K. Ursem.
Differential Evolution Made Easy.
Technical Report 2005-01, Department of Computer Science - University of Aarhus, 2005.

[UV03] Rasmus K. Ursem and Pierré Vadstrup.
Parameter identification of induction motors using differential evolution.
Proceedings of the Fifth Congress on Evolutionary Computation, pages 790–796, 2003.

[UZ04] Konrad Urbański and Krzysztof Zawirski.

Adaptive observer of rotor speed and position for pmsm sensorless control system.
COMPEL: The International Journal for Computation and Mathematics in Electrical and Electronic Engineering, 23, 2004.

[WQ05] Fang Wang and Yuhui Qiu.
Multimodal function optimizing by a new hybrid nonlinear simplex search and particle swarm algorithm.
In *ECML*, pages 759–766, 2005.

This page is left intentionally blank

Simplified hybrid automaton for the single sensor observer

A

This appendix presents the simplified hybrid automaton for the single sensor observer in case there is a load on the BLDCM. This hybrid automaton is derived on basis of the hybrid automaton described in Figure 7.2 on page 76 assuming that the motor can not behave like a generator and therefore can not reverse the currents in the phases. In that case, some of the transitions can not be realized and the new hybrid automaton depicted in Figure A.1 can be used instead.

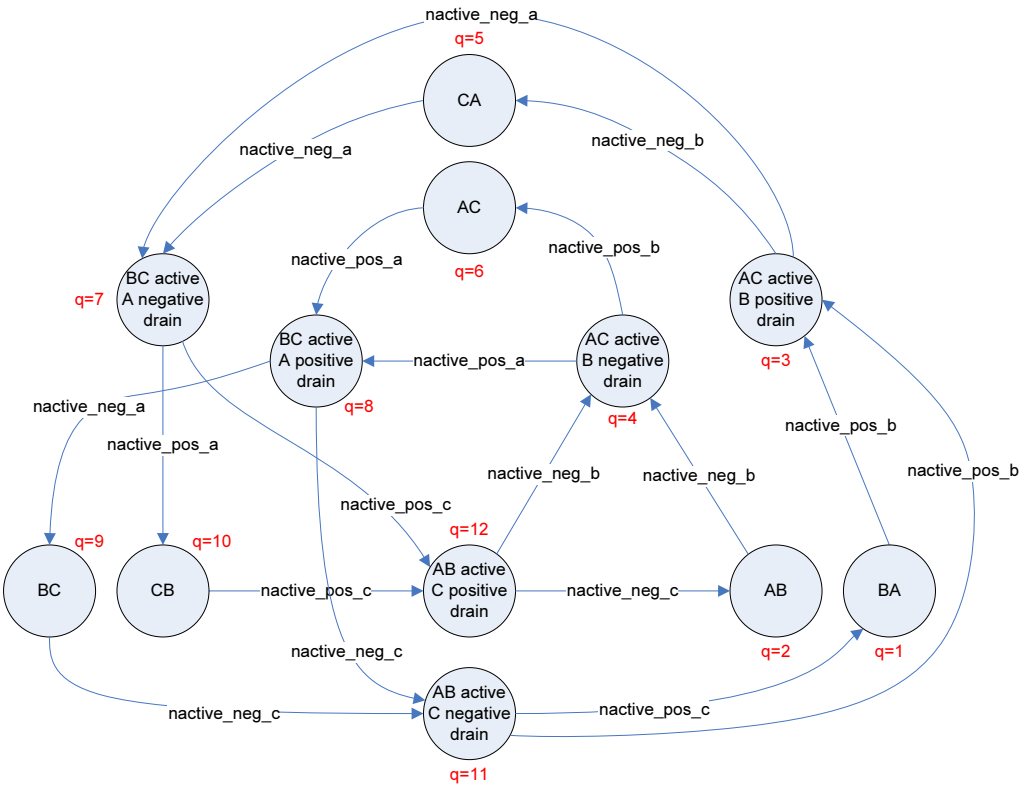

Figure A.1: *Simplified hybrid automaton for the single sensor observer.*

This page is left intentionally blank

REAL TIME IMPLEMENTATION

B

In order to be able to use the observers in closed loop, they need to be able to estimate the angle in real time on the target processor. The implementations need to be reworked so that they can be compiled in dSpace® , and so that the computational complexity is reduced. This chapter only deals with the implementation of the observers, which means that their behaviours are not be changed.

In dSpace® , it is not possible to compile the blocks that are using MATLAB® toolboxes, therefore those parts of the observers are replaced with parts that do not use any toolbox. To reduce the complexity of the observers, the number of calculations made to estimate the states is reduced.

B.1 SIMPLIFICATION OF THE EQUATIONS

In order to reduce the number of calculations used in the observer, all useless calculations are removed. It can be noticed that in the equations of the observers many of the elements of the matrices are zeros. As multiplying with zero always gives zero, those multiplications with zero can be avoided. The idea is to write the equations under a regular form instead of the matrix form that was used before. The equations of the single sensor observer derived in Section 7.3 on page 77 are rewritten as follows:

- **ABC case**, $q \in \{3, 4, 7, 8, 11, 12\}$

$$\begin{aligned}
\frac{d}{dt}i_{as} &= -\frac{r_s}{L_s}i_{as} - \frac{\lambda'_m}{L_s}e_\alpha + \frac{2}{3L_s}V_{as} - \frac{1}{3L_s}(V_{bs} + V_{cs}) \\
\frac{d}{dt}i_{bs} &= -\frac{r_s}{L_s}i_{bs} + \frac{\lambda'_m}{2L_s}e_\alpha - \frac{\sqrt{3}\lambda'_m}{2L_s}e_\beta + \frac{2}{3L_s}V_{bs} - \frac{1}{3L_s}(V_{as} + V_{cs}) \\
\frac{d}{dt}e_\alpha &= -\omega_e e_\beta \\
\frac{d}{dt}e_\beta &= \omega_e e_\alpha
\end{aligned}$$

- **BA case**, $q = 1$, in that case $i_{bs} = -i_{as}$, i.e. $\frac{d}{dt}i_{bs} = -\frac{d}{dt}i_{as}$

$$\begin{aligned}
\frac{d}{dt}i_{as} &= -\frac{r_s}{L_s}i_{as} - \frac{3\lambda'_m}{4L_s}e_\alpha + \frac{\sqrt{3}\lambda'_m}{4L_s}e_\beta + \frac{1}{2L_s}V_{as} - \frac{1}{2L_s}V_{bs} + k_6(\hat{i}_{as} + \frac{i_{cc}}{D_{in}}) \\
\frac{d}{dt}i_{bs} &= -\frac{d}{dt}i_{as} \\
\frac{d}{dt}e_\alpha &= -\omega_e e_\alpha + k_8(\hat{i}_{as} + \frac{i_{cc}}{D_{in}}) \\
\frac{d}{dt}e_\beta &= \omega_e e_\beta + k_9(\hat{i}_{as} + \frac{i_{cc}}{D_{in}})
\end{aligned}$$

- **AB case**, $q = 2$, as for the BA case, $\frac{d}{dt}i_{bs} = -\frac{d}{dt}i_{as}$

$$\begin{aligned}
\frac{d}{dt}i_{as} &= -\frac{r_s}{L_s}i_{as} - \frac{3\lambda'_m}{4L_s}e_\alpha + \frac{\sqrt{3}\lambda'_m}{4L_s}e_\beta + \frac{1}{2L_s}V_{as} - \frac{1}{2L_s}V_{bs} + k_6(\hat{i}_{as} - \frac{i_{cc}}{D_{in}}) \\
\frac{d}{dt}i_{bs} &= -\frac{d}{dt}i_{as} \\
\frac{d}{dt}e_\alpha &= -\omega_e e_\alpha + k_8(\hat{i}_{as} - \frac{i_{cc}}{D_{in}}) \\
\frac{d}{dt}e_\beta &= \omega_e e_\beta + k_9(\hat{i}_{as} - \frac{i_{cc}}{D_{in}})
\end{aligned}$$

- **CA case**, $q = 5$

$$\begin{aligned}
\frac{d}{dt}i_{as} &= -\frac{r_s}{L_s}i_{as} - \frac{3\lambda'_m}{4L_s}e_\alpha - \frac{\sqrt{3}\lambda'_m}{4L_s}e_\beta + \frac{1}{2L_s}V_{as} - \frac{1}{2L_s}V_{cs} + k_{10}(\hat{i}_{as} + \frac{i_{cc}}{D_{in}}) \\
\frac{d}{dt}i_{bs} &= 0 \\
\frac{d}{dt}e_\alpha &= -\omega_e e_\alpha + k_{11}(\hat{i}_{as} + \frac{i_{cc}}{D_{in}}) \\
\frac{d}{dt}e_\beta &= \omega_e e_\beta + k_{12}(\hat{i}_{as} + \frac{i_{cc}}{D_{in}})
\end{aligned}$$

- **AC case**, $q = 6$

$$\begin{aligned}
\frac{d}{dt}i_{as} &= -\frac{r_s}{L_s}i_{as} - \frac{3\lambda'_m}{4L_s}e_\alpha - \frac{\sqrt{3}\lambda'_m}{4L_s}e_\beta + \frac{1}{2L_s}V_{as} - \frac{1}{2L_s}V_{cs} + k_{10}(\hat{i}_{as} - \frac{i_{cc}}{D_{in}}) \\
\frac{d}{dt}i_{bs} &= 0 \\
\frac{d}{dt}e_\alpha &= -\omega_e e_\alpha + k_{11}(\hat{i}_{as} - \frac{i_{cc}}{D_{in}}) \\
\frac{d}{dt}e_\beta &= \omega_e e_\beta + k_{12}(\hat{i}_{as} - \frac{i_{cc}}{D_{in}})
\end{aligned}$$

- **BC case**, $q = 9$

$$\begin{aligned}
\frac{d}{dt}i_{as} &= 0 \\
\frac{d}{dt}i_{bs} &= -\frac{r_s}{L_s}i_{bs} - \frac{\sqrt{3}\lambda'_m}{2L_s}e_\beta + \frac{1}{2L_s}V_{bs} - \frac{1}{2L_s}V_{cs} + k_{13}(\hat{i}_{bs} - \frac{i_{cc}}{D_{in}}) \\
\frac{d}{dt}e_\alpha &= -\omega_e e_\alpha \\
\frac{d}{dt}e_\beta &= \omega_e e_\beta + k_{14}(\hat{i}_{bs} - \frac{i_{cc}}{D_{in}})
\end{aligned}$$

- **CB case**, $q = 10$

$$\begin{aligned}
\frac{d}{dt}i_{as} &= 0 \\
\frac{d}{dt}i_{bs} &= -\frac{r_s}{L_s}i_{bs} - \frac{\sqrt{3}\lambda'_m}{2L_s}e_\beta + \frac{1}{2L_s}V_{bs} - \frac{1}{2L_s}V_{cs} + k_{13}(\hat{i}_{bs} + \frac{i_{cc}}{D_{in}}) \\
\frac{d}{dt}e_\alpha &= -\omega_e e_\alpha \\
\frac{d}{dt}e_\beta &= \omega_e e_\beta + k_{14}(\hat{i}_{bs} + \frac{i_{cc}}{D_{in}})
\end{aligned}$$

The rewritten equations of the observer using two current sensors are derived in the same way, they are as follows:

- **ABC case**, $q \in \{3, 4, 7, 8, 11, 12\}$

$$\begin{aligned}
\frac{d}{dt}i_{as} &= -\frac{r_s}{L_s}i_{as} - \frac{\lambda'_m}{L_s}e_\alpha + \frac{2}{3L_s}V_{as} - \frac{1}{3L_s}(V_{bs} + V_{cs}) + k_1\Delta i_{as} \\
\frac{d}{dt}i_{bs} &= -\frac{r_s}{L_s}i_{bs} + \frac{\lambda'_m}{2L_s}e_\alpha - \frac{\sqrt{3}\lambda'_m}{2L_s}e_\beta + \frac{2}{3L_s}V_{bs} - \frac{1}{3L_s}(V_{as} + V_{cs}) + k_2\Delta i_{bs} \\
\frac{d}{dt}e_\alpha &= -\omega_e e_\beta + k_3\Delta i_{as} + k_4\Delta i_{bs} \\
\frac{d}{dt}e_\beta &= \omega_e e_\alpha + k_5\Delta i_{bs}
\end{aligned}$$

- **BA case**, $q = 1$, in that case $i_{bs} = -i_{as}$, i.e. $\frac{d}{dt}i_{bs} = -\frac{d}{dt}i_{as}$

$$\begin{aligned}
\frac{d}{dt}i_{as} &= -\frac{r_s}{L_s}i_{as} - \frac{3\lambda'_m}{4L_s}e_\alpha + \frac{\sqrt{3}\lambda'_m}{4L_s}e_\beta + \frac{1}{2L_s}V_{as} - \frac{1}{2L_s}V_{bs} + k_6\Delta i_{as} \\
\frac{d}{dt}i_{bs} &= -\frac{d}{dt}i_{as} \\
\frac{d}{dt}e_\alpha &= -\omega_e e_\alpha + k_8\Delta i_{as} \\
\frac{d}{dt}e_\beta &= \omega_e e_\beta + k_9\Delta i_{as}
\end{aligned}$$

- **AB case**, $q = 2$, as for the BA case, $\frac{d}{dt}i_{bs} = -\frac{d}{dt}i_{as}$

$$\begin{aligned}
\frac{d}{dt}i_{as} &= -\frac{r_s}{L_s}i_{as} - \frac{3\lambda'_m}{4L_s}e_\alpha + \frac{\sqrt{3}\lambda'_m}{4L_s}e_\beta + \frac{1}{2L_s}V_{as} - \frac{1}{2L_s}V_{bs} + k_6\Delta i_{as} \\
\frac{d}{dt}i_{bs} &= -\frac{d}{dt}i_{as} \\
\frac{d}{dt}e_\alpha &= -\omega_e e_\alpha + k_8\Delta i_{as} \\
\frac{d}{dt}e_\beta &= \omega_e e_\beta + k_9\Delta i_{as}
\end{aligned}$$

- **CA case**, $q = 5$

$$\begin{aligned}
\frac{d}{dt}i_{as} &= -\frac{r_s}{L_s}i_{as} - \frac{3\lambda'_m}{4L_s}e_\alpha - \frac{\sqrt{3}\lambda'_m}{4L_s}e_\beta + \frac{1}{2L_s}V_{as} - \frac{1}{2L_s}V_{cs} + k_{10}\Delta i_{as} \\
\frac{d}{dt}i_{bs} &= 0 \\
\frac{d}{dt}e_\alpha &= -\omega_e e_\alpha + k_{11}\Delta i_{as} \\
\frac{d}{dt}e_\beta &= \omega_e e_\beta + k_{12}\Delta i_{as}
\end{aligned}$$

- **AC case**, $q = 6$

$$\begin{aligned}
\frac{d}{dt}i_{as} &= -\frac{r_s}{L_s}i_{as} - \frac{3\lambda'_m}{4L_s}e_\alpha - \frac{\sqrt{3}\lambda'_m}{4L_s}e_\beta + \frac{1}{2L_s}V_{as} - \frac{1}{2L_s}V_{cs} + k_{10}\Delta i_{as} \\
\frac{d}{dt}i_{bs} &= 0 \\
\frac{d}{dt}e_\alpha &= -\omega_e e_\alpha + k_{11}\Delta i_{as} \\
\frac{d}{dt}e_\beta &= \omega_e e_\beta + k_{12}\Delta i_{as}
\end{aligned}$$

- **BC case**, $q = 9$

$$\begin{aligned}
\frac{d}{dt}i_{as} &= 0 \\
\frac{d}{dt}i_{bs} &= -\frac{r_s}{L_s}i_{bs} - \frac{\sqrt{3}\lambda'_m}{2L_s}e_\beta + \frac{1}{2L_s}V_{bs} - \frac{1}{2L_s}V_{cs} + k_{13}\Delta i_{bs} \\
\frac{d}{dt}e_\alpha &= -\omega_e e_\alpha \\
\frac{d}{dt}e_\beta &= \omega_e e_\beta + k_{14}\Delta i_{bs}
\end{aligned}$$

- **CB case**, $q = 10$

$$\begin{aligned}
\frac{d}{dt}i_{as} &= 0 \\
\frac{d}{dt}i_{bs} &= -\frac{r_s}{L_s}i_{bs} - \frac{\sqrt{3}\lambda'_m}{2L_s}e_\beta + \frac{1}{2L_s}V_{bs} - \frac{1}{2L_s}V_{cs} + k_{13}\Delta i_{bs} \\
\frac{d}{dt}e_\alpha &= -\omega_e e_\alpha \\
\frac{d}{dt}e_\beta &= \omega_e e_\beta + k_{14}\Delta i_{bs}
\end{aligned}$$

Under matrix form, the number of multiplications required is the same for all different discrete states, as the sizes of the state vector, input vector, and estimation error vector are constants. There are 4 states, 3 inputs, and 2 errors of estimation, this means that the number of multiplications required is:

$$\begin{aligned}
NbMultiplications &= \underbrace{NbStates}_{4} \cdot (\underbrace{NbStates + NbInputs + NbErrors}_{4+3+2=9}) \\
&= 36
\end{aligned}$$

Table B.1 on the following page represents the number of multiplications that are required using the regular equations, i.e. without the matrix form. The table also shows how the complexity of the calculation was reduced by rewriting the equations.

The table shows that rewriting the equations allowed to reduce the number of multiplications to 11 in the worst cases, meaning in ABC, AB, and BA cases. The computation of the derivatives of the states has been reduced with 69% in those cases.

Case	Number of multiplications required	Percentage of multiplications saved
ABC	11	69%
BA	11	69%
AB	11	69%
CA	10	72%
AC	10	72%
BC	8	78%
CB	8	78%

TABLE B.1: *Table of the number of multiplications required depending on the discrete state.*

B.2 FSA

The next element that was taken into consideration, was the Stateflow® diagram of the hybrid automaton. Stateflow® is a MATLAB® toolbox that is used for simulating event-driven systems. This toolbox is a good solution for testing new designs, however it was assumed that direct implementation of the hybrid automaton could benefit in faster performance. The switching sequence was easy to implement as an embedded Simulink® function.

B.3 CHECKMATE REMOVAL

The goal of the observer is to implement it on the real hardware using dSpace®. Therefore, some restrictions are applicable. dSpace® does not support some of the toolboxes like for example CheckMate Toolbox. This toolbox is used for verification and easy implementation of hybrid systems in Simulink®, however dSpace® is not capable of compiling it so that it can run on the target processor.

CheckMate Toolbox was used for implementation of the continuous switched system, that is the continuous equations that are changing depending on the hybrid state. BLDCM Switched Continuous System block includes the implemented differential equations and it integrates them to output the continuous states. This block could be replaced by two separate yet standard Simulink® blocks. One would consists of the switching part of the continuous differential equations, while the second block would integrate the state. This is illustrated in Figure B.1 on the next page.

The reset function is only applied to assure that when the currents are drained, their

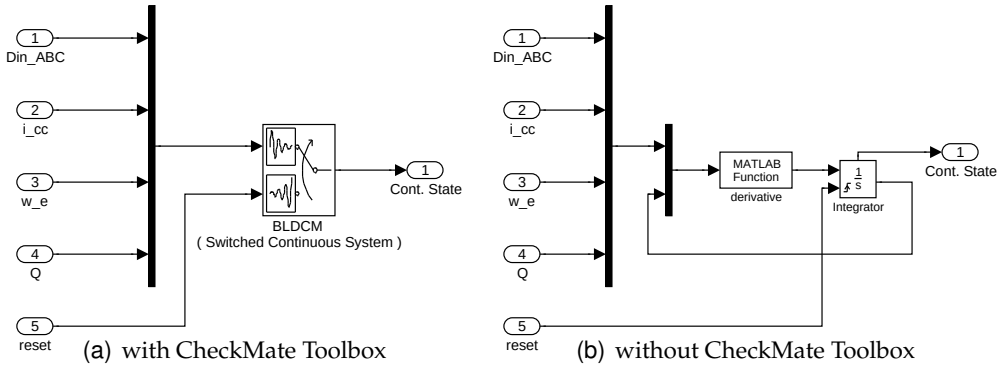

FIGURE B.1: *Simulink® implementation of continuous differential equations (continuous switched system).*

value will be zero. Otherwise it could happen, that due to the solver step size, the values of drained current would cross zero. They would then stay close, but different than zero. This is only caused by the calculation procedure, the smaller solver step size would reduce this problem. However this would slow down the calculations.

The observers can now be compiled with dSpace® and sent to the target processor of the system. The observers were tested online under the same conditions as offline. The test allowed to verify that the observers were able to estimate the angle in real time, while having the same performance as when they estimate offline. The observers can now be used to provide the angle estimate to a closed loop controller in order to check their efficiencies in real conditions.

This page is left intentionally blank

Results of the closed loop tests of the double sensor observer

C

This appendix presents the results of the closed loop tests of the observer using phase measurements to estimate the angle. The results are presented for different values of the maximum angular velocity.

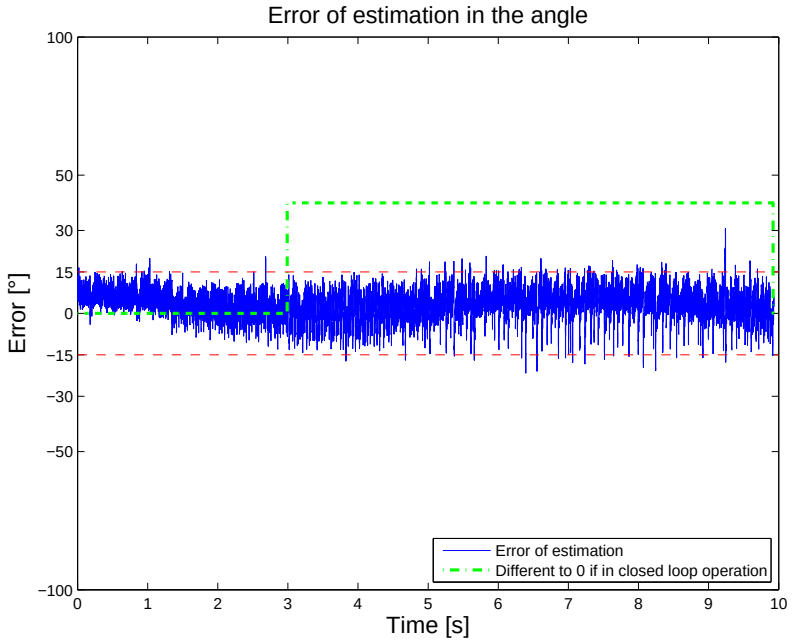

Figure C.1: *Error of estimation in the angle with maximum speed* $\omega_e = 215\,[\mathrm{rad}\cdot\mathrm{s}^{-1}]$ *(*$\omega_r = 680\,[\mathrm{rpm}]$*).*

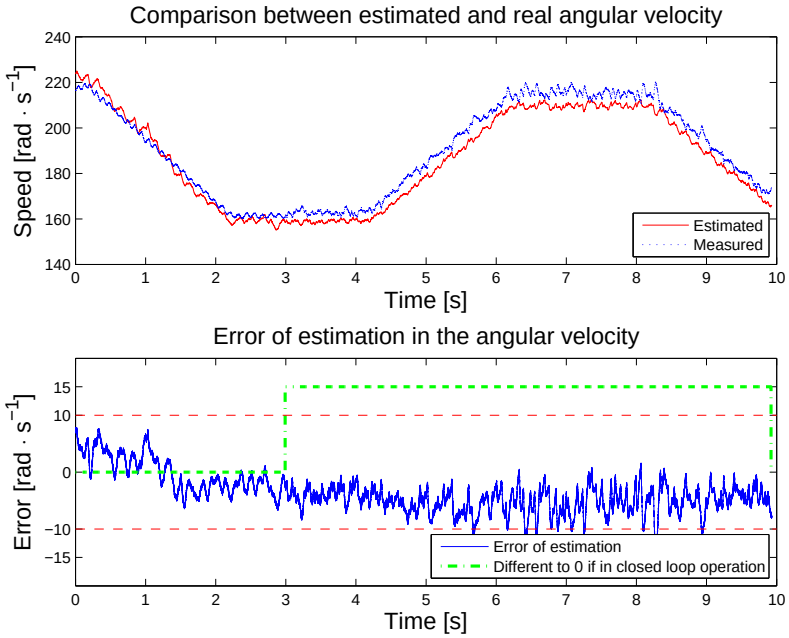

FIGURE C.2: *Speed estimation with maximum speed* $\omega_e = 215\,[\mathrm{rad}\cdot\mathrm{s}^{-1}]$ *(*$\omega_r = 680\,[\mathrm{rpm}]$*).*

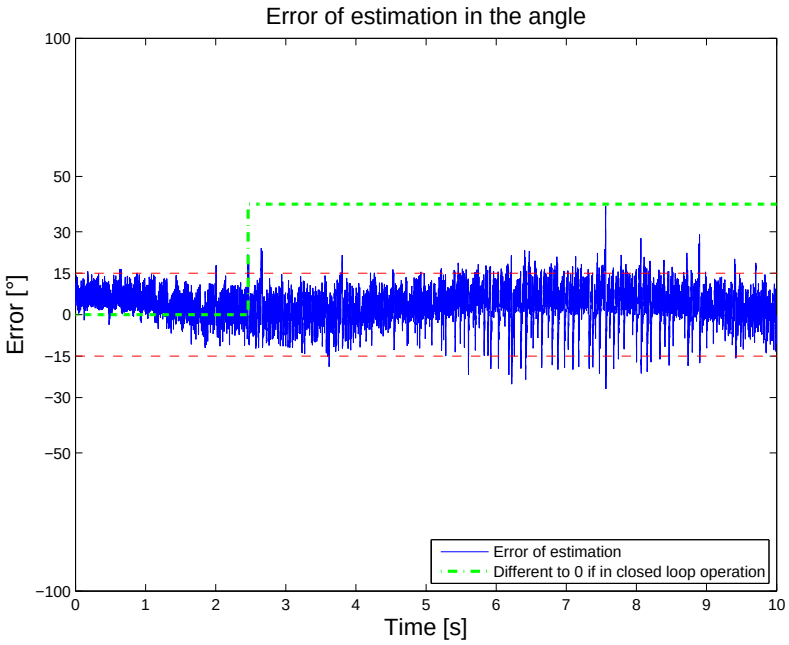

FIGURE C.3: *Error of estimation in the angle with maximum speed* $\omega_e = 235\,[\mathrm{rad}\cdot\mathrm{s}^{-1}]$ *(*$\omega_r = 750\,[\mathrm{rpm}]$*).*

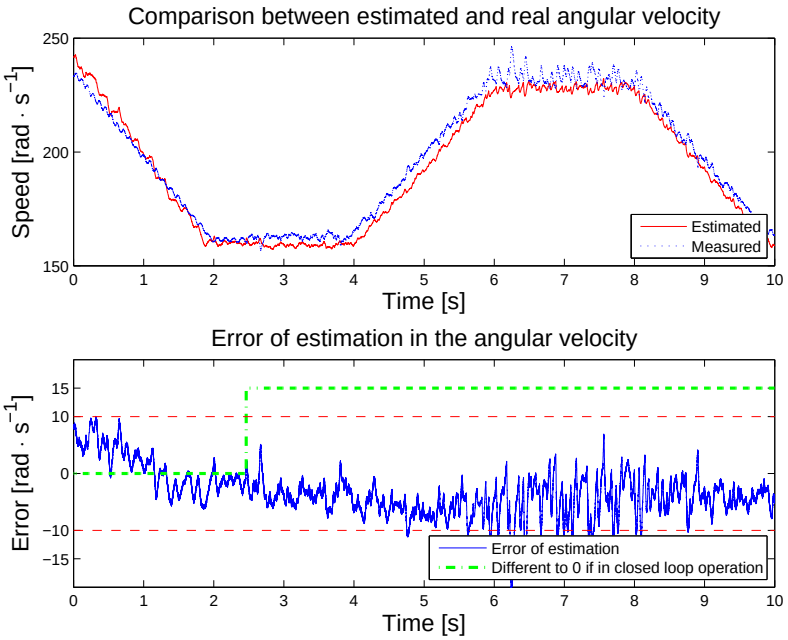

FIGURE C.4: *Speed estimation with maximum speed* $\omega_e = 235\,[\mathrm{rad}\cdot\mathrm{s}^{-1}]$ *(*$\omega_r = 750\,[\mathrm{rpm}]$*).*

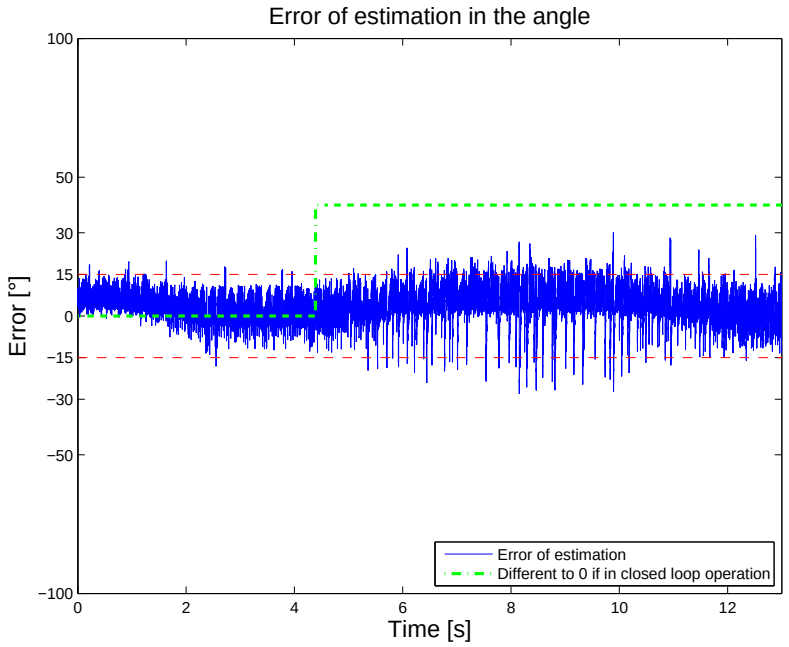

FIGURE C.5: *Error of estimation in the angle with maximum speed* $\omega_e = 255\,[\mathrm{rad}\cdot\mathrm{s}^{-1}]$ *(*$\omega_r = 810\,[\mathrm{rpm}]$*).*

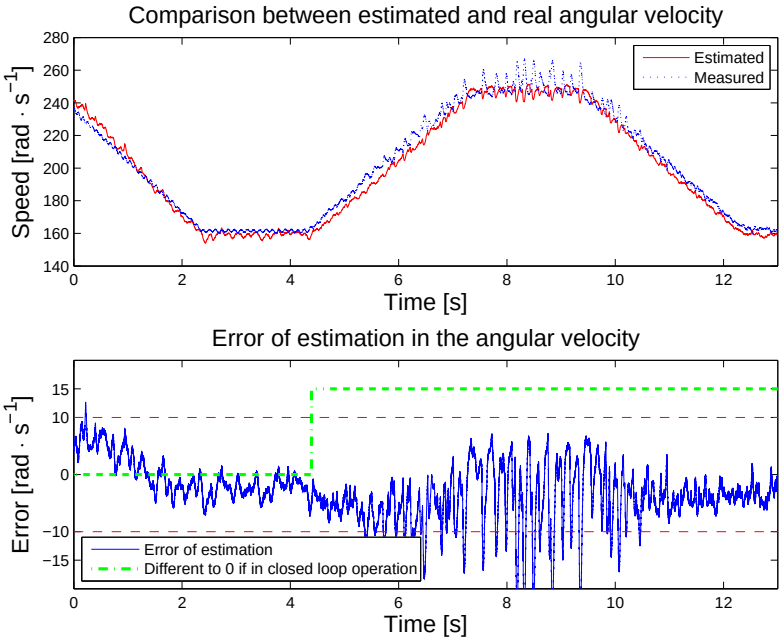

FIGURE C.6: *Speed estimation with maximum speed* $\omega_e = 255\,[\mathrm{rad}\cdot\mathrm{s}^{-1}]$ *(*$\omega_r = 810\,[\mathrm{rpm}]$*).*

NOMENCLATURE

B_m	Damping coefficient of the motor
D_{in}	Input duty cycle to the inverter
e_α, e_β	States that correspond to the back-EMF
e_θ	Error between the electrical angle calculated by the observer, $\hat{\theta}_e$, and the measured angle, θ_e
$\mathbf{i}_{abcs}$	Vector of currents through the phases
i_{cc}	Supply current to the inverter
$\Delta\mathbf{i}$	Difference between estimated and measured currents
$\hat{\mathbf{i}}$	Estimated current vector: $\hat{\mathbf{i}} = \begin{bmatrix} \hat{i}_{as} & \hat{i}_{bs} \end{bmatrix}^T$
i_{xs}	Stator current in phase x
J	Moment of inertia of the rotating part, i.e. rotor and load
${}^q\mathbf{K}$	Proportional gain matrix in the observer in location q
λ	number of offspring in population
λ'_m	Magnitude of the fundamental component of the back-EMF
L_s	Equivalent inductance of a phase
μ	number of parents in population
$\hat{\omega}_e$	Estimated electrical angular velocity
Q	Cost function
r_s	Ohmic resistance of a phase
T_e	Torque produced by the motor
$\hat{\theta}_e$	Estimated electrical angle of the rotor
θ_e	Electrical angle
θ_r	Mechanical angle

T_L	Torque produced by the load
T_{PWM}	Period of the PWM signal, $T_{PWM} = 6.25 \cdot 10^{-5}$ [s]
T_s	Sampling period of the system, $T_s = 6.25 \cdot 10^{-5}$ [s]
$\mathbf{V}_{abcs}$	Vector of input voltages
φ	Mutation coefficient
V_{cc}	Supply voltage of the current inverter
V_n	Neutral node potential
V_{xs}	Input Potential to phase x in stator reference frame
x^o	Offspring individual
ω_e, ω_r	Electrical and mechanical angular velocity
x^p	Parent individual
Z_p	Number of magnetic pole pairs

ACRONYMS

ANN	Artificial Neural Networks
BLDCM	Brushless DC Motor
EA	Evolutionary Algorithm
EC	Evolutionary Computation
EMF	ElectroMotive Force
DE	Differential Evolution
FSA	Finite State Automaton
NSS	Nonlinear Simplex Search
PM	Permanent Magnet
PPT	PWM-PWM-Tristate

PSO Particle Swarm Optimization

PWM Pulse Width Modulation

RWC Random Weight Change

SI Swarm Intelligence

SUS Stochastic Universal Sampling